Fall 2020

EFFECTS OF STORMS ON NITRATE REMOVAL AND GREENHOUSE GAS EMISSIONS FROM FLUVIAL WETLAND DOMINATED SURFACE WATER FLOW PATHS

Sarah Bower
University of New Hampshire, Durham

EFFECTS OF STORMS ON NITRATE REMOVAL AND GREENHOUSE GAS EMISSIONS FROM FLUVIAL WETLAND DOMINATED SURFACE WATER FLOW PATHS

BY

SARAH E. BOWER

B.S. Geoscience, Environmental Studies, William Smith College, 2016

THESIS

Submitted to the University of New Hampshire

in Partial Fulfillment of

the Requirements for the Degree of

Master of Science

in

Natural Resources: Soil and Water Resource Management

September, 2020

EFFECTS OF STORMS ON NITRATE REMOVAL AND GREENHOUSE GAS EMISSIONS

FROM FLUVIAL WETLAND DOMINATED SURFACE WATER FLOW PATHS

BY

SARAH E. BOWER

This thesis was examined and approved in partial fulfillment of the requirements for the degree of Master of Science in Natural Resources: Soil and Water Resource Management by:

Thesis Director, Dr. Wilfred M. Wollheim, Associate Professor
Natural Resources and the Environment

Dr. William H. McDowell, Professor
Natural Resources and the Environment

Dr. Ruth K. Varner, Professor
Earth Sciences

On July 21st, 2020

Approval signatures are on file with the University of New Hampshire Graduate School.

ACKNOWLEDGEMENTS

I would like to thank my advisor, Dr. Wilfred M. Wollheim, for providing me the opportunity to purse a M.S. degree in Natural Resources Management and for his guidance through this project. His endless dedication, enthusiasm, and support were vital to the completion of this project. I would also like to thank my committee members, Drs. Ruth Varner and William H. McDowell, for their support and expertise throughout this project. I sincerely want to thank Eliza Balch, Katherine Perez-Rivera, Cindy Bova, Hannah Miller, Yue Hu and Mackenzie Kalp for their very generous field support, as this project would not have been possible without them and their countless efforts! I'd also like to thank Andrew Robison and Chris Whitney, as well as the rest of the Water Systems Analysis Group (WSAG), for their mentorship and critical feedback during my graduate school experience. Being a part of the Plum Island Ecosystem Long Term Ecological Research (PIE-LTER) network and having the opportunity to work with many devoted researchers from a variety of disciplines, universities, and organizations has been an invaluable experience for me. Also, thank you to Jody Potter, Danielle Chancey, and Jimmy Casey for all of their laboratory help and instruction, and for always being of assistance in a pinch! Lastly, I would like to thank my family and friends for being strong shoulders to lean on along the way and for always encouraging me to pursue my academic and career aspirations. Support for this research was provided by the University of New Hampshire (UNH) Teaching Assistant (TA) Fellowship, the UNH Summer TA Fellowship, the Plum Island Ecosystems Long Term Ecological Research (PIE-LTER) grant (OCE #1637630), and the New Hampshire Agriculture Experiment Station grant (#0225006).

TABLE OF CONTENTS

LIST OF TABLES

LIST OF FIGURES

ABSTRACT

EFFECTS OF STORMS ON NITRATE REMOVAL AND GREENHOUSE GAS EMISSIONS FROM FLUVIAL WETLAND DOMINATED SURFACE WATER FLOW PATHS

By

Sarah E. Bower

University of New Hampshire

Fluvial wetlands, wetlands connected to streams and rivers, can act as buffers in headwaters to limit nitrogen (N) from reaching downstream coastal ecosystems and causing problems, such as coastal eutrophication and loss of habitat. However, as significant hotspots for N removal, fluvial wetland dominated streams are also natural sources of greenhouse gas (GHG) to the atmosphere and contribute to global climate change. With ongoing changes to the flow regime from increased climate variability and intensification of storm events, as well as landscape development, the ability for fluvial wetland dominated streams to regulate downstream N fluxes may decline and come at a greater cost of GHG emissions. To better understand these tradeoffs, I investigated storm influence on nitrate (NO_3^-) removal and GHG evasion along two fluvial wetland dominated flow paths with differing nutrient inputs (high vs. low) in an urbanizing coastal watershed in New England. Results suggest that flow paths with abundant fluvial wetlands are able to remove most NO_3^- (median NO_3^--N removal = 95%) over a wide range of flow conditions. Due to their substantial demand for NO_3^-, fluvial wetland dominated streams were greater sinks of NO_3^- than upstream channels. Although emissions by fluvial wetland dominated reaches are much larger than those by channels when total area is considered, fluvial wetland dominated streams were found to emit lower GHG compared to channelized streams on a per unit area basis. After storms during heightened flow conditions, the flow paths

maintained high NO_3^- removal but showed tendencies for greater GHG evasion, as areal GHG evasion by wetland dominated streams increased on average by more than 19,000 mg m^{-2} d^{-1} for carbon dioxide (CO_2), 49 mg m^{-2} d^{-1} for methane (CH_4), and 0.15 mg m^{-2} d^{-1} for nitrous oxide (N_2O) over an order of magnitude change in discharge. Thus, as climate variability intensifies, we can expect to see pulses in GHG emissions along whole flow paths. However, GHG evasion by wetland dominated streams did not increase in association with higher nutrient loads. Ultimately, the ability for fluvial wetland dominated streams to effectively remove NO_3^- from surface water flow paths draining higher N inputs does not come at the expense of greater GHG emissions beyond those that naturally occur. Understanding these tradeoffs in river networks is important for improving the management of coastal watersheds and predicting how diverse fluvial systems will respond as N loading increases in a changing climate.

CHAPTER 1: INTRODUCTION

Human activity has greatly increased the availability of reactive nitrogen (N) in both terrestrial and aquatic ecosystems over the past several decades (Howarth et al. 2002b, Galloway et al. 2003). With industrial runoff, fertilizer use, and leaky septic tanks enhancing N inputs to the landscape, larger loads of N, typically as nitrate (NO_3^-), are being introduced to river networks and transported downstream to coastal waters (Howarth et al. 2002a, b). Because NO_3^- can be limiting in coastal ecosystems, its availability in excess can have detrimental effects like eutrophication and growth of dead zones (Anderson et al. 2002, Rabalais et al. 2002). Riverine N inputs to coastal ecosystems have been estimated to have increased seven-fold from anthropogenic activity (Howarth et al. 2002b, Galloway et al. 2003), and this trend will likely continue into the future (Chen et al. 2014). If land use and climate change continue at present rates, future riverine export of N could increase by up to 45% (Chen et al. 2014), suggesting that coastal ecosystems may become increasingly vulnerable to the effects of both urban development and climate variability (Faulkner 2004, Talbot et al. 2018).

While N inputs to freshwater ecosystems are growing, less than one-third of these anthropogenic N inputs gets transferred to the ocean, demonstrating that considerable sinks exist in coastal watersheds that aid in both the permanent and temporary removal of N (Boyer et al. 2002, Mulholland et al. 2004). Aquatic ecosystems have been estimated to remove over 50% of the total N inputs from land (Wollheim et al. 2008b), with 15% to 33% of dissolved inorganic N (DIN) removal predicted to be a result of denitrification by rivers (Wollheim et al. 2008a). While streams and rivers contribute to N removal by aquatic ecosystems, proportional N removal is often higher among wetlands (Saunders and Kalff 2001). Wetlands are natural sinks of NO_3^-, as

they are highly efficient at permanently removing N through denitrification, the microbial reduction of NO_3^- to atmospheric N gas (N_2), and temporarily retaining it in plant biomass (Vymazal 2007). Their long water residence times, low oxygen (O_2) conditions, and abundance of labile organic carbon (C) fuel high rates of denitrification in wetlands compared to their channelized counterparts (Saunders and Kalff 2001, Baron et al. 2013, Wollheim et al. 2014, Schmadel et al. 2019).

As hotspots for denitrification and other anaerobic metabolic processes, wetlands are also sources of greenhouse gas (GHG) to the atmosphere (Picek et al. 2007, Ström et al. 2007, Kayranli et al. 2010, Mitsch et al. 2013, Flint and McDowell 2015, Marín-Muñiz et al. 2015). With consistently saturated anoxic soils, wetlands serve as transition zones linking terrestrial and aquatic ecosystems, and are ideal environments for GHG production and emission (Mitsch et al. 2013, Marín-Muñiz et al. 2015). Specifically, wetlands emit methane (CH_4) and nitrous oxide (N_2O) as a consequence of reduced sediment conditions and abundant plant biomass that promote processes like denitrification and methanogenesis (Kayranli et al. 2010). Although denitrification mainly converts NO_3^- to N_2, N_2O can also be released as a byproduct (Gao et al. 2013). Annually, wetlands contribute largely to global GHG emissions as the largest natural source of CH_4 (Dalal et al. 2008). When O_2 is available in sediments, wetlands also produce carbon dioxide (CO_2) from organic matter respiration, which lead to subsequent CO_2 emissions from these systems (Page and Dalal 2011, Marín-Muñiz et al. 2015).

While N removal and GHG production and emissions from wetlands in general have been well studied, fewer studies address these processes and their tradeoffs in *fluvial* wetlands. Fluvial wetlands are wetlands connected to streams and rivers, and thus receive continuous supplies of water and nutrients from any sources upstream. Their presence along surface water

flow paths have been found to lower redox potential and enhance connectivity of advective flows with sediments where anaerobic metabolic processes mainly occur (Stewart et al. 2011, Wollheim et al. 2014, Schmadel et al. 2018). Previous studies revealed headwater or flow-through wetlands were associated with low NO_3^- concentrations (Flint and McDowell 2015; Czuba et al. 2018; Hansen et al. 2018) and high dissolved organic C (DOC) content (Flint and McDowell 2015). Because of their larger reactive surface area and direct connection to advective flows, flow-through wetlands have been found to have a greater effect on watershed NO_3^- removal than geographically isolated wetlands (Czuba et al. 2018), suggesting that they may be larger hotspots of N removal than wetlands separated from advective flow. Studies like Wollheim et al. (2014), revealing higher NO_3^- reaction rates in fluvial wetlands than channelized streams, emphasize that fluvial wetlands increase N processing rates and alter water chemistry in river networks (Czuba et al. 2018).

Fluvial wetlands, however, may be especially vulnerable to changes in hydrology and resource supply because their capacity to both remove NO_3^- and emit GHG depends largely on the availability of key nutrients (Thiere et al. 2011, Kaushal et al. 2014), which become greatly elevated when runoff is increased (Talbot et al. 2018). Connections between main advective flow and fluvial wetlands can expand in response to storm events and land use change, potentially promoting greater N removal and GHG emission along headwater flow paths (Stewart et al. 2011, Kaushal et al. 2014, Talbot et al. 2018). While some studies indicate that N removal may decline with increasing streamflow as NO_3^- becomes saturated and overwhelms demand in the system (Peterson et al. 2001, Wollheim et al. 2005, 2017, 2018), there is evidence suggesting that wetlands help buffer watershed N saturation with increasing flows and NO_3^- loading (Thiere et al. 2011, Wollheim et al. 2018). Since they are generally more reactive than stream channels

and isolated wetlands (Wollheim et al. 2014, Czuba et al. 2018), fluvial wetlands maintain high absolute rates of N removal, especially with higher N loading (Thiere et al. 2011), and likely require larger N inputs to become saturated. Although isolated wetlands have been found to be significant sinks of nitrate following precipitation events (Fink and Mitsch 2004, Griffiths and Mitsch 2017), fluvial wetlands may be more effective at removing N as they potentially intercept a large portion of the total N fluxes within watershed.

To better understand the tradeoffs between NO_3^- removal and GHG emissions from fluvial wetland dominated streams as N loading increases in a changing climate, this paper sought to answer: (1) How do fluvial wetland dominated streams contribute to NO_3^- removal and GHG emissions from river networks? and (2) How does their contribution vary across flow conditions? I hypothesized that fluvial wetland dominated streams would increase NO_3^- removal and areal GHG emissions in N_2O and CH_4 along surface water flow paths because their more reduced conditions would promote higher rates of NO_3^- removal, N_2O production, and CH_4 production compared to channels. Because of their lower O_2 conditions, fluvial wetlands may lower CO_2 production via slower rates of respiration, subsequently reducing CO_2 emissions per unit area along surface water pathways. Further, I hypothesized that NO_3^- removal by fluvial wetland dominated streams would decline at high flow levels because N inputs to the system would surpass sinks, leading to an export of NO_3^- further downstream. Greater NO_3^- availability downstream following storms was predicted to enhance areal N_2O emissions from fluvial wetland systems because of increased N_2O production from denitrification while lowering areal CH_4 emissions as methanogenesis becomes limited by NO_3^-, a more energetically favorable terminal electron acceptor. Areal CO_2 emissions from fluvial wetlands were predicted to increase with higher flows as organic matter respiration increases due to likely higher O_2 conditions

following storms. Findings will enhance our understanding of the role of fluvial wetland dominated streams in river networks and their vulnerability to a changing environment.

CHAPTER 2: METHODS

Study area & design

Two systems of surface water flow paths with an abundance of fluvial wetlands were monitored in this study. The flow paths investigated are situated in the coastal lowland section of northeastern Massachusetts, U.S.A, in the headwaters of the Ipswich River watershed, a Plum Island Ecosystem Long Term Ecological Research (PIE-LTER) watershed (Figure 1). The Ipswich River drains a 400 km^2 watershed, which includes northern suburbs of Boston, MA – the largest major city in New England. Each system is nearly 10 kilometers long, beginning as channelized streams (~2-3 km long) that flow into extensive fluvial wetland habitat (Figure 2). Nutrient inputs to fluvial wetland reaches from upstream river channels were different among the two flow paths due to variation in upstream land cover. Nutrient inputs to the two systems varied, with much higher levels of NO_3^--N (0.67 mg N L^{-1}) in the system with more urbanization upstream, and lower levels (0.17 mg N L^{-1}) in the less urbanized system.

Based on differences in upstream water chemistry, the studied flow paths were termed "higher nutrient" or "lower nutrient" to depict their contrasting nutrient environments. The higher nutrient flow path (HN-FP), located in the upper Ipswich, drains 30% urban, 41% forested, and 23% wetland land cover, while the lower nutrient flow path (LN-FP), located along the more northern tributary of the Ipswich, drains 15% urban, 51% forested, and 32% wetland land cover (Figure 1; Table A2). With more urban and less forested land cover than the LN-FP, the HN-FP experiences greater input of nutrients from the terrestrial landscape. Fluvial wetland cover, however, increases similarly downstream along both flow paths (Table 1; Figure 2).

The two flow paths were sampled synoptically before and during storm events throughout one growing season (June to November 2019). There were 16 study sites where surface waters

were sampled, including 9 from the HN-FP and 7 from the LN-FP (Figure 1). Sampling of transects occurred in the morning until early afternoon to minimize the effects of diel variability. Streams were sampled along the upstream channel portion of a flow path (between 0 and 2-3 km), while fluvial wetlands were sampled along the downstream portion of the flow path (downstream of 2-3 km) where fluvial wetlands are abundant (Figure 2; Table 1). Sampling at fluvial wetlands occurred in constricted locations of advective zones, such that measurements reflect the combined output of advective central channel and adjacent fluvial wetlands.

Surface waters were sampled for dissolved nutrients and GHGs across a range of flow conditions during each storm event to address how changes in hydrology alter estimated nitrate removal and GHG emission dynamics. Estimated GHG emissions focused solely on diffusive fluxes, excluding emissions from ebullition and plant mediated transport; while these additional emission pathways may be important to overall emissions by flow paths, they were not considered here. For each storm sampled, one baseflow sampling was performed, typically the day prior to the storm, to measure how surface waters behave under characteristic baseflow conditions. One or two transects were then collected during each storm, generally 24 and 48 hours after storm flow initiation, in order to assess the response of elevated flow on dissolved nutrient and GHG dynamics along each flow path. Two transects were sampled instead of one to allow for storm pulses to reach downstream fluvial wetlands along the flow paths because advective flows slow as they pass through extensive fluvial wetland habitat.

Four different storms were sampled for each flow path, but only 3 storms per flow path were considered for storm-specific analyses. Storms were targeted on semi-seasonal time scales, such as early summer, mid-summer, late summer and fall, to include a range of storm sizes and streamflow. A total of 8 storms, 4 per flow path, were sampled throughout the study period,

totaling 21 sampling days (4 baseflow and 7 stormflow for the HN-FP, and 4 baseflow and 6 stormflow for the LN-FP; Figure A1); however, storm-specific analyses were limited to 6 of 8 storms, 3 per flow path, because 2 storms were similar to conditions at baseflow such that stormflows did not reach the benchmark of 2x the baseflow conditions (see Storm Event Delineation section of methods; Figure 3; Figure A18). Runoff coefficients for the storms sampled were reasonably low, ranging from 0.045 to 0.175 along the fluvial wetland portion of the flow path and 0.115 to 0.179 along the channelized portion (Table 2), but comparable to previous observations for summer response in the watershed (Pellerin et al. 2004).

Field and laboratory procedure

Water chemistry samples were collected in polypropylene syringes and filtered through pre-combusted Whatman GF/F 0.7 µm glass fiber filters into 60 mL bottles. Samples were kept cold in the field until returned to the lab and stored frozen until analysis. Samples were analyzed in the Water Quality Analysis Lab (WQAL) at the University of New Hampshire (UNH) for concentrations of NO_3^- and other solutes such as ammonium (NH_4^+), total dissolved nitrogen (TDN), DOC, chloride (Cl^-), and sulfate (SO_4^{2-}) to understand controls on NO_3^- and GHG dynamics. Nitrate, Cl^-, and SO_4^{2-} were analyzed using a Dionex ICS-1000, NH_4^+ using a Unity Scientific SmartChem 200 Discrete Analyzer, and TDN and DOC using a Shimadzu TOC-L with a TNM-1 and ASI-V Autosampler.

Dissolved gas samples (CO_2, CH_4, and N_2O) were collected in 60 mL polypropylene syringes fitted with two-way stopcocks. Dissolved gas samples were collected in duplicate at all sites but two (randomly chosen), where samples were collected in triplicate. To capture surface water samples that were clear of air bubbles, syringes were filled to 30 mL with water, expelled

any air bubbles out of the syringe, emptied underwater and refilled to 30 mL. Immediately upon returning to the WQAL at UNH, syringes were introduced with 30 mL of helium and shaken for 5 minutes to equilibrate gases between the sample water and headspace (Mulholland et al. 2004). The 30 mL of equilibrated gas from the headspace was then injected into a 20 mL evacuated, sealed vial and run on the Shimadzu GC-2014 gas chromatograph for concentrations of CH_4, CO_2, and N_2O. Standards of CO_2, CH_4, and N_2O were included in each run at the beginning and end, and after every 12 samples. Using methods from Mulholland et al. (2004), gas concentrations in the headspace were converted to partial pressure of dissolved gas (pCO_2, pCH_4, or pN_2O) in the water sample (in ppm) to account for Henry's Law (environmental conditions such as water temperature and atmospheric pressure) and the Bunsen Solubility Coefficients of each gas at the time of sampling.

Dissolved oxygen (DO) concentration (mg L^{-1}) and percent saturation (%), water temperature (ºC), and specific conductance (µS cm^{-1}) were measured in the field at the time of sampling using a handheld YSI Pro30 conductivity meter and YSI ProODO Optical DO instrument. To detect if denitrification was occurring at study sites, 12 mL vials of surface water were collected in triplicate from each site for N_2:Ar analysis, ensuring no bubbles occurred in the sample vial (O'Brien et al. 2012). Samples for MIMS analysis were stored in the refrigerator for up to 30 days until analyzed for N_2:Ar ratios using a Bay Instruments Membrane Inlet Mass Spectrometer in the WQAL at UNH. N_2:Ar ratios were used instead of N_2 concentration due to superior accuracy by the instrument at measuring the ratios of masses versus individual masses. N_2:Ar disequilibrium between N_2:Ar concentrations measured in surface waters and N_2:Ar at saturation with the atmosphere was analyzed.

Hydrological conditions

Flows were measured periodically across a range of flow conditions at one headwater stream and fluvial wetland dominated stream location along each flow path to assess changes in hydrologic conditions within the channelized and fluvial wetland portions of the transects. Flows at headwater stream locations include SB, a PIE-LTER site, in the HN-FP (drainage area = 3.9 km^2) and IS_135 in the LN-FP (drainage area = 1.8 km^2). Continuous water level and discharge data at SB during the study period was obtained from the PIE-LTER network; continuous water level was not recorded at IS_135 due to logistical constraints. Flows at fluvial wetland locations include MMB-Federal in the HN-FP (drainage area = 20.5 km^2) and FB-BV in the LN-FP (drainage area = 23 km^2). Flows were measured using the area-velocity method with a FlowTracker Velocimeter (Sontek Inc.). HOBO U-20 water level loggers were installed at a fixed depth at wetland sites MMB-Federal and FB-BV along the flow paths. However, continuous water level was not measured at MMB-Federal due to logger malfunction, so continuous discharge data from USGS South Middleton gauge (site 01101500 Ipswich River, drainage area = 115 km^2) was used instead; hydrologic conditions along fluvial wetland reaches will lie somewhere between the channelized headwater stream and the USGS gauge at South Middleton (Figure 3; Figure A1).

As a benchmark to compare logger data to, visual staff gauges were also designed and installed at 13 of 16 sites to record water level at the time of sampling (Table A3). Resultant measurements from loggers were first corrected for atmospheric pressure (recorded at the Plum Island Ecosystems Long Term Ecological Research (PIE-LTER) field station in Newbury, MA) and then set to a consistent benchmark based off of visual staff gauge readings at the time of sampling.

Rating curves were developed for the two channelized sites (SB & IS_135) and fluvial wetland sites (MMB-Federal & FB-BV) to determine relationships between water level and discharge for both logger (when available) and visual staff gauge data (Figure A2, A3). Discharge at the time of collection was then estimated for all study sites on each sampling day based on the rating curve deemed most appropriate for the flow path and site type (stream channel vs. fluvial wetland), scaled by drainage area for each site (Figures A2, A3). For the LN-FP, discharge was estimated at all fluvial wetland locations using discharge from FB-BV based on logger data (Figure A2a). For channelized stream sites within the transect, discharge was determined using the rating curve generated from visual staff gauge data at IS_135 (Figure A3a). For the HN-FP, discharge was determined for each fluvial wetland stream site using the discharge from MMB-Federal (Figure A2b) and for channelized stream sites using discharge estimated from discharge at the long term LTER site at SB (Figure A3b).

Discharge data (L s^{-1}) were converted into runoff rates (mm d^{-1}) to normalize for across site comparison. We assumed that sites with the same site type (channelized vs. fluvial wetland) along a flow path exhibited the same runoff rate on a given sampling day as estimated for the representative channelized or wetland site, but discharge changed depending on upstream drainage area. Similar runoff along the entire fluvial wetland portion of the flow path may not be the case due to time lags but increases in stage height after storms at fluvial wetland study sites suggest that storm pulses peaked at similar times suggesting reasonable assumption. Lags were addressed by comparing runoff estimates to stormflow, particularly peak flow, of continuous discharge measurements from the USGS gauge along the Ipswich River in South Middleton, MA (site 01101500) across the study period (Figure A1).

To assess the timing of peak flow and stormflow samplings, we characterized each storm during the study period (n = 8). Storm events were delineated by assigning a baseflow value that marked the beginning of a storm event; stormflow conditions continued until flows returned to within 5% of baseflow or the recession was cut short by the event of another storm. Two storm events were excluded from storm-specific analyses since stormflows did not meet criteria of returning to at least 2x the baseflow value (Figure A18). Storm-specific analyses (Figure 5, 13, 14, 15) included 3 storms from each flow path, ranging in peak storm runoff between 12.1 and 25.2 mm d^{-1} in channelized streams and between 0.4 and 2.8 mm d^{-1} for fluvial wetland dominated streams (Table 2; Figure 3). Instantaneous discharge ranged from 0 to 0.53 m^3 s^{-1} (runoff range = 0 to 2.21 mm d^{-1}) along the fluvial wetland dominated reaches and 0 to 0.39 m^3 s^{-1} (runoff range = 0.07 to 5.92 mm d^{-1}) along the channelized reaches during the 6-month study period (Figure A1). Storm samplings of channelized streams occurred when runoff was closer to baseflow than peak stormflow due to the much quicker hydrologic responses by channelized streams than fluvial wetland dominated streams (Figure 3; Figure A1).

Nitrate removal and uptake length

Proportional NO_3^- removal was estimated through two separate analyses: (1) whole flow path analysis and (2) site by site analysis. Removal for both analyses were calculated for each sampling day (n = 21) as

$$Removal\ (\%) = \frac{NO_3{:}Cl_{input} - NO_3{:}Cl_{output}}{NO_3{:}Cl_{input}} * 100, \quad \text{(Eq. 1)}$$

where $NO_3{:}Cl_{input}$ is the ratio of NO_3^- to Cl^- (NO_3:Cl) concentrations at the input site, $NO_3{:}Cl_{output}$ is the NO_3:Cl ratio at the output site, and *Removal (%)* is the difference between NO_3:Cl ratios at the input and output sites for a given sampling day, divided by the NO_3:Cl ratio at the input site

and then multiplied by 100. Removal estimates represent some combination of denitrification and assimilation along a flow path. NO_3:Cl ratios were used in removal calculations instead of NO_3^- to account for dilution in the downstream direction (Wollheim et al. 2014, 2017). Chloride, a non-reactive ion, is a conservative tracer in aquatic ecosystems, so Cl^- concentrations are only affected by dilution or new inputs, and not by ecosystem processes. When removal of Cl^- was estimated separately for each transect to determine the potential influence of errors in mass balance, estimates were often above 20%, suggesting that dilution was influencing water chemistry after storms (Figure A4). Using the NO_3:Cl flux ratio, we assume that the effect of dilution or storage on NO_3^- fluxes is accounted for (Figure A5).

For the whole flow path analysis, NO_3^- removal was estimated for each sampling day along the full extent of each flow path. Using Eq. 1 as a basis, $NO_3{:}Cl_{input}$ is the NO_3:Cl ratio at an upstream channelized site and representative of inputs to the flow path, while $NO_3{:}Cl_{output}$ is the NO_3:Cl ratio at the furthest downstream fluvial wetland site and representiave of outputs from the flow path. Eq. 2 and 3 indicate specific sites used in removal estimates for the HN-FP and LN-FP, respectively.

$$Removal\ (\%) = \frac{NO_3{:}Cl_{SB} - NO_3{:}Cl_{MMB-Federal}}{NO_3{:}Cl_{SB}} * 100 \quad \text{(Eq. 2)}$$

$$Removal\ (\%) = \frac{NO_3{:}Cl_{MB-Johnston} - NO_3{:}Cl_{FB-BV}}{NO_3{:}Cl_{MB-Johnston}} * 100 \quad \text{(Eq. 3)}$$

This approach assumes that all inputs along the flow path have similar NO_3:Cl ratios as the upstream input site. This assumption is reasonable because urban land cover declines as wetland land cover increases downstream along the flow paths (Table A2), demonstrating that both NO_3^- and Cl^- should both decline to low levels draining less urban influenced wetlands (Figure 5; Figure A4).

For the site by site removal analysis, NO_3^- removal was calculated between each study site for each sampling day to determine where along the flow paths removal is occurring. Using Eq. 1 as a basis, where $NO_3{:}Cl_{input}$ and $NO_3{:}Cl_{output}$ were determined by:

$$NO_3{:}Cl_{input} = \left(NO_3{:}Cl_{"input"} * UpstreamArea_{"input"}\right) + \left(NO_3{:}Cl_{"direct"} * InterstationArea\right) \quad \text{(Eq. 4)}$$

$$NO_3{:}Cl_{output} = \left(NO_3{:}Cl_{"output"} * UpstreamArea_{"output"}\right). \quad \text{(Eq. 5)}$$

For Eq. 4, $NO_3{:}Cl_{"input"}$ is the ratio of NO_3:Cl concentrations at the input site (site directly upstream along the flow path of the site in question (output site)), $UpstreamArea_{"input"}$ is the total upstream drainage area of the input site, $NO_3{:}Cl_{"direct"}$ is the NO_3:Cl ratio at a joining tributary along the flow path, and *InterstationArea* is the drainage area between the input site and the output site. For Eq. 5 estimating $NO_3{:}Cl_{output}$, $NO_3{:}Cl_{"output"}$ is the NO_3:Cl ratio at the site in question (output site) and $UpstreamArea_{"output"}$ is the total upstream drainage area of the output site. Median NO_3^- removal was estimated at each study site during the study period. It was assumed that NO_3^- and Cl^- inputs from joining tributaries were consistent with that of the tributary input site sampled for each flow path. This assumption is plausible because NO_3:Cl ratios of joining tributaries (Mill-Adams for HN-FP and Ogunquit_Trib for LN-FP) across the study period were mostly comparable to NO_3:Cl ratios at upstream locations along the flow paths (HN-FP: median at SB = 3.52, median at tributary = 3.44; LN-FP: median at MB-Johnston = 1.91, median at tributary = 3.09).

Uptake length (Sw) of NO_3^-, the average distance travelled before being taken up through assimilatory or dissimilatory removal processes, was calculated for each flow path and sampling day. S_w is often determined from nutrient additions (Mulholland et al. 2009, Covino et al. 2010, Beaulieu et al. 2014, Wollheim et al. 2014), but can also be estimated using a network scale

approach (Beaulieu et al. 2015). S_w along the transects was calculated using a linear regression analysis of the relationship between the natural log of the NO_3:Cl ratio (ln(NO_3:Cl)) over downstream distance for the locations where strong gradients in NO_3:Cl occur following methods by (Covino et al. 2010). Strong gradients occur where the channelized stream first enters the fluvial wetland dominated sections and NO_3:Cl ratios decline to nearly zero (Figure 5). All NO_3:Cl ratios were transformed as ln(X+ 0.00001) to allow inclusion of ratios equaling zero. NO_3:Cl ratios were again used to account for dilution (Wollheim et al. 2014, 2017). The slope of the linear regression represents the longitudinal uptake rate (k_L) in km^{-1}. Sw in km was then calculated as the negative inverse of k_L for each sampling day (n=21) using the Eq. 6 (Covino et al. 2010). Estimates of S_w are maximum daily values.

$$S_w = -\frac{1}{k_L} \quad \text{(Eq. 6)}$$

Gas evasion

Gas evasion from surface waters are a function of the concentration of dissolved gas in the water and air, surface water hydraulics, and air-water gas transfer velocities at a given temperature. Fluxes for CO_2, CH_4, and N_2O across the air-water interface for every sampling day were estimated as (Raymond et al. 1997, 2012):

$$F(g) = (C_w - Kh * C_a)k_{gas.} \quad \text{(Eq. 7)}$$

For Eq. 7, *F(g)* is flux in mg m^{-2} d^{-1}, C_w is the concentration of the gas in water in mg m^{-3}, C_a is the concentration of the gas in the atmosphere in mg m^{-3}, k_h Henry's Law constant for a select gas, and k_{gas} is the gas transfer velocity for a selected gas in m d^{-1} (Raymond et al. 1997, 2012). Henry's Law constant (k_h) is temperature dependent and accounts for the solubility of a select gas in the water (given water temperature on sampling days). Gas concentrations (C_w and C_a)

were determined from the partial pressure of dissolved gases in water and air, given water temperature and gas solubility. The partial pressure of CO_2, CH_4, and N_2O at saturation with the atmosphere are 407.4, 1.975, and 0.331 ppm, but these values vary marginally day to day as a function of water temperature.

Air-water gas transfer velocities for select gases at each sample location and time were determined as a function of hydraulic geometry and water temperature. Gas transfer velocities at study sites on each sampling day were calculated using Eq. 8,

$$k_{gas} = \frac{k_{600}}{(\frac{600}{Sc_{gas}})^{-0.5}}, \quad \text{(Eq. 8)}$$

where k_{gas} is the water transfer velocity, k_{600} is the gas transfer coefficient in m d^{-1}, and Sc_{gas} is the Schmidt number of 600 (Raymond et al. 2012). Temperature dependent Schmidt numbers of 600 (Sc_{gas}) were found for each gas (CO_2, CH_4 and N_2O) using Eq. 9 and methods from Raymond et al. (2012):

$$Sc_{gas} = A + BT + CT^2 + DT^3, \quad \text{(Eq. 9)}$$

where T is water temperature at time of collection (ºC) and A, B, C, and D are coefficients for selected gases. Gas transfer coefficients (k_{600}) were calculated for all study sites on each sampling day using the following equation:

$$k_{600} = (VS)^{0.89\pm0.020} \times D^{0.54\pm0.030} \times 5037 \pm 604, \quad \text{(Eq. 10)}$$

where V is velocity, S is slope, and D is depth (Raymond et al. 2012). Slope at study sites along the transects was estimated using Google Earth Pro; slope is the difference in elevation between the sample site in question and the study site directly upstream divided by the distance between the two (Table A2). Hydraulic geometry for channelized study sites were determined using linear regression analysis between the natural log of discharge and depth (y = -0.895 + 0.294x), width (y = -1.64 + 0.285x), and velocity (y = 2.56 +0.423x) acquired from Raymond et al. (2012).

Because hydraulic relationships from Raymond et al. (2012) pertain only to channelized systems, hydraulic geometry relationships for fluvial wetland sites were developed using data measured in this study. For fluvial wetland sites, linear relationships were developed for each flow path from discharge measurements (mean depth, width, velocity) at downstream fluvial wetland sites, MMB-Federal (HN-FP) and FB-BV (LN-FP) (Figure A2). For wetland sites in the HN-FP, the linear regression analysis between the natural log of discharge and depth (y = -0.4851 + 0.0874), width (y = 2.1299 + 0.0845) and velocity (y = -1.6448 +0.8281x) were used. For wetland sites in the LN-FP, hydraulic geometry relationships for depth (y = -0.7175 + 0.2162x), width (y = 1.785 + 0.0594x) and velocity (y = -1.0675 + 0.7244x) were used. This method assumes hydraulic geometry relationships are consistent across all wetland sites for a given flow path and that these measurements are representative of the channelized portion connecting fluvial wetlands, not the wetlands themselves.

Potential errors associated with evasion estimates were calculated assuming deviations in both k_{gas} and partial pressure of a gas in the water. I assumed that k_{gas} deviates by a reasonable error of ± 20% and that the partial pressure of dissolved gas in the water differs by ± the mean standard deviation of the gas observed across the study period. For each flow path, estimates of daily CO_2, CH_4 and N_2O contributions (kg or g) from the channelized portion and fluvial wetland dominated portion of the flow paths were calculated by multiplying median gas fluxes by the upstream areal extent of the stream channel or fluvial wetland area (Table 5).

Fluvial wetland delineation

Fluvial wetland extent within each transect was quantified to estimate how it changes downstream with increasing drainage area (Table 1, Figure 2). Fluvial wetlands were defined as

wetlands intersected by the river network. Additionally, areal extent of connected wetlands (those adjacent to any fluvial wetlands) and isolated wetlands (those not connected to the river network, fluvial wetlands, or connected wetlands) were also quantified to determine total wetland influence for each flow path (HN-FP: 23.4%; LN-FP: 32.4%; Table A2). Wetland extent (fluvial, connected, and isolated) was delineated using QGIS, an open source Geographic Information System.

Wetland land cover and river network hydrography data layers for the watershed were obtained from MassGIS (https://docs.digital.mass.gov/massgis). Wetland extent for each flow path was first fixed by the watershed boundary, a data layer obtained from the Plum Island Ecosystem Long Term Ecological Research (PIE-LTER) network (https://pie-lter.ecosystems.mbl.edu). Interstation drainage areas, or the catchment area between study sites, were generated using River GIS from GPS coordinate locations of study sites and 120 m resolution gridded flow accumulation acquired from the PIE-LTER network. Wetlands were selected and identified by type (fluvial, connected, or isolated) for each interstation area. Wetland areal extent for the entire upstream drainage basin for each site was found by totaling wetland area from all interstation areas upstream. Interstation fluvial wetland influence (the percent fluvial wetland land cover between a given site and the site directly upstream) and upstream fluvial wetland influence (the total percent of fluvial wetland land cover upstream in sub-catchment) were then calculated for each study site (Table 1).

Statistical analyses

Data transformations were performed on data for most statistical tests to improve assumptions of normality and homogeneity of variance. General log transformations were

applied to NO_3^- concentration, NO_3^- uptake length, CO_2 evasion, and CH_4 evasion data, log (x + min) transformations were applied to N_2O evasion data, and arcsine square root transformations were applied to whole-flow path % NO_3^- removal data. To test for differences in NO_3^- concentration and GHG evasion between channelized streams and fluvial wetlands, as well as between flow paths, two-way factorial analysis of variance (ANOVA) and Tukey-Kramer (Tukey HSD) tests were performed. To examine the influence of streamflow on NO_3^- removal and GHG evasion dynamics for sample groups (fluvial wetland dominated streams and channelized streams), simple linear regressions were used to summarize bivariate relationships between runoff rate and whole-flow path % NO_3^- removal, NO_3^- uptake length, N_2:Ar disequilibrium, and mean GHG evasion rates along the flow paths on sampling days. SB-Chest, the first fluvial wetland dominated stream location along the HN-FP, was excluded from site type comparative analyses because it is a fluvial wetland reach with relatively little impact compared to all other fluvial wetland study reach locations. Analysis of covariance (ANCOVA) was then used to test for the interactive effect of flow path on bivariate relationships between runoff rate and whole-flow path NO_3^- removal (%) and N_2:Ar disequilibrium. One-sample t-tests were conducted to determine if mean N_2O evasion rates were different from 0 for fluvial wetland dominated and channelized streams along each flow path. Lastly, to further asses the effect of storm events, I tested for differences in NO_3^- concentrations and GHG evasion before and after storms across sample sites using paired t-tests for multiple comparisons. All statistical analyses were performed using JMP® Pro 15.0.0.

CHAPTER 3: RESULTS

Water chemistry in fluvial wetland dominated and channelized streams

NO_3^- concentrations were statistically lower in the fluvial wetland portions of the flow path compared to the channelized portion over the entire 6-month sampling period for both flow paths (HN-FP $p < 0.0001$; LN-FP $p = 0.0002$). Channelized stream study sites along the HN-FP and LN-FP ranged in NO_3^--N concentration from 0.37 to 0.91 mg N L^{-1} (median = 0.66 mg N L^{-1}, mean = 0.67 mg N L^{-1}) and 0.01 to 0.41 mg N L^{-1} (median = 0.16 mg L^{-1}; mean = 0.17 mg N L^{-1}), respectively (Figure 4). NO_3^--N concentrations at study sites along the fluvial wetland portion of the flow paths were low or below detection, ranging from 0 to 0.10 mg N L^{-1} (HN-FP median = 0.01 mg N L-1, mean = 0.01 mg N L^{-1} ; LN-FP median = 0.04 mg N L^{-1}, mean = 0.04 mg N L^{-1}; Figure 5). The HN-FP exhibited greater NO_3^- concentrations in the fluvial wetland portion of the flow path than the LN-FP during the study period ($p < 0.0001$). NO_3^- declined downstream along both flow paths in similar fashion, where the steepest decline occurred as the flow paths transition from a channelized stream into a fluvial wetland dominated stream (~2-3 km downstream) (Figure 5). Fluvial wetland sites were always a sink for NO_3^- but not for NH_4^+ or dissolved organic nitrogen (DON) (Figure A10, A12). There was no consistent pattern in NH_4^+ concentrations longitudinally along the flow paths while DON tended to increase downstream (Figure A10, A12).

DO and SO_4^{2-} tended to decline in concentration downstream similar to NO_3^- while DOC increased (Figure A8, A9, A13). DO saturation (%) was always less than 66% in the fluvial wetland dominated portion of the flow paths (HN-FP median = 19%; LN-FP median = 32%) while DO saturation (%) reached greater than 94% in the channelized portion of the flow path (HN-FP median = 73.5%; LN-FP median = 83.8%; Figure A8). Concentrations of SO_4^{2-} ranged

from 2.08 to 7.71 mg S L^{-1} (HN-FP median = 5.32 mg S L^{-1}; LN-FP median = 2.97 mg S L^{-1}) in the channelized portion of the flow paths and 0.28 to 7.73 mg S L^{-1} (HN-FP median = 1.48 mg S L^{-1}; LN-FP median = 1.67 mg S L^{-1}) in the fluvial wetland portion (Figure A9). DOC concentrations, however, were greater in the fluvial wetland portion of the flow path than the channelized portion for both flow paths and increased faster in the LN-FP than the HN-FP (Figure A13).

Nitrate removal along fluvial wetland dominated flow paths

NO_3^- removal, a function of both denitrification and assimilation, by fluvial wetland dominated flow paths was high for both flow paths but was overall greater in the HN-FP throughout the study period (Figure 6). Removal estimates of NO_3^--N ranged from 94% to 99% (median = 98%) by the HN-FP and 11% to 96% (median = 63%) by the LN-FP (Figure 6). The LN-FP showed more variability in NO_3^- removal across the sample period (Figure 6). The LN-FP also exhibited longer uptake lengths of NO_3^--N by fluvial wetland dominated streams (range = 0.60 to 2.70 km; median 1.19 km) than the HN-FP (range = 0.42 to 0.69 km; median = 0.48 km; Figure 7). Fluvial wetland dominated streams removed a much greater proportion of NO_3^- compared to channelized streams throughout the study period (Figure 8b). Channelized streams were typically locations of NO_3^- sources while fluvial wetland dominated streams were locations of high NO_3^- removal (Figure 8b). Median NO_3^--N removal along the fluvial wetland portion of the flow paths ranged from 29% to 98% compared to the channelized portion ranging from -99% to 22% (Figure 8b), where negative values imply there are NO_3^- sources to the system.

NO_3^--N removal along the transects was greatest where established fluvial wetland habitat began for each flow path (median HN-FP: MMB-OldCanal = 98%, MMB-38 = 96%;

median LN-FP: MB-Foster = 92%; Figure 8b). While SB-Chest is the first fluvial wetland reach along the HN-FP, the reach is relatively small and the removal signal is thus not strong yet (median NO_3^--N removal SB-Chest = 8%; Figure 8b). Locations of high removal (fluvial wetland dominated reaches) coincided with predominately positive N_2:Ar disequilibrium, indicating that that N_2 production via denitrification was occurring throughout the wetland portion of the flow paths (Figure 8a). Channelized streams at the start of the flow paths experienced no or limited removal and were also locations of additional NO_3^- sources beyond the representative headwater tributary site sampled (Figure 8a). The channelized portion of the flow path also showed variable patterns in N_2:Ar disequilibrium, serving as locations of denitrification as well as N fixation (Figure 8a).

GHG evasion along fluvial wetland dominated flow paths

Fluvial wetland dominated streams exhibited predominately higher pCH_4 and pCO_2 but lower pN_2O than channelized streams in both flow paths over the 6-month study period (Table 3; Figure A14, A15, A16). The pCH_4 in the fluvial wetland portion of the flow paths ranged from < 2 to 741 ppm (HN-FP median pCH_4 = 71.2 ppm; LN-FP median = 36.5 ppm) while pCO_2 ranged from 6810 to > 24980 ppm (HN-FP median pCO_2 = 13269 ppm; LN-FP median = 9578 ppm; Table 3). The pCH_4 and pCO_2 were typically lower upstream in the channelized portion of the flow paths, ranging in pCH_4 from 0 to 336 (HN-FP median pCH_4 = 58.9 ppm; LN-FP median = 16.9 ppm) and pCO_2 from < 1951 to > 34600 (HN-FP median pCO_2 = 6314 ppm; LN-FP median = 3313 ppm; Table 3). Fluvial wetland dominated and channelized streams were normally oversaturated in CH_4 and always oversaturated in CO_2 (saturation levels of $pCH_4 \approx 1.975$ ppm and $pCO_2 \approx 407.4$ ppm) throughout the study (Table 3). However, channelized streams were

normally oversaturated in N_2O while fluvial wetland dominated streams tended to straddle the equilibrium level and were sometimes undersaturated in N_2O (saturation level of $pN_2O \approx 0.331$ ppm; Table 3). The channelized portion of the flow paths ranged in pN_2O from 0.12 to 2.57 (HN-FP median pN_2O = 0.94 ppm; LN-FP median = 0.42 ppm) while the fluvial wetland portion ranged from 0.03 to 1.18 ppm (HN-FP median pN_2O = 0.20 ppm; LN-FP median = 0.36 ppm; Table 3).

Air-water gas transfer velocities were lower and more constrained in the fluvial wetland portion of the flow paths than the channelized portion across the study months (Table 4). As a function of hydrologic geometry (width, depth, and streamflow velocity) on sampling days, median gas transfer velocities of CH_4, CO_2, and N_2O at channelized stream locations were 1.16 m d^{-1}, 1.25 m d^{-1}, and 0.85 m d^{-1}, respectively (Table 4). Median gas transfer velocities in fluvial wetland dominated streams were much lower (CH_4 = 0.15 m d^{-1}, CO_2 = 0.16 m d^{-1}, and N_2O = 0.11 m d^{-1}; Table 4). As a result, evasion per unit area was lower in fluvial wetland dominated streams than channelized streams despite higher partial pressure of dissolved gases (Figure 9).

Fluvial wetland dominated streams along the two headwater flow paths had statistically lower diffusive CH_4, CO_2, and N_2O evasion per unit area compared to channelized streams (CH_4: HNFP $p < 0.0001$, LN-FP $p = 0.0016$; CO_2: HN-FP $p < 0.0001$, LN-FP $p = 0.0004$; N_2O: HN-FP $p < .0001$; LN-FP $p = 0.0022$). The fluvial wetland portion of the flow paths ranged in CH_4 evasion from 0.03 to 113 mg CH_4-C m^{-2} d^{-1} (HN-FP: mean = 10.6 mg CH_4-C m^{-2} d^{-1}, median = 6.8 mg CH_4-C m^{-2} d^{-1}; LN-FP: mean = 22.3 mg CH_4-C m^{-2} d^{-1}, median = 12.2 mg CH_4-C m^{-2} d^{-1}) while the channelized portion ranged higher from – 0.11 to 428 mg CH_4-C m^{-2} d^{-1} (HN-FP: mean = 46.9 mg CH_4-C m^{-2} d^{-1}, median = 41.8 mg CH_4-C m^{-2} d^{-1}; LN-FP: mean = 72. 6 mg CH_4-C m^{-2} d^{-1}, median = 20.1 mg CH_4-C m^{-2} d^{-1}; Figure 9). Along the flow paths, CO_2 evasion ranged from

118 to > 28500 mg CO_2-C m^{-2} d^{-1} in fluvial wetland dominated streams (HN-FP: mean = 3871 mg CO_2-C m^{-2} d^{-1}, median = 2997 mg CO_2-C m^{-2} d^{-1}; LN-FP: mean = 8936 mg CO_2-C m^{-2} d^{-1}, median = 6809 mg CO_2-C m^{-2} d^{-1}) and 2387 to > 64500 mg CO_2-C m^{-2} d^{-1} in channelized streams (HN-FP: mean = 16970 mg CO_2-C m^{-2} d^{-1}, median = 15213 mg CO_2-C m^{-2} d^{-1}; LN-FP: mean = 17306 mg CO_2-C m^{-2} d^{-1}, median = 12490 mg CO_2-C m^{-2} d^{-1}; Figure 9). N_2O evasion rates were considerably lower along the flow paths, ranging from -0.09 to 1.19 mg N_2O-N m^{-2} d^{-1} in fluvial wetland dominated streams (HN-FP: mean = 0.00 mg N_2O-N m^{-2} d^{-1}, median = -0.01 mg N_2O-N m^{-2} d^{-1}; LN-FP: mean = 0.26 mg N_2O-N m^{-2} d^{-1}, median = 0.09 mg N_2O-N m^{-2} d^{-1}) and -0.13 to 6.17 mg N_2O-N m^{-2} d^{-1} in channelized streams (HN-FP: mean = 1.17 mg N_2O-N m^{-2} d^{-1}, median = 0.90 mg N_2O-N m^{-2} d^{-1}; LN-FP: mean = 0.88 mg N_2O-N m^{-2} d^{-1}, median = 0.44 mg N_2O-N m^{-2} d^{-1}; Figure 9). For the HN-FP, N_2O evasion rates were not statistically different from 0 in fluvial wetland dominated stream locations ($p = 0.5556$), but were statistically different from 0 for fluvial wetlands in LN-FP ($p = 0.0043$) and channelized locations for both flow paths (HN-FP $p < 0.0001$; LN-FP $p = 0.0006$).

Both fluvial wetlands and channels did not differ in CH_4 or CO_2 evasion between the two flow paths but did differ in N_2O evasion. Methane and CO_2 evasion by fluvial wetlands were statistically similar between the flow paths (CH_4 $p = 0.8696$; CO_2 $p = 0.3631$; Figure 9). Likewise, channels exhibited similar CH_4 or CO_2 evasion in the HN-FP and LN-FP (CH_4 $p = 0.9896$; CO_2 $p = 0.9873$; Figure 9). The flow paths, however, did differ in N_2O evasion by both fluvial wetlands and channels (fluvial wetlands $p = 0.0002$; channels $p = 0.0319$; Figure 9).

Due to larger surface area of fluvial wetland ecosystems compared to that of channelized streams, total daily GHG emissions are greater from fluvial wetland dominated streams than channelized stream (Table 5). When flux rates are applied to total surface area extent, median

estimates of total CH_4 emissions by fluvial wetland ecosystems were found to be 12.9 kg CH_4-C d^{-1} for the HN-FP and 55.4 kg CH_4-C d^{-1} for the LN-FP while estimated emissions by channelized stream ecosystems were much less (median HN-FP = 2.3 kg CH_4-C d^{-1}; median LN-FP = 2.0 kg CH_4-C d^{-1}; Table 5). Likewise, estimates of total CO_2 evasion by fluvial wetlands were greater compared to channels (median Fluvial wetlands: HN-FP = 5726 kg CO_2-C d^{-1}, LN-FP = 31074 kg CO_2-C d^{-1}; median channels: HN-FP = 822 kg CO_2-C d^{-1}, LN-FP = 1222 kg CO_2-C d^{-1}). Fluvial wetland ecosystems in the LN-FP were greater sources of N_2O (median N_2O evasion = 397 g N_2O-N d^{-1}) than channelized stream ecosystems (median HN-FP = 48.7 g N_2O-N d^{-1}; median LN-FP= 43.3 g N_2O-N d^{-1}). Although median estimates of N_2O evasion by fluvial wetland ecosystems in the HN-FP were found to be -9.8 g N_2O-N d^{-1}, areal N_2O evasion were not significantly different from 0, indicating that total N_2O evasion is minor (Table 5).

Nitrate removal dynamics after storms under heightened flows

Storm events or heightened flow conditions were not observed to influence NO_3^- concentrations in fluvial wetland dominated streams (Figure 5). After storms events, NO_3^- concentrations showed essentially identical declining patterns along the flow paths from channelized streams to fluvial wetland dominated streams, suggesting little evidence of saturation of NO_3^- removal in the flow paths as a whole (Figure 5). Declines in NO_3^- concentration after storms were observed upstream in the channelized portion of the flow paths and at the first fluvial wetland dominated (transitional) study location along the HN-FP, but were likely a result of storm event dilution as Cl^- also declined in similar fashion (Figure 5; Figure A4); increases in NO_3:Cl in channels after storms suggest that Cl declined more than NO_3^- (Figure A4). The channelized portion of the flow paths exhibited no significant change in mean

N_2:Ar disequilibrium with increasing runoff over the study months but showed a tendency to shift from locations of N fixation to denitrification at intermediate flows ($p = 0.0797$; Figure 10b). Cl^- patterns after storms in the fluvial wetland dominated portion of the flow paths remained relatively unchanged, demonstrating a lack of dilution in fluvial wetland dominated streams following storm events (Figure A3); no changes were observed in NO_3:Cl in fluvial wetland reaches suggests that NO_3^- declined more than Cl^- because of its reactivity in the system (Figure A4). Paired t-tests revealed no significant differences in NO_3^--N concentration before and after storms along the fluvial wetland portion of the flow paths ($p > 0.05$ for all storms; $n = 6$; Figure 5). No change in positive N_2:Ar disequilibrium in fluvial wetlands across flows for both flow paths (Figure 10a) demonstrates that NO_3^- removal via denitrification abilities does not come at the expense of increasing flow conditions.

NO_3^- removal and uptake length dynamics by fluvial wetland systems were not observed to change across flow conditions for the HN-FP but tended to decline and increase, respectively, for the LN-FP (Figure 11). There was a significant effect of flow path on the bivariate relationship between runoff and NO_3^- removal ($p < 0.0001$), suggesting the flows paths differed in their NO_3^--N removal abilities across flows (Figure 11). The HN-FP maintained higher NO_3^- removal and shorter NO_3^- uptake length under heightened streamflow than those the LN-FP (Figure 11). NO_3^--N removal and uptake length remained steady (removal range = 94% to 99%; median = 98%; uptake length range = 0.42 to 0.69 km) under higher flows for the HN-FP, with no effect of runoff observed on NO_3^- removal ($p = 0.6925$) or uptake length ($p = 0.2030$; Figure 11). Although there was also no significant relationship between runoff and NO_3^- removal observed for the LN-FP ($p = 0.9102$), NO_3^--N removal was more variable for the LN-FP (range = 11% to 96%; median = 63%) and showed a tendency for lower removal at intermediate flow

conditions (Figure 11b). Uptake lengths of NO_3^--N also increased by 2.1 km with increasing runoff ($p = 0.0072$; $R^2 = 0.62$; Figure 11a), indicating that NO_3^- was being transported longer distances before uptake after storms in the LN-FP.

GHG evasion dynamics after storms under heightened flows

Fluvial wetland dominated streams showed tendencies for greater mean daily CO_2 evasion per unit area under elevated flows for both flow paths (Figure 12b). Carbon dioxide evasion increased on average from 310 to 19398 mg CO_2-C m^{-2} d^{-1} over an order of magnitude change in discharge in the LN-FP, but only to 7321 mg CO_2-C m^{-2} d^{-1} in the HN-FP (HN-FP $p \leq 0.0001$, $R^2 = 0.97$; LN-FP $p \leq 0.0001$, $R^2 = 0.98$; Figure 12b). Significant differences between baseflow and stormflow CO_2 evasion were found for each storm analyzed in the LN-FP during the 6-month study period (Storm D: $p = 0.0071$; Storm E: Day 1 $p = 0.0269$, Day 2 = 0.0148; Storm F: $p = 0.0067$; Figure 13). For the HN-FP, significant differences between baseflow and stormflow CO_2 evasion were only observed during the second stormflow sampling for each storm (Storm A: Day 2 $p = 0.0091$; Storm B: Day 2 $p < 0.0001$; Storm C: Day 2 $p < 0.0001$; Figure 13). On average, pCO_2 in fluvial wetland dominated streams following storm events were variable, but often showed a declining pattern (Table 5; Figure A14).

Similar to CO_2, fluvial wetland dominated streams exhibited tendencies for greater mean daily CH_4 evasion per unit area under heightened streamflow (Figure 12c). Across the sampling period, average CH_4 increased from 0.95 to 50.1 mg CH_4-C m^{-2} d^{-1} in the LN-FP but only to 27.7 mg CH_4-C m^{-2} d^{-1} in the HN-FP, although increases in mean daily CH_4 evasion with runoff was only significant for the HN-FP (HN-FP $p = 0.0012$, $R^2 = 0.70$; LN-FP $p = 0.1999$; Figure 12c). Trends of greater CH_4 evasion with increasing flows, however, were less apparent when specific

storms were analyzed; only 2 of 6 storms (runoff coefficients of 0.119 and 0.094 in the HN-FP; Table 2) showed significantly greater CH_4 evasion after storms (HN-FP Storm A: Day 1 $p = 0.0015$, Day 2 $p = 0.0034$; Storm B: Day 1 $p = 0.0308$; Figure 14). In fluvial wetland dominated streams, pCH_4 increased on average following storm events where differences in baseflow and stormflow were significant, suggesting that observed increasing tendency in CH_4 evasion with increasing flows is due in part to increases in pCH_4 in the water (Table 5; Figure A15).

Under higher flows, fluvial wetlands dominated streams in the LN-FP tended to increase in N_2O evasion while those in the HN-FP exhibited no change in evasion, demonstrating that N_2O evasion from fluvial wetland dominated streams under heightened flows were variable (Figure 12a). Although minimal, the LN-FP increased in N_2O evasion on average from 0 to 0.15 mg N_2O-N m^{-2} d^{-1} as discharge increased by over an order of magnitude while the HN-FP showed no change in mean daily N_2O evasion with increasing flows (HN-FP $p = 0.6513$; LN-FP $p = 0.0038$, $R^2 = 0.67$; Figure 12a). However, 4 of 6 storms (2 from each flow path) exhibited significant changes in N_2O evasion in fluvial wetland dominated streams (HN-FP Storm A: Day 1 $p = 0.0381$; Storm B: Day 1 $p = 0.0299$; LN-FP Storm E: Day 1 $p = 0.0314$, Storm F: $p = 0.0215$; Figure 15). N_2O evasion after storms predominately increased in fluvial wetlands, although minimally, with the greatest increase of only 1.91 mg N_2O-N m^{-2} d^{-1} in the LN-FP during a substantial fall storm (Storm F; runoff coefficient = 0.145; Table 2; Figure 15). Fluvial wetland dominated streams tended to increase in pN_2O after storms where there were significant differences found between baseflow and stormflow N_2O evasion, demonstrating that tendencies for greater evasion at higher flows in the LN-FP were in part driven by rises in pN_2O along the fluvial wetland portion of the flow path (Table 5; Figure A16).

The channelized portion of the flow paths also showed tendencies of greater CO_2, CH_4, and N_2O evasion under elevated flows throughout the study months (Figure 16). CO_2 evasion increased by nearly 37000 mg CO_2-C m^{-2} d^{-1} in the LN-FP as discharge rose by over an order of magnitude ($p = 0.0002$; $R^2 = 0.84$; Figure 16B). While the tendency for greater CO_2 evasion was not as strong in channelized streams of the HN-FP, evasion was rose on average to than 27800 mg CO_2-C m^{-2} d^{-1} under high flow conditions compared to nearly 4600 mg CO_2-C m^{-2} d^{-1} observed at lower flows ($p = 0.4323$; Figure 16B). Channelized streams also showed tendencies of greater mean daily CH_4 evasion under higher flow conditions (HN-FP range = 8.5 to 207 mg CH_4-C m^{-2} d^{-1}; LN-FP range = 9.5 to 96.1 mg CH_4-C m^{-2} d^{-1}), although these trends were not significant (HN-FP $p = 0.2488$; LN-FP $p = 0.2598$; Figure 16C). Channelized streams increased in N_2O evasion with increasing discharge on average from 0.04 to 3.56 mg N_2O-N m^{-2} d^{-1} in the LN-FP and from 0.3 to 2.8 mg N_2O-N m^{-2} d^{-1} in the HN-FP (HN-FP $p = 0.0045$, $R^2 = 0.61$; LN-FP $p \leq 0.0001$, $R^2 = 0.98$; Figure 16A). After storm events, pCO_2, pCH_4, and pN_2O predominately increased in the channelized portion of the flow paths, suggesting that tendencies for increasing GHG evasion under higher flows were due in part to rises in the partial pressure of dissolved gases (Table 5; Figure A14, A15, A16).

CHAPTER 4: DISCUSSION

High nitrate removal by fluvial wetland dominated streams

The presence of fluvial wetlands leads to lower NO_3^- by river networks than if the network consists only of channelized streams. Results from this study were consistent with previous findings that demonstrate the net effect of fluvial wetlands is to decrease NO_3^- concentration along surface-water flow paths (Johnston et al. 1990, Wollheim et al. 2014, Flint and McDowell 2015, Czuba et al. 2018, Hansen et al. 2018). The steep decline in NO_3^- concentration along flow paths with fluvial wetlands suggests that such wetlands can substantially reduce NO_3^- concentrations downstream. Higher NO_3^--N concentrations observed in channels (range = 0.37 to 0.91 mg N L^{-1}) were comparable to mean concentrations reported for urban-suburban streams across the US (0.298 mg N L^{-1}; Mulholland et al. 2009), while very low NO_3^--N concentrations (range 0 to 0.10 mg N L^{-1}) found in fluvial wetland dominated streams were on the lower end of concentrations (range < detection limit to 4.17 mg N L^{-1}) for headwater wetlands (Flint and McDowell 2015) and comparable to simulated concentrations (mean = 0 mg N L^{-1}) for flow-through wetlands (Czuba et al. 2018).

Fluvial wetland dominated streams promote high removal of NO_3^- in river networks, as they were greater sinks of NO_3^- than channels due to their greater demand. Wetland dominated surface water flow paths removed nearly 100% of NO_3^- inputs in the HN-FP and often more than 60% in the LN-FP during the 6-month study period, while channels were locations of NO_3^- sources or low removal (Figure 6, 8b). Removal was greatest when the flow paths first entered the fluvial wetland dominated portion (Figure 8b), indicating that large inputs of NO_3^- do not travel far distances in fluvial wetland systems before being readily taken up through avenues of microbial denitrification and autotroph assimilation (Vymazal 2007). The proportion of NO_3^-

removed by fluvial wetland dominated reaches declines somewhat further downstream along the flow paths because relatively little NO_3^- is reaching these systems as a result of high removal occurring upstream. My findings are consistent with previous studies that found higher NO_3^- reaction and uptake rates by fluvial wetlands (also termed in-channel and flow-through wetlands) than channelized streams (O'Brien et al. 2012, Wollheim et al. 2014, Czuba et al. 2018). A previous study of NO_3^--N removal by 72 streams across the US using 15N isotopes, which included the PIE-LTER site SB, revealed gross uptake to be much higher (nearly 64% over a 1 km reach) than reported here for net uptake in channelized streams (Mulholland et al. 2009).

Consistent with findings in the literature, results from this study support my hypothesis of increased NO_3^- removal by fluvial wetlands in river networks. Fluvial wetlands are effective at removing NO_3^- because of their direct connection to adjective flow, large area of reactive sediments, abundance of labile organic C, and low DO conditions that fuel denitrification and encourage assimilation of NO_3^- into abundant plant biomass (Vymazal 2007, O'Brien et al. 2012, Czuba et al. 2018). There is evidence of lowered redox potential and greater organic C content along the flow paths, as both DO and SO_4^{2-} declined considerably downstream while DOC increased where fluvial wetland habitat was abundant (Figure A8, A9, A13). Denitrification is likely contributing to high NO_3^- removal by fluvial wetland systems as N_2:Ar was often oversaturated (Figure 8A); although TDN does not decline as much, so it is unclear to what extent NO_3^- was denitrified (Figure A11).

Although demand for NO_3^- is high among the fluvial wetland dominated streams, the demand seems to differ between low and high nutrient conditions. When comparing the two flow paths, the HN-FP exhibited consistently greater NO_3^- removal than the LN-FP (Figure 6), indicating that demand for NO_3^- keeps up with supply more closely in the higher nutrient

environment than in lower nutrient environment where demand in the system is likely lower and can be more easily overwhelmed. Results are consistent with previous research that found proportional N retention to be 5x higher by wetlands receiving greater N inputs (Thiere et al. 2011), suggesting that fluvial systems have the ability to adapt their demand for NO_3^- to changing inputs. Demand in the HN-FP is likely greater a result of more reduced conditions, demonstrated by lower DO and SO_4^{2-} conditions by fluvial wetlands in the HN-FP (median DO = 19%, SO_4^{2-} = 1.48 mg S L^{-1}) than those in the LN-FP (median DO = 32%, SO_4^{2-} =1.67 mg S L^{-1}; Figure A8, A9), promoting the utilization of NO_3^- as a terminal electron acceptor during anaerobic respiration (Vymazal 2007). It is unlikely that organic C abundance is driving greater demand and removal in the HN-FP because DOC increased faster in the fluvial wetland portion of the LN-FP than the HN-FP, perhaps due to greater DOC inputs by more forested land cover upstream (Figure A13).

Low areal GHG evasion by fluvial wetland dominated streams

Estimates of GHG (CH_4, CO_2, and N_2O) evasion by channelized streams in this study were consistent with previous reports of average and median diffusive GHG emissions by headwater streams (Hope et al. 2001, Beaulieu et al. 2008, 2011, Billett and Harvey 2013, Schade et al. 2016, Stanley et al. 2016). Evasion estimates for CH_4 from channelized streams in this study (Figure 9) were on the lower end of the range of diffusive fluxes from nearly 400 streams globally but are relatively close the median estimate (range = -166.8 to 6929 mg CH_4-C m^{-2} d^{-1}; median = 13.8 mg CH_4-C m^{-2} d^{-1}; Stanley et al. 2016). CO_2 evasion reported here by channels (Figure 9) were greater than a maximum estimate found in the literature for headwater streams in NH (3494 mg CO_2-C m^{-2} d^{-1}; Schade et al. 2016) but are consistent with other studies

that report a range in CO_2 fluxes between 259 and 45878 mg CO_2-C m^{-2} d^{-1} (Hope et al. 2001) and a median estimate of 11491 mg CO_2-C m^{-2} d^{-1} (Billett and Harvey 2013). Results of N_2O evasion by channels reported here were comparable to some studies where the reported range from headwater streams was 0.21 to 6.4 mg N_2O-N m^{-2} d^{-1} (Beaulieu et al. 2008) and average evasion was 0.89 mg N_2O-N m^{-2} d^{-1} (Beaulieu et al. (2011), but also fall on the lower end of the range reported recently by Borges et al. (2019) (-2.3 to 14.0 mg N_2O-N m^{-2} d^{-1}).

Results reported here of areal GHG evasion by wetland dominated streams were lower than most estimates of evasion by channelized headwater streams reported in the literature and in this study, supporting my hypothesis for areal CO_2 evasion but refuting it for N_2O and CH_4. Estimates of CH_4, CO_2, and N_2O by wetland streams were often on the lower end of ranges reported by many studies for stream channels over the past two decades (Hope et al. 2001, Beaulieu et al. 2008, 2011, Billett and Harvey 2013, Stanley et al. 2016, Borges et al. 2019). Similarly, this study found overall lower evasion on a per unit area basis for each GHG by wetland dominated streams than by channelized streams (Figure 9); however, when total surface area is considered, emissions by fluvial wetland dominated reaches are much larger (Table 5). Lower estimates of areal CH_4 evasion by wetland dominated reaches may be due to only capturing diffusive fluxes and ignoring fluxes from ebullition and plant-mediated transport (Bastviken et al. 2011). Measurements of evasion were taken predominately during summer months when vegetation emergent along the margins of the fluvial wetlands is abundant, suggesting that areal CH_4 and CO_2 evasion estimates reported here may have been lower due to higher loss of CH_4 and CO_2 by vegetative transport during the growing season (Altor and Mitsch 2006, 2008). Measurements for dissolved gases in this study were taken at constricted points in

advective flow, which are locations where evasion may have already occurred and where fluvial wetlands are potentially less reactive.

Lower areal GHG evasion by wetland dominated streams compared to channels were in part due to slower air-water gas exchange rates in reaches where fluvial wetlands dominate, despite higher dissolved CO_2 and CH_4 concentrations. As fluvial wetland habitat increases downstream, the hydrologic geometry widens and deepens, further lengthening the water residence time and slowing streamflow velocity. Gas transfer velocities were estimated to be nearly 8x faster along the channelized portion than the wetland dominated portion of the flow paths for each GHG (Table 4), although these are estimates derived from linear relationships between hydrologic geometry (following methods by Raymond et al. (2012)) and thus come with considerable uncertainty. With more turbulent surface waters due to generally steeper slopes (Table A2) and smaller streambed area, upstream channels promote faster streamflow and exchange of gases with the atmosphere, driving higher evasion in channels versus wetland streams (Raymond et al. 2012). Slower release of gases across the air-water interface in wetland dominated streams allows gases to accumulate along low-gradient slopes and spend longer in surface waters before being evaded (Stanley et al. 2016). Higher pCO_2 and pCH_4 found in most fluvial wetland dominated study sites than channelized sites throughout the study period can be partly explained by slower gas exchange promoting accumulation of CO_2 and CH_4 in fluvial wetland surface waters (Table 3).

Despite mostly higher pCO_2 and pCH_4 downstream in reaches dominated by fluvial wetlands than in upstream channels, lower areal evasion of CO_2 and CH_4 by these systems suggests that production and/or delivery of CO_2 and CH_4 per unit area were also lower in wetland dominated streams than in channels. With a steep O_2 gradient between surface waters and

underlying sediments, CO_2 production via aerobic respiration in wetlands is likely limited to the sediment-water interface as oxygen quickly depletes with sediment depth, fostering environments for anaerobic respiration (Kadlec 2012). Slower rates of both aerobic and anaerobic respiration in fluvial wetlands compared to channelized streams, where aerobic conditions dominate, likely explains the lower CO_2 production per unit area along fluvial wetland dominated reaches. Although wetlands are the largest natural source of CH_4 emissions due to their anoxic bottom sediments, emitting roughly 5.4x more than streams and rivers (Whalen 2005, Stanley et al. 2016), lower CH_4 production per unit area in fluvial wetland dominated streams may be a result of two potential mechanisms: (1) low nutrient availability directly limiting CH_4 producers and oxidizers (Palma-Silva et al. 2013, Bodelier and Steenbergh 2014, Stanley et al. 2016), and/or (2) favorability of other terminal electron acceptors such as NO_3^- and SO_4^{2-} in anaerobic respiration (Stanley et al. 2016). Lower CH_4 evasion per unit area in wetland dominated streams is more likely due to mechanism (2), as we did not see greater pCH_4 at SB-Chest (the first fluvial wetland reach in series along the HN-FP) where NO_3^- was not limited (Table 3; Figure 5). Delivery of terrestrial inputs from the surrounding environment are generally greater in upstream headwaters due to stronger intrinsic connections between surface waters and the terrestrial environment (Alexander et al. 2007), indicating that terrestrial inputs from the watershed contribute less to overall evasion further downstream along these flow paths while internal processes contribute more. Thus, it is likely that greater delivery of CO_2 and CH_4 to upstream channels where it can be quickly evaded ultimately limits pCO_2 and pCH_4 downstream along fluvial wetland dominated reaches.

Lower N_2O evasion per unit area and generally lower pN_2O in reaches dominated by wetland dominated streams than channels were likely due to NO_3^- limitation downstream and

elevated delivery of terrestrial produced N_2O upstream. N_2O is produced in terrestrial and aquatic ecosystems through the microbial processes of denitrification under anaerobic conditions and nitrification under aerobic conditions in sediments (Vymazal 2007). While N fixation was prevalent at most channelized study sites, headwater streams have been found to have high rates of denitrification because of elevated N loading from the landscape, great contact between overlying surface water flow and underlying sediment area, and anoxic conditions at shallow sediment depths in small streams (Beaulieu et al. 2011, Hampton et al. 2020). NO_3^- and N_2O produced in terrestrial soils and transported to highly connected headwaters is also likely contributing to greater pN_2O in channelized streams, as more NO_3^- can promote denitrification in subsurface sediments and large inputs of N_2O increase in-stream concentrations (Seitzinger et al. 2006). In this study, higher pN_2O were observed mostly in channelized streams but also at SB-Chest, the first fluvial wetland reach along the HN-FP (Table 3, Figure 5, A16). SB-Chest had NO_3^- concentrations that matched more closely to those observed in channels because it is a relatively smaller fluvial wetland system and is located closer to NO_3^- sources upstream (Figure 5). pN_2O was also observed to be greater at SB-Chest than all other fluvial wetland study locations along the flow paths (Table 3), suggesting that low NO_3^- in fluvial wetland dominated reaches largely limits N_2O production downstream and leads to lower concentrations and evasion of N_2O in these systems.

While observed differences in areal N_2O evasion between the flow paths for both the channelized and fluvial wetland dominated portions are likely due to NO_3^- availability, no differences found in flow path CH_4 and CO_2 evasion by streams or wetlands suggest there is likely no C limitations along both transects. Findings from several studies suggest that greater availability of organic C can be an important factor driving higher CH_4 and CO_2 emissions (Altor

and Mitsch 2006, 2008, Cole et al. 2007, Stanley et al. 2016). Despite a faster increase in DOC along the fluvial wetland dominated portion of the LN-FP than the HN-FP, likely due to larger wetlands (Table A2; Figure 13), there was no significant differences in CH_4 or CO_2 by wetland dominated streams or channels, suggesting that both flow paths are likely not C limited. Similarities in warm water temperature and light abundance along the transects may also be contributing to similarities in CO_2 evasion, as these factors along with organic C drive rates of CO_2 evasion and pCO_2 controlled by the tradeoffs between photosynthesis and aerobic respiration (Cole et al. 2007).

Nitrate removal and GHG evasion by fluvial wetlands vs. isolated wetlands

High NO_3^- demand and removal by fluvial wetlands suggest these systems may be greater hotspots of NO_3^- removal than geographically isolated (i.e. non-fluvial) wetlands, especially in high nutrient environments where removal is far from saturation for the flow path. Several studies investigating NO_3^- removal by isolated wetlands report proportional removal estimates (~35%) lower than the majority of estimates determined by fluvial wetland dominated streams in this study and by in-channel wetlands investigated by Czuba et al. (2018) (Kovacic et al. 2000, Mitsch et al. 2005). Previous research has observed isolated wetlands to have the highest NO_3^- concentrations at their outflows and smallest impact on total NO_3^- inputs to the watershed compared to wetlands located the river networks (Hansen et al. 2018). While there is evidence from this study and others that suggest fluvial wetlands may be greater hotspots of NO_3^- removal than isolated wetlands in higher nutrient environments (Czuba et al. 2018, Hansen et al. 2018), research on NO_3^- removal efficiencies by fluvial versus isolated wetlands needs further consideration (Cohen et al. 2016).

Similarly, more research is needed to evaluate differences in evasion between various wetland types, as GHG evasion by fluvial wetlands is still largely unknown and lacking in the literature. Areal GHG evasion from streams with significant fluvial wetlands were often found to be on the lower end of estimates for geographically isolated wetlands, suggesting that these systems may emit less GHG than wetlands separated from advective flow. Maximum CH_4 evasion by fluvial wetlands reported here (113 mg CH_4-C m^{-2} d^{-1}) was on the lower end of ranges between 27 and 2232 mg CH_4-C m^{-2} d^{-1} (Picek et al. 2007, Marín-Muñiz et al. 2015) reported for isolated wetlands in the literature. Estimates of areal CO_2 evasion by fluvial wetlands were also considerably lower than estimates reported previously for isolated wetlands (range 1390 to 77500 mg CO_2-C m^{-2} d^{-1}, Ström et al. 2007) but comparable to those reported by other studies ranging between 150 and 18000 mg CO_2-C m^{-2} d^{-1} (Picek et al. 2007, Marín-Muñiz et al. 2015). Previous studies reporting areal N_2O evasion by isolated wetlands found much larger ranges (-0.85 to 11.56 mg N_2O-N m^{-2} d^{-1}, Jacinthe et al. 2012) and average fluxes (4.32 mg N_2O-N m^{-2} d^{-1}, Bonnett et al. 2013) than observed by fluvial wetlands in this study. While generally lower GHG emissions by fluvial wetlands compared to isolated wetlands may also be due to sampling methods disregarding other pathways for emission (ebullitive and plant-mediated transport), it may also be related to their continuous supplies of water and nutrients from all sources upstream. Thus, fluvial wetlands are less likely than isolated wetlands to become source limited, which may be influencing lower GHG evasion by these system on a per unit area basis compared to isolated wetlands.

Nitrate removal and GHG evasion dynamics after storms under heightened flow

Opposed to what was hypothesized, fluvial wetland dominated streams maintain an apparent high NO_3^- buffering ability during stormflows (runoff ranging from 0 to 2.21 mm d^{-1} in this study), as demand for NO_3^- in the system remained high under elevated streamflow. There was essentially no breakthrough of NO_3^- evident after storms along the fluvial wetland dominated portion of the HN-FP (Figure 5), suggesting saturation was not met as removal and uptake length kept pace under high flow conditions (Figure 11). Previous studies demonstrate that NO_3^- loading from the landscape to stream and river networks increases during storms due to the mobilization of nutrients, especially N, from both terrestrial and groundwater storage (Wollheim et al. 2014, Hansen et al. 2018). Greater delivery of N to headwaters often leads to lower NO_3^- removal potential by river networks and higher transport of NO_3^- downstream as riverine NO_3^- becomes saturated and overwhelms demand in the system (Peterson et al. 2001, Mulholland et al. 2008, Wollheim et al. 2008a, 2018, Baron et al. 2013, Czuba et al. 2018). Unmet NO_3^- demand observed along much of the HN-FP after storms may be due in part to (1) very minimal changes in DO (Figure A8) which allows denitrification to continue with high efficiency under heightened flows (Figure 10a), and/or (2) flow conditions not being high enough to overcome flow thresholds where NO_3^- supply > demand (Wollheim et al. 2018). After large rain events, hydrologic connectivity is enhanced as more wetland area becomes inundated and available for anaerobic processes like denitrification to occur, which may promote high removal abilities to continue under elevated streamflow (Burkett and Kusler 2000, Wollheim et al. 2008a, Baron et al. 2013).

However, demand in the system was observed to be more easily overwhelmed under higher flows along the fluvial wetland portion of the LN-FP where overall demand is likely lower, suggesting that option 2 is probably driving the relationships observed in the HN-FP. The

slight increase in uptake length and declining tendency in NO_3^- removal as runoff increased indicated that NO_3^- was being transported longer distances before uptake after storms by fluvial wetland reaches in the LN-FP (Figure 11). However, there was no evident pulse in NO_3^- downstream after storms along much of the LN-FP (Figure 5), suggesting that the fluvial wetland dominated flow path is long enough to accommodate slight increases in uptake length and continue limiting NO_3^- at elevated flows.

As fluvial wetland dominated reaches reported here sustain generally high NO_3^- removal abilities under heightened flows, with storm removal estimates consistent with some findings in the literature (Fink and Mitsch 2004, Griffiths and Mitsch 2017, Czuba et al. 2018), previous studies have also demonstrated that N removal efficiency can decline in ponded waters/isolated wetlands with heightened flows (Spieles and Mitsch 2000, Schmadel et al. 2018). Similar to findings reported here, Czuba et al. (2018) found that flow-through wetlands connected directly to the river network were largely effective at removing NO_3^- across flow conditions. As well, Griffiths and Mitsch (2017) reported greater N removal from geographically isolated, constructed wetlands in Florida during wetter seasons when flows were higher, while Fink and Mitsch (2004) found relatively no change in N retention in a created wetland in Ohio during large storm events. However, other studies have reported opposite findings of lower N removal/retention efficiency in ponded waters/wetlands (Spieles and Mitsch 2000, Schmadel et al. 2018).

While higher flow conditions had little to no influence on NO_3^- removal by long flow paths with abundant fluvial wetlands, GHG evasion exhibited tendencies to generally increase with runoff due to enhanced exchange and production/delivery of GHGs. Besides the lack of change in N_2O evasion observed across flows for the HN-FP, there were tendencies for elevated

CO_2, CH_4, and N_2O evasion in fluvial wetland dominated and channelized streams at higher streamflow (Figure 12, 13, 14, 15, 16). Gas evasion is inherently driven by both the concentration of gas in the water and the air-water gas transfer velocity (Raymond et al. 2012). Mostly higher pCH_4 and pN_2O, and sometimes higher pCO_2, in wetland dominated streams following storms where GHG evasion was significantly different under baseflow conditions (Table 5; Figure A14, A15, A16) suggest that higher flows mostly increased production and/or delivery of GHGs, as quicker exchange of gases to the atmosphere due to faster flow velocity would lead to lower partial pressure of gases if production remained the same or delivery of terrestrially derived gases did not occur. This was also true for the channelized streams studied, as channels exhibited generally greater pCO_2, pCH_4, and pN_2O following storms (Table 5; Figure A14, A15, A16). Declines in partial pressure of GHG, especially CO_2, at some fluvial wetland study sites after storms suggest that increased in gas exchange is primarily driving increased evasion at those locations.

Delivery of terrestrially produced GHG may be driving increased partial pressure of gases in surfaces waters after storms, especially in upstream headwater channels where connectivity between terrestrial and aquatic ecosystems is inherently high (Alexander et al. 2007, Crawford et al. 2013). Warmer temperatures and abundant organic C have been found to promote methanogenesis and aerobic respiration, driving CH_4 and CO_2 evasion by aquatic systems (Altor and Mitsch 2006, 2008, Cole et al. 2007, Kaushal et al. 2014). Slight increases in DOC in channels and some fluvial wetland dominated sites due to greater delivery of nutrients when flows are high (Hall et al. 2016, Stanley et al. 2016), as well as sometimes warmer surface waters along the flow paths, suggest that DOC and temperature could be contributing to increased pCO_2 and pCH_4 after storms (Figure A7, A13). However, we did not see strong

patterns of increasing DOC and temperature after storms along the flow paths across the study period, suggesting it is more likely that delivery of terrestrial produced GHG from soil-water runoff and groundwater inputs (upstream and locally) that become enhanced following precipitation events are supplying greater amounts of GHG along the transects, further promoting evasion of these GHGs (Bodelier and Steenbergh 2014, Stanley et al. 2016, Talbot et al. 2018, Borges et al. 2019). Delivery of GHGs produced outside stream channels is often enhanced under higher flows as stronger linkages between terrestrial and aquatic environments promote delivery of gases to stream channels (Stanley et al. 2016).

As discussed earlier, NO_3^- availability and lower DO conditions can also enhance GHG production and subsequent evasion in these systems (Mulholland et al. 2004, Beaulieu et al. 2008, Bodelier and Steenbergh 2014, Stanley et al. 2016). While elevated runoff typically increases NO_3^- loading from the landscape to headwater streams (Talbot et al. 2018), NO_3^- concentrations declined in channels upstream after storms due to dilution, but was still elevated compared the wetland sites (Figure 5; Figure A 4). NO_3^- also remained low along fluvial wetland dominated reaches after storms (Figure 5), suggesting that we can rule NO_3^- out as a probable control on CH_4 and N_2O production along the flow paths, particularly in the fluvial wetland dominated portion. Likewise, changes in DO were mostly minimal after storms, suggesting that changes in redox potential along these flow paths is also unlikely driving GHG production (Figure A8).

There were no apparent nutrient limitations on increasing GHG evasion after storms as fluvial wetland dominated streams showed greater increases in GHG evasion in the LN-FP than the HN-FP. When runoff increased by 1 mm d^{-1}, mean evasion by fluvial wetland dominated streams in the LN-FP increased by 9765 mg CO_2-C m^{-2} d^{-2} for CO_2 and 0.46 mg N_2O-N m^{-2} d^{-2}

for N_2O, and showed tendencies of increasing by ~11 mg CH_4-C m^{-2} d^{-2} for CH_4 (Figure 12). Mean GHG evasion in the HN-FP, however, increased at a slower rate for CO_2 (3135 mg CO_2-C m^{-2} d^{-2} per 1 mm d^{-1} runoff) among fluvial wetland dominated streams, and showed tendencies of increasing at a slower rate for CH_4 (~9.0 mg CH_4-C m^{-2} d^{-2} per 1 mm d^{-1} runoff) and nearly no change in N_2O (~0 mg N_2O-N m^{-2} d^{-2} per 1 mm d^{-1} runoff) (Figure 12). Tendencies for greater GHG evasion with increasing flows along the LN-FP than the HN-FP suggest that GHG evasion is not limited by upstream N inputs.

Elevated GHG evasion by fluvial wetland dominated reaches receiving lower nutrient inputs may be a result of (1) greater localized inputs of terrestrially produced GHG to fluvial wetland systems, (2) greater availability of organic C fueling aerobic and anaerobic respiration, and/or (3) faster air-water gas exchange. The LN-FP likely has more localized GHG inputs from soil-water runoff and groundwater as the drainage area of the LN-FP has roughly 10% more forested and more wetland land cover than the HN-FP (Table A2). As perhaps a result of more forested and wetland upstream land cover, DOC was also observed to be slightly greater among downstream fluvial wetland dominated reaches in the LN-FP and maintained during higher stormflows (Figure A13), which may be promoting more GHG production along the LN-FP (Altor and Mitsch 2006, 2008, Kaushal et al. 2014). GHG evasion was estimated here to be strongly controlled by hydrologic variability, suggesting that differences in gas transfer velocities between the two flow paths may be driving the disparity in production and evasion patterns with increasing flow. When estimates of gas transfer velocities during stormflows were averaged for fluvial wetland dominated study sites between the two flow paths, the LN-FP exhibited greater gas transfer (Table A4). Although, average gas exchange was also estimated to be higher in

channels of the LN-FP than the HN-FP where we did not see greater increases in mean GHG evasion with runoff (Figure 16; Table A4), suggesting that option 3 is a less reliable justification.

While the mechanisms validating my hypotheses may still hold true for N_2O and CH_4, findings from this study demonstrating tendencies for greater GHG evasion by wetland dominated streams at higher flows ultimately refuted my hypothesis of lower areal N_2O and CH_4 evasion following storms; my hypothesis of greater CO_2 evasion after storms was supported, however it was likely due to increased delivery from terrestrial produced CO_2 than increased DO conditions (as changes in DO were variable and minimal following storms). Although there is inconsistency among the literature on the effect of hydrologic changes on GHG emissions from streams and wetlands due to the collective influence of various ecosystem factors (Kaushal et al. 2014), these findings were consistent with previous studies reporting no or negative relationships between GHG evasion and flood flows or water table height in wetlands (Altor and Mitsch 2008), peatlands (Merbach et al. 1996), riparian zones (Pacific et al. 2009, Soosaar et al. 2011), and streams (Tortosa et al. 2011, Stanley et al. 2016). However, like the results presented here, many studies have also found pulses of GHG emission to be correlated with higher flow conditions from these various systems (Harms and Grimm 2012, Bonnett et al. 2013, Kaushal et al. 2014, Vidon et al. 2014, Stanley et al. 2016, Audet et al. 2017, Marx et al. 2017, Hampton et al. 2020), suggesting that changes in the hydrologic regime can have profound effects on rates of GHG emissions from surface waters. This apparent discrepancy among the literature further reiterates the complexity of abiotic and biotic factors all interacting to influence GHG emissions by aquatic ecosystems (Kaushal et al. 2014).

Although possible, it is unlikely that the patterns we see in both NO_3^- removal and GHG emissions after storms are the product of stored water being flushed from transient storage zones

to advective channels, as storm pulse signals were apparent in other measured parameters. Storm pulses appear to have made their way downstream along the flow paths as water level increased between baseflow and stormflows across all fluvial wetland dominated study sties for each storm (Table A3). Additionally, specific conductance was found to decline after storms along fluvial wetland dominated reaches (Figure A6), suggesting that stormflow samplings were characteristic of the storm pulses and not of stored water. Despite being certain there were storm responses present along these reaches, Cl^- and NO_3:Cl showed relatively no response to storms along the fluvial wetland dominated portion of the flow paths (Figure A3, A4), alternatively suggesting that some of the storm signal could be getting stored in transient storage zones upstream instead of being transferred downstream.

Tradeoffs and management implications

Fluvial wetland dominated streams are shown here to be crucial locations of NO_3^- removal in river networks, especially in more urban catchments where N availability is greater. Elevated N loading to river networks in catchments draining more urban land cover often leads to larger export of N to coastal ecosystems due to diminished removal capabilities (Mulholland et al. 2008, Flint and McDowell 2015, Czuba et al. 2018). However, results reported here demonstrate that fluvial wetland dominated streams can thrive in higher nutrient environments because their demand for NO_3^- is substantial – potentially even more substantial than those in lower nutrient environments – and in this case, always prevents anthropogenic N from breaking through (Figure 5). In the Ipswich River watershed, urban land cover is skewed towards the headwaters upstream of fluvial wetland systems, enhancing DIN inputs to headwater flow paths (Mineau et al. 2015), yet fluvial wetland dominated reaches show no limitations on their

response to elevated DIN inputs (Figure 5, 6, 7). Despite ongoing land use change, suburban headwater catchments of the Ipswich River watershed continue to have high N retention (Morse and Wollheim 2014), suggesting that fluvial wetland dominated flow paths serve as strong buffers in coastal watersheds against growing N sources across flow conditions.

Enhanced NO_3^- loading in headwaters has seemingly no negative impact on GHG emissions from fluvial wetland dominated surface water flow paths. Although N loading to headwater streams is heightened by intensification of upstream urban land cover (Howarth et al. 2002b, Mineau et al. 2015), GHG emissions by fluvial wetland dominated streams were not elevated as a result. In fact, CO_2 and CH_4 evasion from channels and fluvial wetland dominated streams were observed to be similar despite differences in upstream NO_3^- loading between the two flow paths investigated (Figure 9). While N_2O evasion was found to be slightly elevated in channels where nutrient loading was greater (HN-FP), there was essentially no N_2O evasion observed by fluvial wetland dominated streams in the higher nutrient environment, yet there was evidence of small emissions by these systems in the lower nutrient environment (Figure 9). These patterns in GHG emissions by fluvial wetland dominated streams in more urban influenced catchments suggest that increased N availability in headwater channels does not necessarily encourage GHG evasion along extensive fluvial wetland dominated surface water flow paths, especially evasion of CO_2 and CH_4, and can even potentially limit evasion of N_2O in fluvial wetland dominated streams as inflowing NO_3^- continues to be actively removed by these systems.

As fluvial wetland dominated streams in higher nutrient environments seem to be unaltered by high N inputs, they are also potentially less affected by storms than pathways receiving overall lower nutrient inputs. While the wetland dominated streams in the LN-FP

showed tendencies for possibly lower NO_3^- removal and greater N_2O evasion with increasing streamflow, those in the HN-FP exhibited no change in removal ability or N_2O emission across flow conditions (Figure 11, 12). N_2O has a global warming potential 298 times that of carbon dioxide over a 100-year time scale, so the ability for fluvial wetland dominated streams to act as neither a source nor a sink of N_2O across flow conditions in higher nutrient environments demonstrates the substantial impact these systems may have on total GHG emissions. Despite generally greater CO_2 and CH_4 evasion after storms along the transects, reaches dominated by fluvial wetlands in the HN-FP showed lower rates of increase compared to those reaches in the LN-FP (Figure 12, 16). Thus, there is evidence that suggests the effects of hydrologic changes due to storms on both NO_3^- removal and GHG emission dynamics can be further limited in river networks where N is more available.

Results from this study ultimately reveal that fluvial wetland dominated surface water flow paths receiving both high and low N loads can be vulnerable to the impacts of climate variability with respect to GHG emissions. Despite differences in nutrient loading, both flow paths showed tendencies to greater GHG emissions under heightened streamflow (Figure 12, 16). Flooding from heavy precipitation events can change biogeochemical dynamics in aquatic ecosystems like wetlands by delivering nutrients, recharging groundwater, and expanding reactive surfaces (Talbot et al. 2018), which often fuel greater GHG emissions (Bodelier and Steenbergh 2014, Kaushal et al. 2014). Wetlands contribute largely to total GHG emissions, especially CH_4, suggesting that increases in GHG evasion by fluvial wetland dominated streams in response to storm events will likely increase total GHG emissions (Figure 12; Table 5) as storm events become more frequent and stronger in magnitude (Talbot et al. 2018).

Representative of the transition zone between aquatic and terrestrial ecosystems, with continuous supplies of water and nutrients from all sources upstream, fluvial wetland dominated streams should be critical focal points of future broad scale management efforts due to their abilities to promote greater NO_3^- removal in river networks without increasing areal GHG emissions more than most channels and geographically isolated wetlands. While they do emit greater total GHG emissions than channels due to their much greater surface area, they tend to emit generally less GHG per unit area and may even be greater hotspots of NO_3^- removal than most channels and isolated wetlands, especially in high nutrient environments where removal is far from saturation for the flow path. As NO_3^- loading to headwater systems will likely continue increasing with the intensification of storms and urban development (Faulkner 2004, Talbot et al. 2018), management efforts geared towards restoring fluvial wetland habitat in urbanizing coastal watersheds where N inputs are enhanced could help improve coastal water quality by limiting NO_3^- export downstream (Hansen et al. 2018) at a lower cost of GHG emission than what naturally occurs in more pristine environments. Thus, systems of fluvial wetlands along surface water flow paths are undervalued, instrumental players in coastal watersheds, whose improved management and potential restoration could help mitigate future impacts from broad scale environmental changes.

CHAPTER 5: CONCLUSION

Fluvial wetland dominated streams are important freshwater ecosystems that are understudied and therefore largely undervalued by the management community. My results suggest that the presence of fluvial wetlands along surface water flow paths contribute substantially to river network NO_3^- removal, including in urbanizing coastal watersheds where N loading to headwaters is elevated. It was shown here that fluvial wetland dominated streams can remain effective in higher nutrient environments as their demand for NO_3^- is substantial. Although GHG emissions by fluvial wetland reaches are much larger than those by channels when total area is considered, wetland dominated streams emit lower GHG compared to channelized streams on a per unit area basis due to slower air-water gas exchange and lower production/delivery of gases per unit area. GHG evasion by wetland dominated streams, importantly N_2O, did not increase in association with higher nutrient loads, demonstrating that increased N loading from the landscape need-not lead to higher GHG evasion by these systems.

While the ability of fluvial wetland dominated streams to act as strong NO_3^- buffers seems to be largely unaffected by storms/heightened flow conditions as demand in the systems remains high, their GHG emission potential may be more vulnerable to hydrologic changes. With enhanced gas exchange and production/delivery of gases following storms, there were tendencies for greater GHG evasion by wetland dominated flow paths at higher runoff rates, with the exception of N_2O by wetland dominated streams in the HN-FP. Increased runoff as a result of more urban development causes even higher flow conditions after storms along river networks (Faulkner 2004), which could subsequently lead to higher GHG evasion. With climate variability intensifying both the frequency and magnitude of storm events (Faulkner 2004), we can expect to see pulses of GHG emissions along whole flow paths – both channelized and fluvial wetland

dominated. Ultimately, the ability for fluvial wetland dominated streams to effectively remove NO_3^- from surface water flow paths draining higher N inputs does not come at the expense of greater GHG emissions beyond what naturally occurs. Understanding the complex tradeoffs of fluvial wetlands along surface water flow paths is critical for prioritizing future management activities to lessen coastal eutrophication and emissions of GHG, and for predicting how coastal watersheds will respond as N loading increases in a changing climate.

LIST OF REFERENCES

ALEXANDER, R. B., E. W. BOYER, R. A. SMITH, G. E. SCHWARZ, AND R. B. MOORE. 2007. The role of headwater streams in downstream water quality. Journal of the American Water Resources Association 43:41–59.

ALTOR, A. E., AND W. J. MITSCH. 2006. Methane flux from created riparian marshes: Relationship to intermittent versus continuous inundation and emergent macrophytes. Ecological Engineering 28:224–234.

ALTOR, A. E., AND W. J. MITSCH. 2008. Pulsing hydrology, methane emissions and carbon dioxide fluxes in created marshes: A 2-year ecosystem study. Wetlands 28:423–438.

ANDERSON, D. M., P. M. GLIBERT, AND J. M. BURKHOLDER. 2002. Harmful algal blooms and eutrophication: Nutrient sources, composition, and consequences. Estuaries 25:704–726.

AUDET, J., M. B. WALLIN, K. KYLLMAR, S. ANDERSSON, AND K. BISHOP. 2017. Nitrous oxide emissions from streams in a Swedish agricultural catchment. Agriculture, Ecosystems and Environment 236:295–303.

BARON, J. S., E. K. HALL, B. T. NOLAN, J. C. FINLAY, E. S. BERNHARDT, J. A. HARRISON, F. CHAN, AND E. W. BOYER. 2013. The interactive effects of excess reactive nitrogen and climate change on aquatic ecosystems and water resources of the United States. Biogeochemistry 114:71–92.

BASTVIKEN, D., L. J. TRANVIK, J. A. DOWNING, P. M. CRILL, AND A. ENRICH-PRAST. 2011. Freshwater methane emissions offset the continental carbon sink. Science 331:50.

BEAULIEU, J. J., C. P. ARANGO, S. K. HAMILTON, AND J. L. TANK. 2008. The production and emission of nitrous oxide from headwater streams in the Midwestern United States. Global Change Biology 14:878–894.

BEAULIEU, J. J., H. E. GOLDEN, C. D. KNIGHTES, P. M. MAYER, S. S. KAUSHAL, M. J. PENNINO, C. P. ARANGO, D. A. BALZ, C. M. ELONEN, K. M. FRITZ, AND B. H. HILL. 2015. Urban stream burial increases watershed-scale nitrate export. PLoS ONE 10:1–14.

BEAULIEU, J. J., P. M. MAYER, S. S. KAUSHAL, M. J. PENNINO, C. P. ARANGO, D. A. BALZ, T. J. CANFIELD, C. M. ELONEN, K. M. FRITZ, B. H. HILL, H. RYU, AND J. W. S. DOMINGO. 2014. Effects of urban stream burial on organic matter dynamics and reach scale nitrate retention. Biogeochemistry 121:107–126.

BEAULIEU, J. J., J. L. TANK, S. K. HAMILTON, W. M. WOLLHEIM, R. O. HALL, P. J. MULHOLLAND, B. J. PETERSON, L. R. ASHKENAS, L. W. COOPER, C. N. DAHM, W. K. DODDS, N. B. GRIMM, S. L. JOHNSON, W. H. MCDOWELL, G. C. POOLE, H. M. VALETT, C. P. ARANGO, M. J. BERNOT, A. J. BURGIN, C. L. CRENSHAW, A. M. HELTON, L. T. JOHNSON, J. M. O'BRIEN, J. D. POTTER, R. W. SHEIBLEY, D. J. SOBOTA, AND S. M. THOMAS. 2011. Nitrous oxide

emission from denitrification in stream and river networks. Proceedings of the National Academy of Sciences 108:214–219.

BILLETT, M. F., AND F. H. HARVEY. 2013. Measurements of CO_2 and CH_4 evasion from UK peatland headwater streams. Biogeochemistry 114:165–181.

BODELIER, P. L. E., AND A. K. STEENBERGH. 2014. Interactions between methane and the nitrogen cycle in light of climate change. Current Opinion in Environmental Sustainability 9–10:26–36.

BONNETT, S. A. F., M. S. A. BLACKWELL, R. LEAH, V. COOK, M. O'CONNOR, AND E. MALTBY. 2013. Temperature response of denitrification rate and greenhouse gas production in agricultural river marginal wetland soils. Geobiology 11:252–267.

BORGES, A. V., F. DARCHAMBEAU, T. LAMBERT, C. MORANA, G. H. ALLEN, E. TAMBWE, A. TOENGAHO SEMBAITO, T. MAMBO, J. N. WABAKHANGAZI, J. P. DESCY, C. R. TEODORU, AND S. BOUILLON. 2019. Variations in dissolved greenhouse gases (CO_2, CH_4, N_2O) in the Congo River network overwhelmingly driven by fluvial-wetland connectivity. Biogeosciences 16:3801–3834.

BOYER, E. W., C. L. GOODALE, A. NORBERT, AND R. W. HOWARTH. 2002. Anthropogenic nitrogen sources and relationships to riverine nitrogen export in the northeastern U.S.A. Biogeochemistry 57/58:137–169.

BURKETT, V., AND J. KUSLER. 2000. Climate change: potential impacts and interactions in wetlands of the United States 36.

CHEN, D., H. HUANG, M. HU, AND R. A. DAHLGREN. 2014. Influence of lag effect, soil release, and climate change on watershed anthropogenic nitrogen inputs and riverine export dynamics. Environmental Science and Technology 48:5683–5690.

COHEN, M. J., I. F. CREED, L. ALEXANDER, N. B. BASU, A. J. K. CALHOUN, C. CRAFT, E. D'AMICO, E. DEKEYSER, L. FOWLER, H. E. GOLDEN, J. W. JAWITZ, P. KALLA, L. K. KIRKMAN, C. R. LANE, M. LANG, S. G. LEIBOWITZ, D. B. LEWIS, J. MARTON, D. L. MCLAUGHLIN, D. M. MUSHET, H. RAANAN-KIPERWAS, M. C. RAINS, L. SMITH, AND S. C. WALLS. 2016. Do geographically isolated wetlands influence landscape functions? Proceedings of the National Academy of Sciences of the United States of America 113:1978–1986.

COLE, J. J., Y. T. PRAIRIE, N. F. CARACO, W. H. MCDOWELL, L. J. TRANVIK, R. G. STRIEGL, C. M. DUARTE, P. KORTELAINEN, J. A. DOWNING, J. J. MIDDELBURG, AND J. MELACK. 2007. Plumbing the global carbon cycle: Integrating inland waters into the terrestrial carbon budget. Ecosystems 10:171–184.

COVINO, T. P., B. L. MCGLYNN, AND R. A. MCNAMARA. 2010. Tracer additions for spiraling curve characterization (TASCC): Quantifying stream nutrient uptake kinetics from ambient

to saturation. Limnology and Oceanography: Methods 8:484–498.

CRAWFORD, J. T., R. G. STRIEGL, K. P. WICKLAND, M. M. DORNBLASER, AND E. H. STANLEY. 2013. Emissions of carbon dioxide and methane from a headwater stream network of interior Alaska. Journal of Geophysical Research: Biogeosciences 118:482–494.

CZUBA, J. A., A. T. HANSEN, E. FOUFOULA-GEORGIOU, AND J. C. FINLAY. 2018. Contextualizing wetlands within a river network to assess nitrate removal and inform watershed management. Water Resources Research 54:1312–1337.

DALAL, R. C., D. E. ALLEN, S. J. LIVESLEY, AND G. RICHARDS. 2008. Magnitude and biophysical regulators of methane emission and consumption in the Australian agricultural, forest, and submerged landscapes: a review. Plant and Soil 309:43–76.

FAULKNER, S. 2004. Urbanization impacts on the structure and function of forested wetlands. Urban Ecosystems 7:89–106.

FINK, D. F., AND W. J. MITSCH. 2004. Seasonal and storm event nutrient removal by a created wetland in an agricultural watershed. Ecological Engineering 23:313–325.

FLINT, S. A., AND W. H. MCDOWELL. 2015. Effects of headwater wetlands on dissolved nitrogen and dissolved organic carbon concentrations in a suburban New Hampshire watershed. Freshwater Science 34:456–471.

GALLOWAY, J. N., J. D. ABER, J. W. ERISMAN, S. P. SEITZINGER, R. W. HOWARTH, E. B. COWLING, AND B. J. COSBY. 2003. The nitrogen cascade. BioScience 53:341.

GAO, Y., X. LIU, N. YI, Y. WANG, J. GUO, Z. ZHANG, AND S. YAN. 2013. Estimation of N_2 and N_2O ebullition from eutrophic water using an improved bubble trap device. Ecological Engineering 57:403–412.

GRIFFITHS, L. N., AND W. J. MITSCH. 2017. Removal of nutrients from urban stormwater runoff by storm-pulsed and seasonally pulsed created wetlands in the subtropics. Ecological Engineering 108:414–424.

HALL, R. O., J. L. TANK, M. A. BAKER, E. J. ROSI-MARSHALL, AND E. R. HOTCHKISS. 2016. Metabolism, gas exchange, and carbon spiraling in rivers. Ecosystems 19.

HAMPTON, T. B., J. P. ZARNETSKE, M. A. BRIGGS, F. MAHMOODPOOR DEHKORDY, K. SINGHA, F. D. DAY-LEWIS, J. W. HARVEY, S. R. CHOWDHURY, AND J. W. LANE. 2020. Experimental shifts of hydrologic residence time in a sandy urban stream sediment–water interface alter nitrate removal and nitrous oxide fluxes. Biogeochemistry 149:195–219.

HANSEN, A. T., C. L. DOLPH, E. FOUFOULA-GEORGIOU, AND J. C. FINLAY. 2018. Contribution of wetlands to nitrate removal at the watershed scale. Nature Geoscience 11:127–132.

HARMS, T. K., AND N. B. GRIMM. 2012. Responses of trace gases to hydrologic pulses in desert floodplains. Journal of Geophysical Research: Biogeosciences 117:1–14.

HOPE, D., S. M. PALMER, M. F. BILLETT, AND J. J. C. DAWSON. 2001. Carbon dioxide and methane evasion from a temperate peatland stream. Limnology and Oceanography 46:847–857.

HOWARTH, R. W., E. W. BOYER, W. J. PABICH, AND J. N. GALLOWAY. 2002a. Nitrogen use in the United States from 1961-2000 and potential future trends. Ambio 31:88–96.

HOWARTH, R. W., A. SHARPLEY, AND D. A. N. WALKER. 2002b. Sources of nutrient pollution to coastal waters in the United States: Implications for achieving coastal water quality goals 25:656–676.

JACINTHE, P. A., J. S. BILLS, L. P. TEDESCO, AND R. C. BARR. 2012. Nitrous oxide emission from riparian buffers in relation to vegetation and flood frequency. Journal of Environmental Quality 41:95–105.

JOHNSTON, C. A., N. E. DETENBECK, AND G. J. NEIMI. 1990. The cumulative effect of wetlands on stream water quality and quantity. A landscape approach. Biogeochemistry 10:105–141.

KADLEC, R. H. 2012. Constructed marshes for nitrate removal. Critical Reviews in Environmental Science and Technology 42:934–1005.

KAUSHAL, S. S., P. M. MAYER, P. G. VIDON, R. M. SMITH, M. J. PENNINO, T. A. NEWCOMER, S. DUAN, C. WELTY, AND K. T. BELT. 2014. Land use and climate variability amplify carbon, nutrient, and contaminant pulses: A review with management implications. Journal of the American Water Resources Association 50:585–614.

KAYRANLI, B., M. SCHOLZ, A. MUSTAFA, AND Å. HEDMARK. 2010. Carbon storage and fluxes within freshwater wetlands: A critical review. Wetlands 30:111–124.

KOVACIC, D. A., M. B. DAVID, L. E. GENTRY, K. M. STARKS, AND R. A. COOKE. 2000. Effectiveness of constructed wetlands in reducing nitrogen and phosphorus export from agricultural tile drainage. Journal of Environmental Quality 29:1262–1274.

MARÍN-MUÑIZ, J. L., M. E. HERNÁNDEZ, AND P. MORENO-CASASOLA. 2015. Greenhouse gas emissions from coastal freshwater wetlands in Veracruz Mexico: Effect of plant community and seasonal dynamics. Atmospheric Environment 107:107–117.

MARX, A., J. DUSEK, J. JANKOVEC, M. SANDA, T. VOGEL, R. VAN GELDERN, J. HARTMANN, AND J. A. C. BARTH. 2017. A review of CO_2 and associated carbon dynamics in headwater streams: A global perspective. Reviews of Geophysics 55:560–585.

MERBACH, W., J. AUGUSTIN, T. KALETTKA, AND H. J. JACOB. 1996. Nitrous Oxide and Methane Emissions from riparian areas of ponded depressions of northeast Germany. Journal of

Applied Botany-Angewandte Botanik 70:134–136.

MINEAU, M. M., W. M. WOLLHEIM, AND R. J. STEWART. 2015. An index to characterize the spatial distribution of land use within watersheds and implications for river network nutrient removal and export. Geophysical Research Letters 42.

MITSCH, W. J., B. BERNAL, A. M. NAHLIK, Ü. MANDER, L. ZHANG, C. J. ANDERSON, S. E. JØRGENSEN, AND H. BRIX. 2013. Wetlands, carbon, and climate change. Landscape Ecology 28:583–597.

MITSCH, W. J., J. W. DAY, L. ZHANG, AND R. R. LANE. 2005. Nitrate-nitrogen retention in wetlands in the Mississippi River Basin. Ecological Engineering 24:267–278.

MORSE, N. B., AND W. M. WOLLHEIM. 2014. Climate variability masks the impacts of land use change on nutrient export in a suburbanizing watershed. Biogeochemistry 121:45–59.

MULHOLLAND, P. J., R. O. HALL, D. J. SOBOTA, W. K. DODDS, E. G. STUART, N. B. GRIMM, S. K. HAMILTON, W. H. MCDOWELL, J. M. O. BRIEN, J. L. TANK, L. R. ASHKENAS, L. W. COOPER, C. N. DAHM, S. V GREGORY, S. L. JOHNSON, J. L. MEYER, B. J. PETERSON, G. C. POOLE, H. M. VALETT, J. R. WEBSTER, C. P. ARANGO, J. J. BEAULIEU, M. J. BERNOT, A. J. BURGIN, C. L. CRENSHAW, A. M. HELTON, L. T. JOHNSON, B. R. NIEDERLEHNER, J. D. POTTER, R. W. SHEIBLEY, AND S. M. THOMAS. 2009. Nitrate removal in stream ecosystems measured by ^{15}N addition experiments: Denitrification. Limnology and Oceanography 54:666–680.

MULHOLLAND, P. J., A. M. HELTON, G. C. POOLE, R. O. HALL, S. K. HAMILTON, B. J. PETERSON, J. L. TANK, L. R. ASHKENAS, L. W. COOPER, C. N. DAHM, W. K. DODDS, S. E. G. FINDLAY, S. V. GREGORY, N. B. GRIMM, S. L. JOHNSON, W. H. MCDOWELL, J. L. MEYER, H. M. VALETT, J. R. WEBSTER, C. P. ARANGO, J. J. BEAULIEU, M. J. BERNOT, A. J. BURGIN, C. L. CRENSHAW, L. T. JOHNSON, B. R. NIEDERLEHNER, J. M. O'BRIEN, J. D. POTTER, R. W. SHEIBLEY, D. J. SOBOTA, AND S. M. THOMAS. 2008. Stream denitrification across biomes and its response to anthropogenic nitrate loading. Nature 452:202–205.

MULHOLLAND, P. J., H. M. VALETT, J. R. WEBSTER, S. A. THOMAS, L. W. COOPER, S. K. HAMILTON, AND B. J. PETERSON. 2004. Stream denitrification and total nitrate uptake rates measured using a field ^{15}N tracer addition approach. Limnology and Oceanography 49:809–820.

O'BRIEN, J. M., S. K. HAMILTON, L. E. KINSMAN-COSTELLO, J. T. LENNON, AND N. E. OSTROM. 2012. Nitrogen transformations in a through-flow wetland revealed using whole-ecosystem pulsed 15N additions. Limnology and Oceanography 57:221–234.

PACIFIC, V. J., B. L. MCGLYNN, D. A. RIVEROS-IREGUI, H. E. EPSTEIN, AND D. L. WELSCH. 2009. Differential soil respiration responses to changing hydrologic regimes. Water Resources Research 45:6–11.

PAGE, K. L., AND R. C. DALAL. 2011. Contribution of natural and drained wetland systems to

carbon stocks, CO_2, N_2O, and CH_4 fluxes: An Australian perspective. Soil Research 49:377–388.

PALMA-SILVA, C., C. C. MARINHO, E. F. ALBERTONI, I. B. GIACOMINI, M. P. FIGUEIREDO BARROS, L. M. FURLANETTO, C. R. T. TRINDADE, AND F. DE A. ESTEVES. 2013. Methane emissions in two small shallow neotropical lakes: The role of temperature and trophic level. Atmospheric Environment 81:373–379.

PELLERIN, B. A., W. M. WOLLHEIM, C. S. HOPKINSON, W. H. MCDOWELL, M. R. WILLIAMS, C. J. VÖRÖSMARTY, AND M. L. DALEY. 2004. Role of wetlands and developed land use on dissolved organic nitrogen concentrations and DON/TDN in northeastern U.S. rivers and streams. Limnology and Oceanography 49:910–918.

PETERSON, B. J., W. M. WOLLHEIM, P. J. MULHOLLAND, J. R. WEBSTER, J. L. MEYER, J. L. TANK, E. MARTI, W. B. BOWDEN, H. M. VALETT, A. E. HERSHEY, W. . MCDOWELL, W. K. DODDS, S. K. HAMILTON, S. GREGORY, AND D. D. MORRALL. 2001. Control of nitrogen export from watersheds by headwater streams. Science 292:86–91.

PICEK, T., H. ČÍŽKOVÁ, AND J. DUŠEK. 2007. Greenhouse gas emissions from a constructed wetland-Plants as important sources of carbon. Ecological Engineering 31:98–106.

RABALAIS, N. N., R. E. TURNER, AND W. J. WISEMAN. 2002. Gulf of Mexico hypoxia, a.k.a. "The dead zone." Annual Review of Ecology and Systematics 33:235–263.

RAYMOND, P. A., N. F. CARACO, AND J. J. COLE. 1997. Carbon dioxide concentration and atmospheric flux in the Hudson River. Estuaries 20:381–390.

RAYMOND, P. A., C. J. ZAPPA, D. BUTMAN, T. L. BOTT, J. POTTER, P. MULHOLLAND, A. E. LAURSEN, W. H. MCDOWELL, AND D. NEWBOLD. 2012. Scaling the gas transfer velocity and hydraulic geometry in streams and small rivers. Limnology and Oceanography: Fluids and Environments 2:41–53.

SAUNDERS, D. L., AND J. KALFF. 2001. Nitrogen retention in wetlands, lakes and rivers. Hydrobiologia 443:205–212.

SCHADE, J. D., J. BAILIO, AND W. H. MCDOWELL. 2016. Greenhouse gas flux from headwater streams in New Hampshire, USA: Patterns and drivers. Limnology and Oceanography 61:S165–S174.

SCHMADEL, N. M., J. W. HARVEY, R. B. ALEXANDER, G. E. SCHWARZ, R. B. MOORE, K. ENG, J. D. GOMEZ-VELEZ, E. W. BOYER, AND D. SCOTT. 2018. Thresholds of lake and reservoir connectivity in river networks control nitrogen removal. Nature Communications 9.

SCHMADEL, N. M., J. W. HARVEY, G. E. SCHWARZ, R. B. ALEXANDER, J. D. GOMEZ-VELEZ, D. SCOTT, AND S. W. ATOR. 2019. Small Ppnds in headwater catchments are a dominant influence on regional nutrient and sediment budgets. Geophysical Research Letters 46.

SEITZINGER, S., J. A. HARRISON, J. K. BÖHLKE, A. F. BOUWMAN, R. LOWRANCE, B. PETERSON, C. TOBIAS, AND G. VAN DRECHT. 2006. Denitrification across landscapes and waterscapes: A synthesis. Ecological Applications 16:2064–2090.

SOOSAAR, K., Ü. MANDER, M. MADDISON, A. KANAL, A. KULL, K. LÕHMUS, J. TRUU, AND J. AUGUSTIN. 2011. Dynamics of gaseous nitrogen and carbon fluxes in riparian alder forests. Ecological Engineering 37:40–53.

SPIELES, D. J., AND W. J. MITSCH. 2000. The effects of season and hydrologic and chemical loading on nitrate retention in constructed wetlands: A comparison of low- and high-nutrient riverine systems. Ecological Engineering 14:77–91.

STANLEY, E. H., N. J. CASSON, S. T. CHRISTEL, J. T. CRAWFORD, L. C. LOKEN, AND S. K. OLIVER. 2016. The ecology of methane in streams and rivers: patterns, controls, and global significance. Ecological Monographs 86:146–171.

STEWART, R. J., W. M. WOLLHEIM, M. N. GOOSEFF, M. A. BRIGGS, J. M. JACOBS, B. J. PETERSON, AND C. S. HOPKINSON. 2011. Separation of river network-scale nitrogen removal among the main channel and two transient storage compartments. Water Resources Research 47:1–19.

STRÖM, L., A. LAMPPA, AND T. R. CHRISTENSEN. 2007. Greenhouse gas emissions from a constructed wetland in southern Sweden. Wetlands Ecology and Management 15:43–50.

TALBOT, C. J., E. M. BENNETT, K. CASSELL, D. M. HANES, E. C. MINOR, H. PAERL, P. A. RAYMOND, R. VARGAS, P. G. VIDON, W. WOLLHEIM, AND M. A. XENOPOULOS. 2018. The impact of flooding on aquatic ecosystem services. Biogeochemistry:1–23.

THIERE, G., J. STADMARK, AND S. E. B. WEISNER. 2011. Nitrogen retention versus methane emission: Environmental benefits and risks of large-scale wetland creation. Ecological Engineering 37:6–15.

TORTOSA, G., D. CORREA, A. J. SÁNCHEZ-RAYA, A. DELGADO, M. A. SÁNCHEZ-MONEDERO, AND E. J. BEDMAR. 2011. Effects of nitrate contamination and seasonal variation on the denitrification and greenhouse gas production in La Rocina Stream (Doñana National Park, SW Spain). Ecological Engineering 37:539–548.

VIDON, P., P. A. JACINTHE, X. LIU, K. FISHER, AND M. BAKER. 2014. Hydrobiogeochemical controls on riparian nutrient and greenhouse gas dynamics: 10 years post-restoration. Journal of the American Water Resources Association 50:639–652.

VYMAZAL, J. 2007. Removal of nutrients in various types of constructed wetlands. Science of the Total Environment 380:48–65.

WHALEN, S. C. 2005. Natural wetlands and the atmosphere. Environmental Engineering Science 22:73–94.

WOLLHEIM, W. M., S. BERNAL, D. A. BURNS, J. A. CZUBA, C. T. DRISCOLL, A. T. HANSEN, R. T. HENSLEY, J. D. HOSEN, S. INAMDAR, S. S. KAUSHAL, L. E. KOENIG, Y. H. LU, A. MARZADRI, P. A. RAYMOND, D. SCOTT, R. J. STEWART, P. G. VIDON, AND E. WOHL. 2018. River network saturation concept: factors influencing the balance of biogeochemical supply and demand of river networks. Biogeochemistry. https://doi.org/10.1007/s10533-018-0488-0

WOLLHEIM, W. M., T. K. HARMS, B. J. PETERSON, K. MORKESKI, C. S. HOPKINSON, R. J. STEWART, M. N. GOOSEFF, AND M. A. BRIGGS. 2014. Nitrate uptake dynamics of surface transient storage in stream channels and fluvial wetlands. Biogeochemistry 120:239–257.

WOLLHEIM, W. M., G. K. MULUKUTLA, C. COOK, AND R. O. CAREY. 2017. Aquatic nitrate retention at river network scales across flow conditions determined using nested in situ sensors. Water Resources Research 53:9740–9756.

WOLLHEIM, W. M., B. A. PELLERIN, C. J. VÖRÖSMARTY, AND C. S. HOPKINSON. 2005. N retention in urbanizing headwater catchments. Ecosystems 8:871–884.

WOLLHEIM, W. M., B. J. PETERSON, S. M. THOMAS, C. H. HOPKINSON, AND C. J. VÖRÖSMARTY. 2008a. Dynamics of N removal over annual time periods in a suburban river network. Journal of Geophysical Research: Biogeosciences 113:1–17.

WOLLHEIM, W. M., C. J. VÖRÖSMARTY, A. F. BOUWMAN, P. GREEN, J. HARRISON, E. LINDER, B. J. PETERSON, S. P. SEITZINGER, AND J. P. M. SYVITSKI. 2008b. Global N removal by freshwater aquatic systems using a spatially distributed, within-basin approach. Global Biogeochemical Cycles 22:1–14.

TABLES

Table 1. Study sites along each flow path with site specific characteristics, including site type (channelized or fluvial wetland dominated stream), distance downstream along a flow path, total upstream drainage area, total upstream fluvial wetland influence, and interstation fluvial wetland influence. Upstream fluvial wetland influence is the total percent of fluvial wetland land cover upstream. Interstation fluvial wetland influence is the percent fluvial wetland land cover between a given site and the site directly upstream. Sites along the higher nutrient flow path (HN-FP) are shaded while those along the lower nutrient flow path (LN-FP) are unshaded. Study sites for each flow path are in order of distance downstream where distance downstream is benchmarked to the first sample locations. Study sites with an * are tributary input sites that feed into a flow path at the specified distance.

Site	Site Type	Distance Downstream (km)	Upstream Drainage Area (km^2)	Upstream Fluvial Wetland Influence (%)	Interstation Fluvial Wetland Influence (%)
IS_101	Channelized	0.0	2.7	0.0	0.0
SB	Channelized	1.1	3.9	0.5	1.5
SB-Chest	Fluvial Wetland	2.3	4.8	2.0	8.8
MMB-OldCanal	Fluvial Wetland	3.5	10.0	8.4	14.3
MMB-38	Fluvial Wetland	4.0	11.6	7.2	0.2
MMB-Lowell	Fluvial Wetland	4.5	12.2	7.3	8.3
Mill-Adams*	Channelized	6.1	5.4	7.3	7.3
MMB	Fluvial Wetland	6.2	19.9	8.8	20.6
MMB-Federal	Fluvial Wetland	7.0	20.5	9.3	27.3
IS_135	Channelized	0.0	1.8	7.4	7.4
MB-Johnston	Channelized	0.9	2.4	6.5	3.6
MB-Salem	Channelized	2.3	5.7	7.9	8.9
MB-Foster	Fluvial Wetland	4.19	8.14	8.77	8.26
Ogunquit_Trib*	Channelized	6.54	2.59	13.87	13.87
FB-Lawrence	Fluvial Wetland	7.17	18.03	17.97	29.69
FB-BV	Fluvial Wetland	9.12	23.04	19.81	26.42

Table 2. Characterization of the 6 storms sampled in the study, 3 for each flow path. Storms for each flow path are ordered by date from earliest to latest. Labels A through F for each storm correspond to Figure 3. HN-FP and LN-FP are the higher nutrient and lower nutrient flow paths, respectively. SB represents the storm responses of channelized stream sites along the HN-FP. USGS South Middleton and FB-BV represent the storm responses for fluvial wetland dominated stream sites along the HN-FP and LN-FP, respectively. Statistics on total precipitation, storm volume, runoff depth, baseflow runoff condition, and peak stormflow runoff condition are included for each storm. Runoff coefficient is a dimensionless measure relating the amount of runoff to the amount of precipitation received. Grey shading used to visually separate different storms sampled.

Flow Path	Site	Storm Date	Total Precipitation (mm)	Storm Volume (m^3)	Storm Runoff Depth (mm)	Runoff Coefficient	Runoff at Baseflow (mm d^{-1})	Peak Storm Runoff (mm d^{-1})
HN-FP	SB	6/5/19 (A)	19.8	8,920	2.28	0.115	0.88	12.13
	USGS South Middleton	6/5/19 (A)	19.8	271,716	2.36	0.119	0.30	0.63
	SB	7/22/19 (B)	47.2	34,028	8.69	0.184	0.66	17.65
	USGS South Middleton	7/22/19 (B)	47.2	509,343	4.42	0.094	0.15	0.57
	SB	8/28/19 (C)	27.7	19,466	4.97	0.179	0.44	25.15
	USGS South Middleton	8/28/19 (C)	27.7	143,233	1.24	0.045	0.03	0.17
LN-FP	FB-BV	6/20/19 (D)	24.9	100,378	4.36	0.175	1.12	2.77
	FB-BV	8/7/19 (E)	51.3	25,865	1.12	0.022	0.04	0.41
	FB-BV	10/16/19 (F)	68.3	227,956	9.89	0.145	0.04	2.36

Table 3. Median methane (CH_4), carbon dioxide (CO_2), and nitrous oxide (N_2O) partial pressures in ppm for each study site. Median mass ratios of nitrogen gas and argon (N_2:Ar) were also reported for each study site. N_2:Ar ratios were used instead of concentrations due to superior accuracy by the instrument at measuring the ratios of masses versus individual masses. Partial pressure of CH_4, CO_2, N_2O at equilibrium with the atmosphere are roughly 1.975, 407.4, and 0.331 ppm, respectively, but vary daily by Henry's Law (based on water temperature and atmospheric pressure). N_2:Ar ratios at saturation in this study are 26.9 on average, but also vary daily depending on temperature and atmospheric pressure. HN-FP and LN-FP are the higher nutrient and lower nutrient flow paths, respectively. Study sites for each flow path are in order of distance downstream where distance downstream is benchmarked to the first sample locations. Sample size for sites along the HN-FP and LN-FP is 11 and 10, respectively. Fluvial wetland dominated stream sites are shaded and channelized stream sites are unshaded. The 1st and 3rd quartiles (25th and 75th percentiles) in parentheses.

Flow Path	Site	*p*CH_4 (ppm)	*p*CO_2 (ppm)	*p*N_2O (ppm)	N_2:Ar
HN-FP	IS_101	93.9 (73.7, 142.2)	10388 (6880, 13337)	1.00 (0.89, 1.34)	27.1 (26.7, 27.1)
	SB	24.2 (22.3, 46.9)	5994 (4252, 7118)	0.83 (0.55, 1.15)	26.9 (26.5, 27.0)
	SB-Chest	26.5 (25.8, 59.8)	4574 (3912, 5495)	0.75 (0.65, 0.86)	27.1 (26.5, 27.2)
	MMB-OldCanal	116.1 (71.1, 173.9)	13430 (11998, 15629)	0.25 (0.11, 0.31)	27.3 (26.8, 27.4)
	MMB-38	117.6 (74.3, 223.5)	13352 (11425, 14350)	0.21 (0.13, 0.27)	27.2 (26.9, 27.3)
	MMB-Lowell	98.1 (64.8, 163.3)	13828 (11608, 15308)	0.28 (0.13, 0.33)	27.1 (26.7, 27.2)
	MMB	33.8 (23.3, 105.4)	13781 (11147, 15025)	0.13 (0.11, 0.25)	27.4 (27.0, 27.7)
	MMB-Federal	39.2 (19.7, 52.2)	12172 (10145, 13063)	0.19 (0.14, 0.22)	27.5 (27.1, 27.8)
LN-FP	IS_135	101.0 (70.4, 189.0)	8234 (7744, 8806)	0.48 (0.36, 0.59)	26.7 (26.5, 27.0)
	MB-Johnston	14.3 (9.8, 23.3)	2507 (2188, 3010)	0.37 (0.31, 0.49)	26.7 (26.4, 27.0)
	MB-Salem	8.7 (7.1, 10.3)	3191 (2969, 3402)	0.47 (0.34, 0.57)	26.8 (26.5, 27.0)
	MB-Foster	103.8 (32.4, 195.8)	12107 (10624, 12815)	0.34 (0.27, 0.37)	27.0 (26.7, 27.5)
	FB-Lawrence	42.7 (37.7, 94.8)	9249 (7388, 10951)	0.41 (0.32, 0.93)	27.1 (26.9, 27.4)
	FB-BV	28.1 (19.9, 33.0)	8141 (7746, 8738)	0.41 (0.33, 0.51)	27.0 (26.9, 27.4)

Table 4. Range in air-water gas transfer velocities *(k)* for methane (CH_4), carbon dioxide (CO_2), and nitrous oxide (N_2O). Median gas transfer velocities in parentheses. Gas transfer velocities vary between channelized and fluvial wetland dominated stream study sites due to differences in site characteristics (width, depth), hydrology (streamflow velocity), and water temperature.

Site Type	k_{CH4} (m d^{-1})	k_{CO2} (m d^{-1})	k_{N2O} (m d^{-1})
Channelized	0.36 – 4.89 (1.16)	0.58 – 6.14 (1.25)	0.36 – 4.89 (0.85)
Fluvial Wetland	0.01 – 1.66 (0.15)	0.01 – 1.73 (0.16)	0.01 – 1.39 (0.11)

Table 5. Median estimates of areal evasion (mg m^{-2} d^{-1}) and total daily evasion accounting for upstream fluvial wetland extent (kg d^{-1} or g d^{-1}) for methane (CH_4), carbon dioxide (CO_2), and nitrous oxide (N_2O) from fluvial wetlands dominated and channelized streams along each flow path. HN-FP and LN-FP are the higher nutrient and lower nutrient flow paths, respectively. Total area of fluvial wetlands and streams along each flow path are included.

Site Type	Flow Path	Area (km^2)	CH_4 Evasion (mg m^{-2} d^{-1})	CO_2 Evasion (mg m^{-2} d^{-1})	N_2O Evasion (mg m^{-2} d^{-1})	Total CH_4 Evasion (kg d^{-1})	Total CO_2 Evasion (kg d^{-1})	Total N_2O Evasion (g d^{-1})
Fluvial Wetland	HN-FP	1.91	6.76	2997	-0.01	12.92	5726	-9.8
	LN-FP	4.56	12.15	6809	0.09	55.43	31074	396.8
Channelized	HN-FP	0.05	41.77	15213	0.90	2.26	822	48.7
	LN-FP	0.10	20.08	12490	0.44	1.96	1222	43.3

Table 6. Mean methane (CH_4), carbon dioxide (CO_2), and nitrous oxide (N_2O) partial pressures in ppm for stream and fluvial wetland sites along during baseflow and stormflow conditions for the a) HN-FP and b) LN-FP. HN-FP and LN-FP are the higher nutrient and lower nutrient flow paths, respectively. Mean mass ratios of nitrogen gas and argon (N_2:Ar) were also reported for stream and fluvial wetland sites during baseflow and stormflow conditions. N_2:Ar ratios were used instead of concentrations due to superior accuracy by the instrument at measuring the ratios of masses versus individual masses. Partial pressure of CH_4, CO_2, N_2O at equilibrium with the atmosphere are roughly 1.975, 407.4, and 0.331 ppm, respectively, but vary daily by Henry's Law (based on water temperature and atmospheric pressure). N_2:Ar ratios at saturation in this study are 26.9 on average, but also vary daily depending on temperature and atmospheric pressure. Sample size for stream sites along the HN-FP and LN-FP is 2 and 3, respectively. Sample size for fluvial wetland sites along the HN-FP and LN-FP is 5 and 3, respectively. A total of 6 storms were sampled, 3 per flow path (labels for storms A through F correlate with Figure 3 and Table 2). Standard deviation in parentheses.

a) HN-FP

Storm Date	Site Type	Baseflow pCH_4	Stormflow pCH_4	Baseflow pCO_2	Stormflow pCO_2	Baseflow pN_2O	Stormflow pN_2O	Baseflow N_2:Ar	Stormflow N_2:Ar
6/5/19 (A)	Channelized	24.0 (NA)	47.4 (30.8)	6315 (NA)	11447 (5217)	1.35 (NA)	1.26 (0.66)	26.9 (NA)	27.0 (0.27)
	Fluvial Wetland	40.0 (24.3)	67.4 9 (45.9)	12549 (2396)	14696 (4254)	0.26 (0.06)	0.30 (0.13)	27.3 (0.24)	27.4 (0.39)
7/22/19 (B)	Channelized	17.2 (7.6)	81.3 (45.6)	4881 (1604)	7759 (3095)	0.75 (0.17)	1.35 (0.82)	27.0 (0.08)	27.0 (0.11)
	Fluvial Wetland	128.1 (173)	146.8 (97.5)	16248 (7809)	14099 (1565)	0.21 (0.13)	0.13 (0.06)	27.2 (0.25)	27.6 (0.39)
8/28/19 (C)	Channelized	60.5 (51.3)	88.9 (84.2)	19735 (21046)	4827 (3146)	0.66 (0.29)	0.70 (0.31)	27.0 (0.10)	26.8 (0.33)
	Fluvial Wetland	323.1 (279)	138.6 (69.3)	16979 (1523)	13156 (1224)	0.11 (0.03)	0.15 (0.07)	27.4 (0.09)	27.1 (0.42)

b) LN-FP

Storm Date	Site Type	Baseflow pCH_4	Stormflow pCH_4	Baseflow pCO_2	Stormflow pCO_2	Baseflow pN_2O	Stormflow pN_2O	Baseflow N_2:Ar	Stormflow N_2:Ar
6/20/19 (D)	Channelized	46.4 (50.7)	31.4 (34.3)	4502 (2744)	6913 (4168)	0.42 (0.07)	0.52 (0.05)	27.0 (0.00)	27.0 (0.00)
	Fluvial Wetland	96.2 (97.3)	69.9 (62.0)	8704 (2822)	9181 (2785)	0.41 (0.04)	0.32 (0.01)	27.0 (0.01)	27.0 (0.01)
8/7/19 (E)	Channelized	19.8 (15.8)	122.2 (138)	3464 (1605)	5190 (4405)	0.23 (0.10)	0.53 (0.37)	26.7 (0.10)	27.0 (0.20)
	Fluvial Wetland	216.0 (338)	133.9 (161)	14012 (5557)	10869 (1842)	0.33 (0.07)	0.51 (0.30)	27.4 (0. 09)	27.9 (0.48)
10/16/19 (F)	Channelized	66.2 (94.1)	30.9 (34.2)	5742 (3372)	5021 (3105)	0.44 (0.41)	0.79 (0.40)	26.5 (0.15)	26.5 (0.02)
	Fluvial Wetland	90.6 (77.9)	22.1 (7.3)	11821 (2699)	7775 (583)	0.23 (0.09)	0.91 (0.38)	27.0 (0.18)	26.5 (0.01)

FIGURES

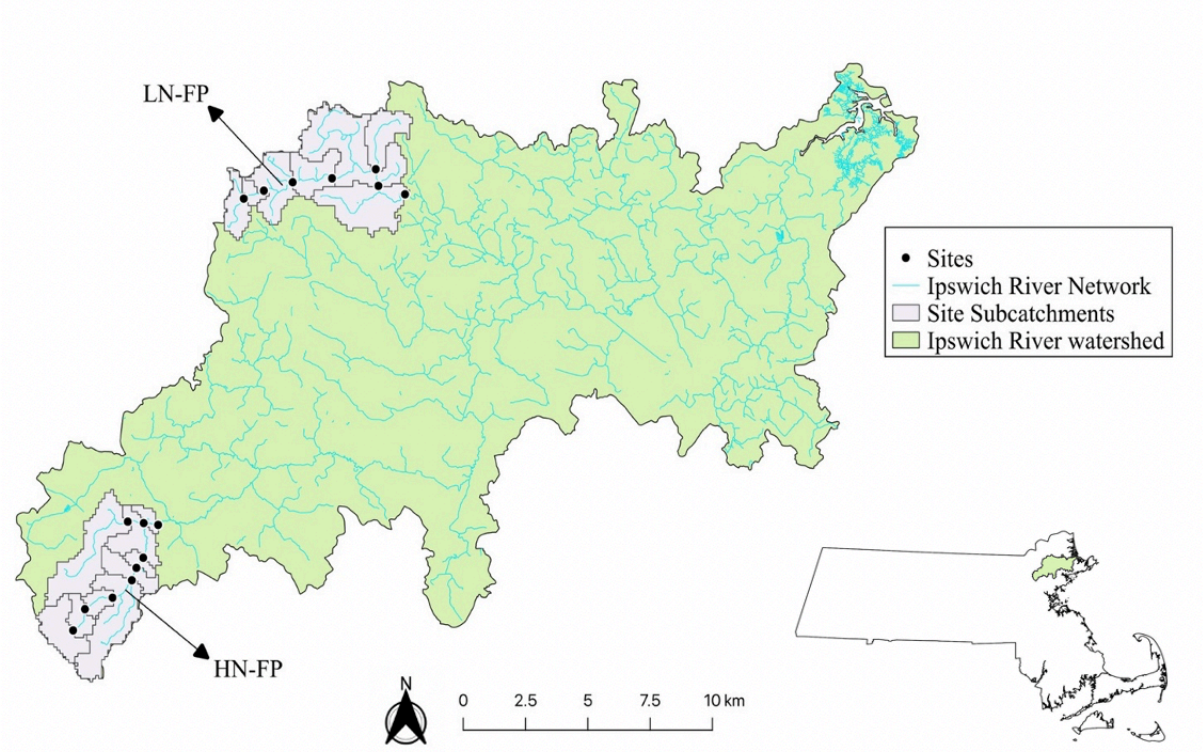

Figure 1. Map of study sites (black dots) along two fluvial wetland dominated surface water flow paths in the Ipswich River watershed (green) in northeastern Massachusetts. HN-FP and LN-FP are the higher nutrient and lower nutrient flow paths, respectively. Interstation drainage areas, or the catchment area between study sites, are represented in light grey with dark grey borders.

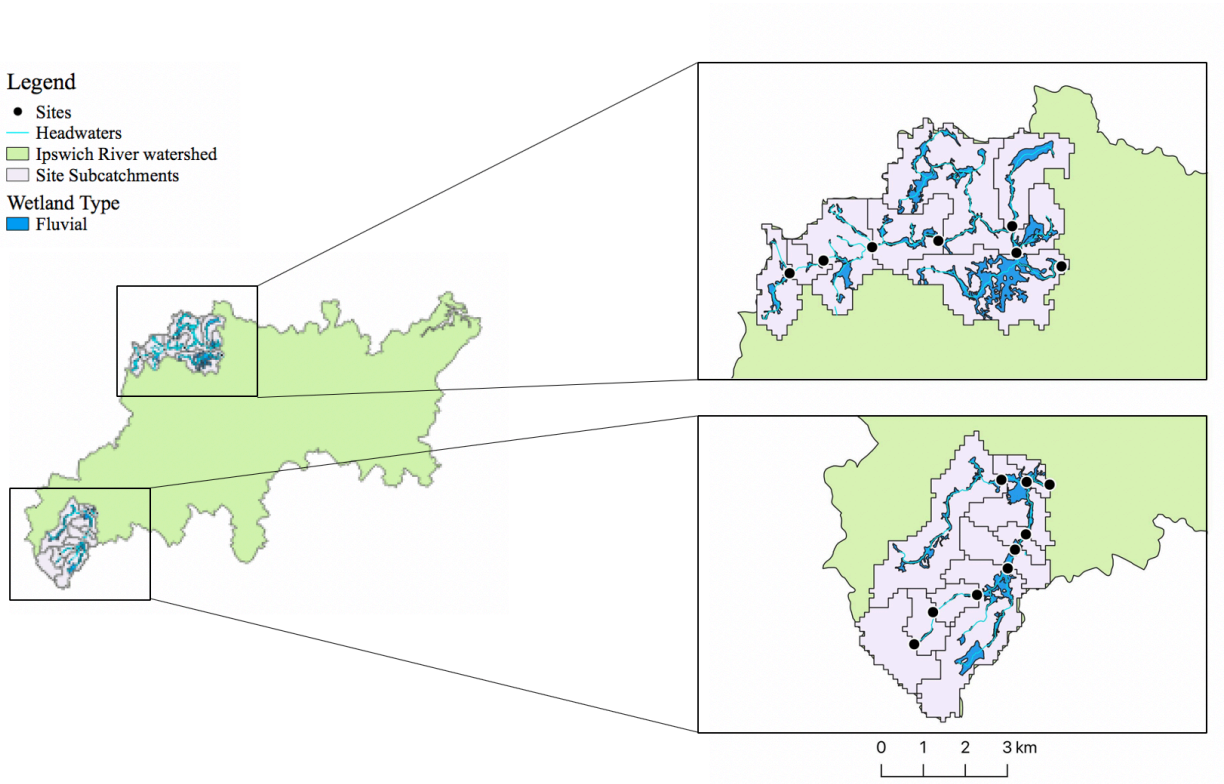

Figure 2. Fluvial wetland extent (blue polygons) along two surface water flow paths in the Ipswich River watershed, MA. HN-FP and LN-FP are the higher nutrient and lower nutrient flow paths, respectively. The HN-FP is found in the upper portion (bottom) of the watershed while the LN-FP is found in the lower portion (top). A closer look at the fluvial wetland extent along the LN-FP and HN-FP are presented at the top right and bottom right, respectively. Interstation drainage areas, or the catchment area between study sites, are represented in light grey with dark grey borders.

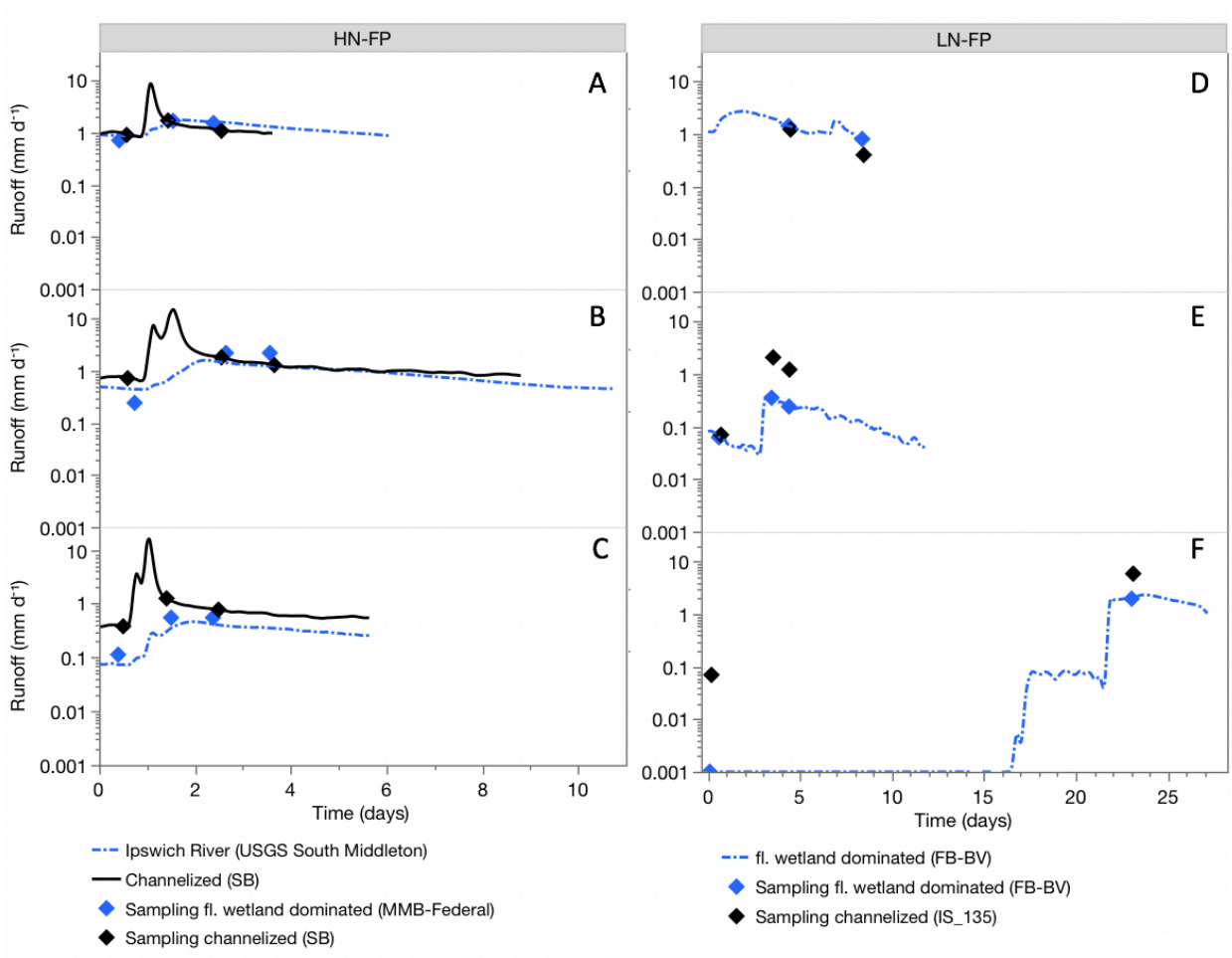

Figure 3. Runoff rate over time for the 6 storms (3 per flow path) sampled and analyzed in this study. HN-FP (left) and LN-FP (right) are the higher nutrient and lower nutrient flow paths, respectively. Storm responses on the left (A, B, C) represent the storms where study sites along the HN-FP were sampled, while storm responses on the right (D, E, F) represent the storms where study sites along the LN-FP were sampled. Storms top to bottom are in order of earliest date to latest date (A: 6/5/19, B: 7/22/19, C: 8/28/19, D: 6/20/19, E: 8/7/19, F: 10/16/19). Black lines represent the storm responses at Sawmill Brook (SB), which was used to characterize the responses at channelized streams along the HN-FP. Blue dashed lines in the HN-FP represent the storm responses at the USGS gauge at South Middleton along the Ipswich River (just downstream of the last fluvial wetland dominated site, MMB-Federal, in the HN-FP); the storm response at fluvial wetland dominated stream sites along the HN-FP were expected to be somewhere between SB and USGS South Middleton. Blue dashed lines in the LN-FP represent the storm response at FB-BV, the furthest downstream fluvial wetland dominated study site along the LN-FP. There was no continuous runoff data available to characterize the storm response in channelized streams of the LN-FP. Black and blue diamonds are estimated runoff at the representative channelized stream study sites (SB for HN-FP and IS_135 for LN-FP) and fluvial wetland dominated stream study sites (MMB-Federal for HN-FP and FB-BV for LN-FP), respectively, at the time of sampling.

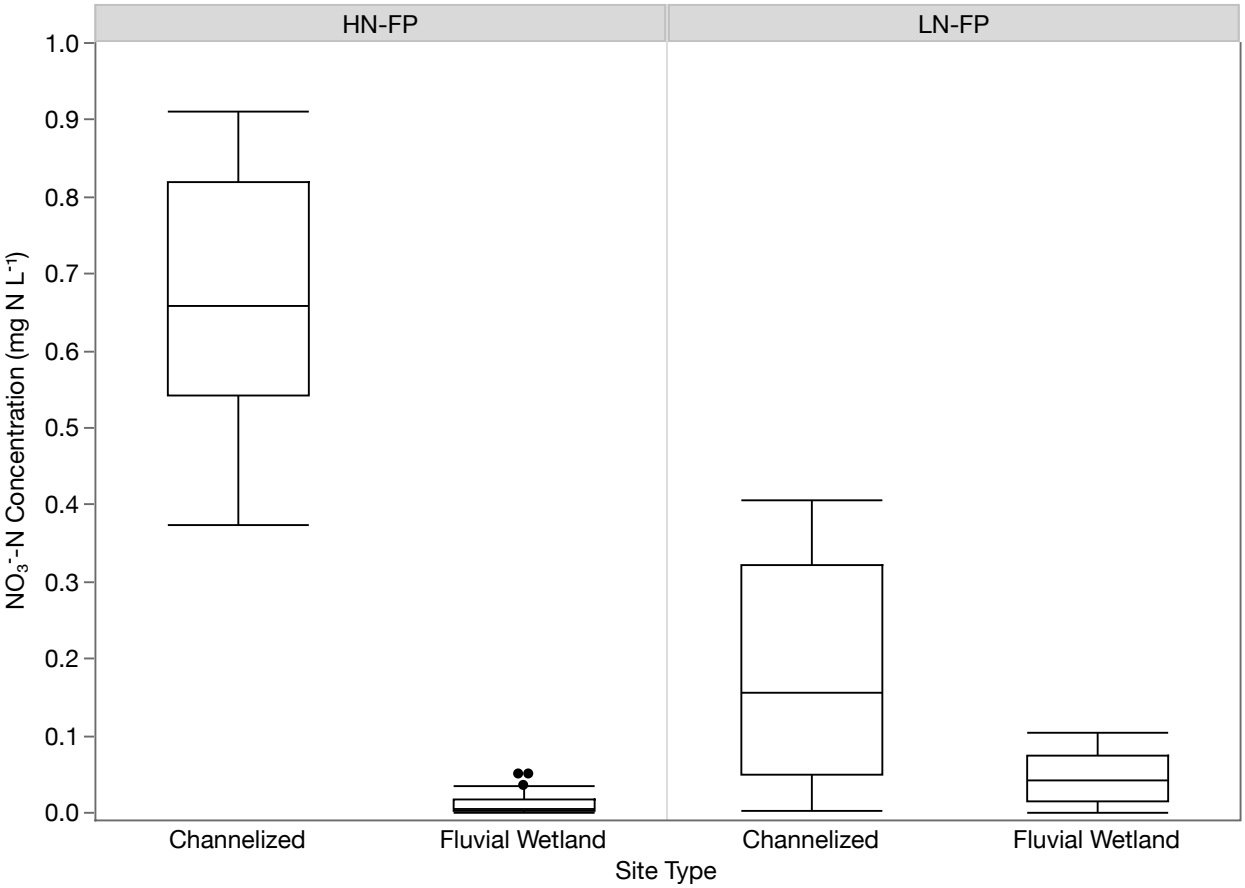

Figure 4. Box plots of nitrate (NO_3^--N) concentrations measured throughout the study period at study sites along two fluvial wetland dominated surface water flow paths in the Ipswich River watershed, MA. Study sites were separated by site type (channelized stream or fluvial wetland dominated stream) for each flow path. HN-FP (left) and LN-FP (right) are the higher nutrient and lower nutrient flow paths, respectively. Box plots display the minimum concentration, 25th percentile, 50th percentile (median), 75th percentile, and the maximum concentration (outliers excluded). Black dots represent outliers on a given sampling day. SB-Chest, a fluvial wetland dominated stream in the beginning stages, was excluded for the HN-FP.

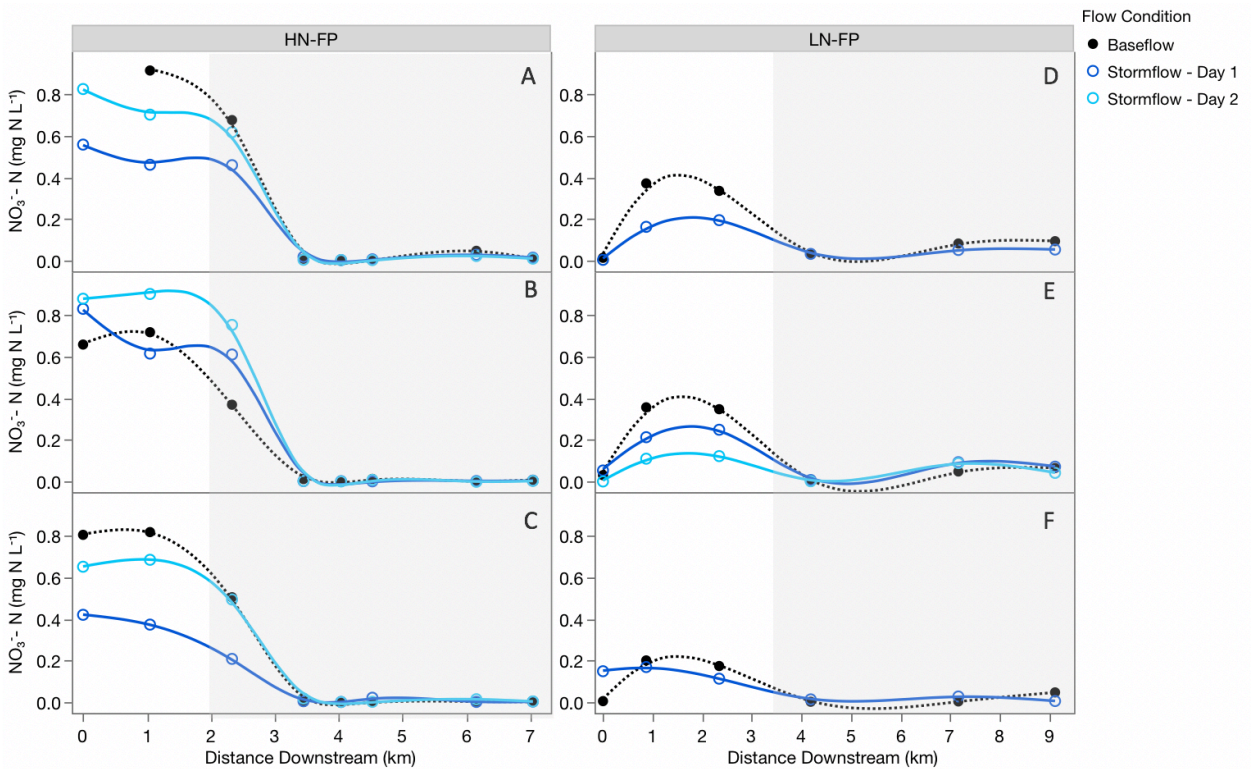

Figure 5. Nitrate (NO_3^--N) concentrations at study sites along two surface water flow paths at baseflow and stormflows following 6 storms (3 per flow path). HN-FP (left) and LN-FP (right) are the higher nutrient and lower nutrient flow paths, respectively. Storms on the left (A, B, C) represent the storms where study sites along the HN-FP were sampled, while storms on the right (D, E, F) represent the storms where study sites along the LN-FP were sampled. Storms top to bottom are in order of earliest date to latest date (A: 6/5/19, B: 7/22/19, C: 8/28/19, D: 6/20/19, E: 8/7/19, F: 10/16/19). Dots (solid black or hollow blue) are measured NO_3^--N concentrations at study sites along the flow paths. Black dots and dashed lines represent baseflow concentrations, usually prior to a storm. Stormflow – Day 1 (dark blue dots and solid lines) and Stormflow – Day 2 (light blue dots and solid lines) represent concentrations measured typically 24 and 48 hours after a storm, respectively. Grey shaded regions indicate the fluvial wetland dominated portions of the flow paths. Non-shaded regions (between 0 and ~2-3.5 km) indicate the channelized portion of the flow paths.

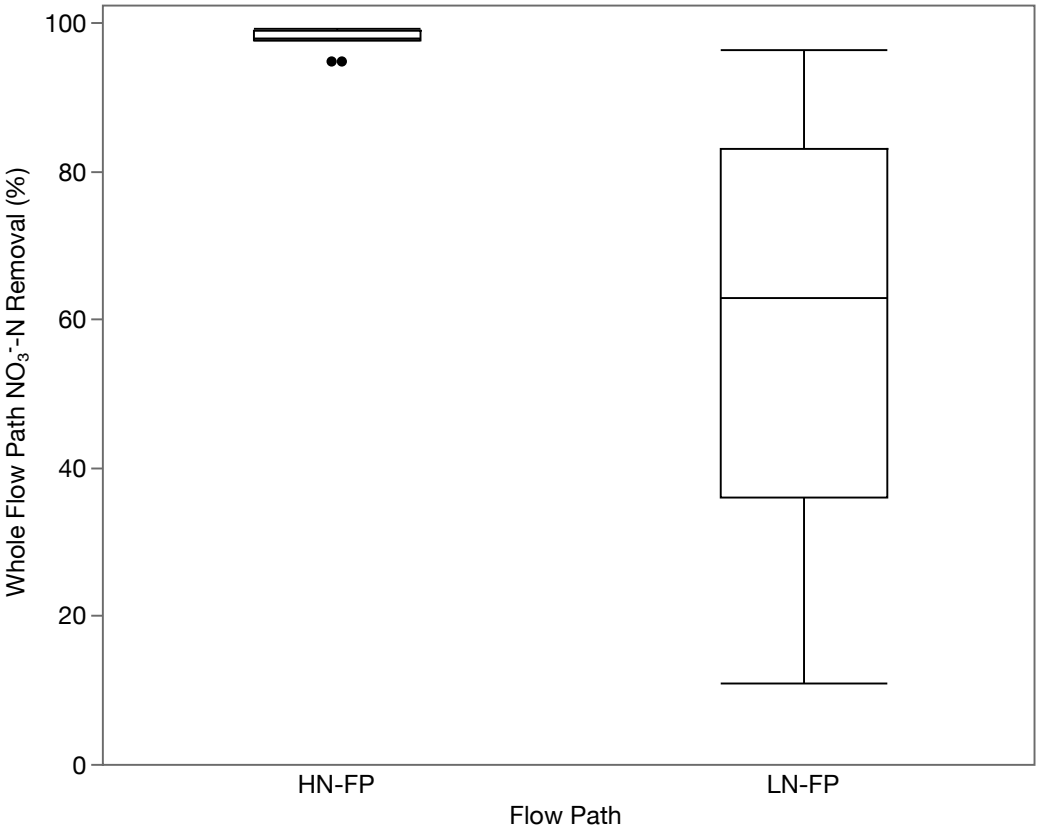

Figure 6. Box plots of percent nitrate (NO_3^--N) removal for each sampling day by two fluvial wetland dominated surface water flow paths in the Ipswich River watershed, MA. HN-FP and LN-FP are the higher nutrient and lower nutrient flow paths, respectively. Whole flow path NO_3^--N removal were determined from NO_3:Cl ratios from representative upstream channels (SB for the HN-FP and MB-Johnston) and downstream fluvial wetland dominated streams (MMB-Federal for HN-FP and FB-BV for LN-FP, see Methods), assuming NO_3:Cl ratios from at the representative upstream channel sites are characteristic of all runoff in the catchment. Box plots display the minimum concentration, 25th percentile, 50th percentile (median), 75th percentile, and the maximum concentration (outliers excluded). Black dots represent outliers on a given sampling day.

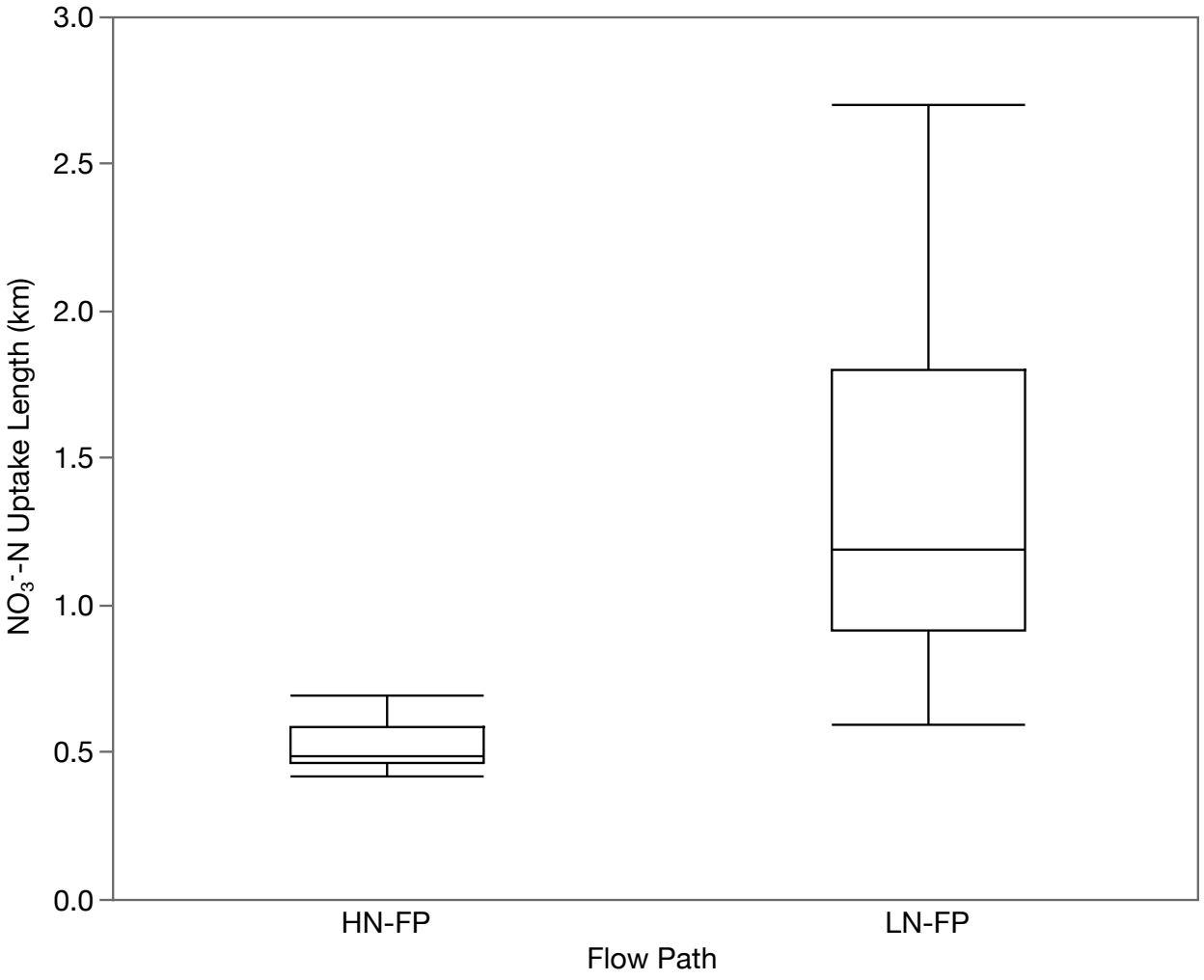

Figure 7. Box plots of nitrate (NO_3^--N) uptake length for each sampling day by two fluvial wetland dominated surface water flow paths in the Ipswich River watershed, MA. HN-FP and LN-FP are the higher nutrient and lower nutrient flow paths, respectively. Uptake lengths were determined from NO_3:Cl ratios along the transitional zone (where uptake is greatest) as the flow paths transform from channelized to fluvial wetland dominated streams (see Methods). Box plots display the minimum concentration, 25th percentile, 50th percentile (median), 75th percentile, and the maximum concentration.

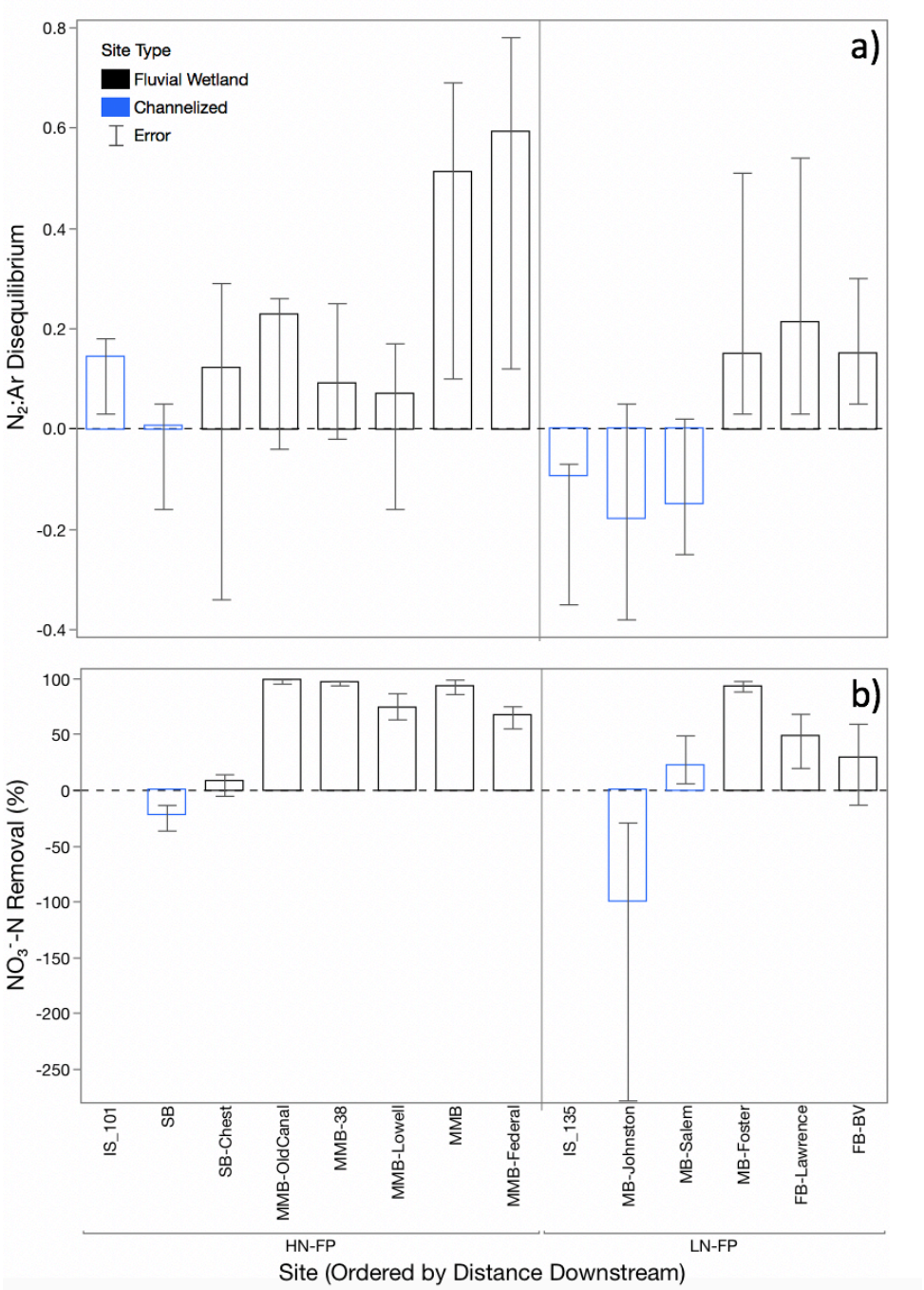

Figure 8. Median a) N_2:Ar disequilibrium for each study site and b) percent NO_3^--N removal for each stream reach between the study site directly upstream and the named study site during the 6-month study period. N_2:Ar ratios at saturation in this study are 26.9 on average, but also vary daily depending on temperature and atmospheric pressure. Error bars represent the 1st and 3rd quartiles (25th and 75th percentiles) of the data for each study site. Fluvial wetland dominated stream sites are outlined in black and channelized stream sites are outlined in blue. Study sites are ordered for each flow path by their distance downstream with reference to the first upstream study site. HN-FP (left) and LN-FP (right) are the higher nutrient and lower nutrient flow paths, respectively.

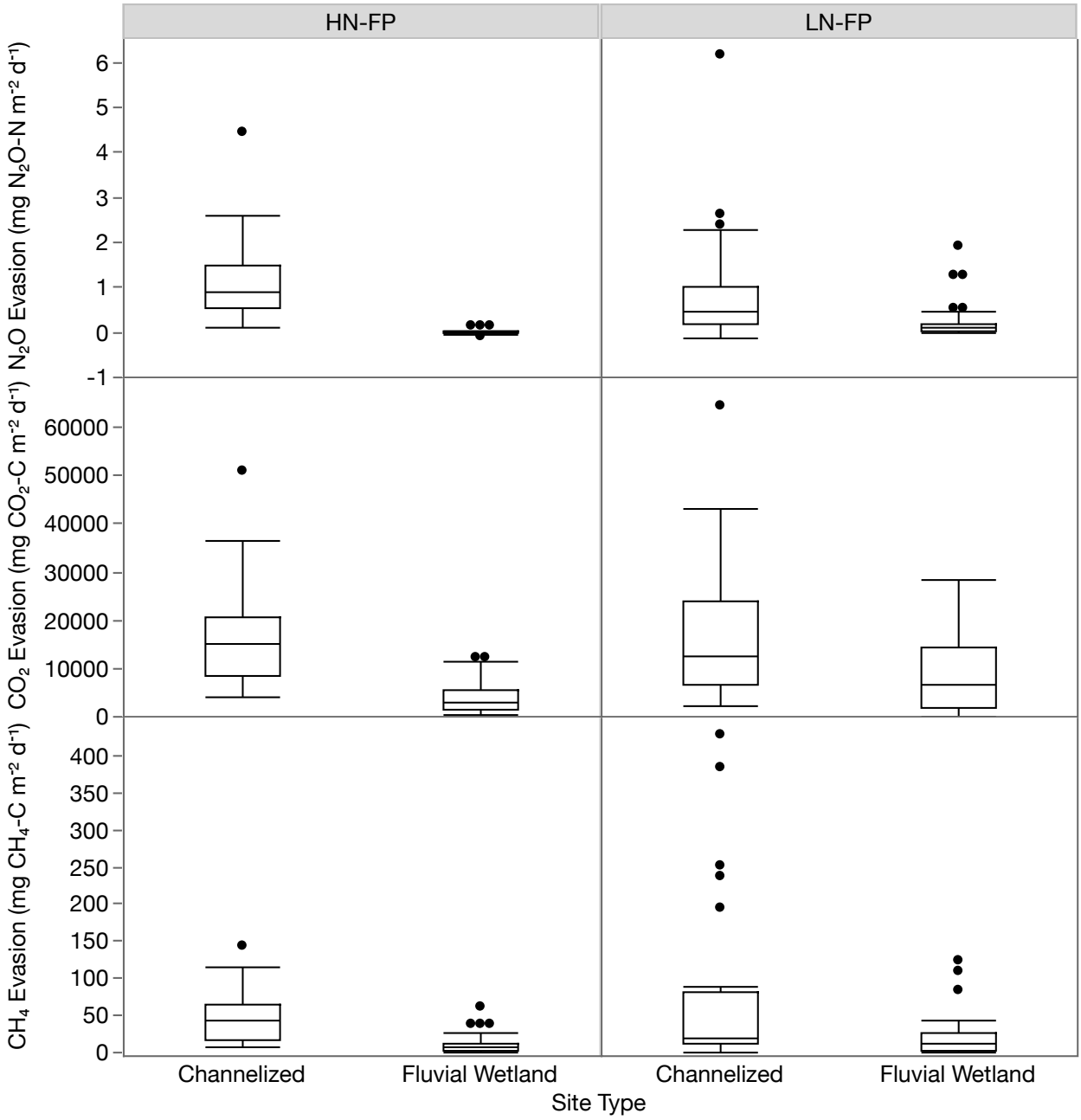

Figure 9. Box plots of greenhouse gas fluxes for each sampling day for channelized stream and fluvial wetland dominated stream study sites along two surface water flow paths in the Ipswich River watershed, MA. HN-FP (left) and LN-FP (right) are the higher nutrient and lower nutrient flow paths, respectively. Methane (CH_4) evasion rates are depicted in the bottom panel, carbon dioxide (CO_2) evasion rates in the middle panel, and nitrous oxide (N_2O) evasion rates in the top panel for each flow path. Box plots display the minimum concentration, 25th percentile, 50th percentile (median), 75th percentile, and the maximum concentration (outliers excluded). Black dots represent outliers on a given sampling day.

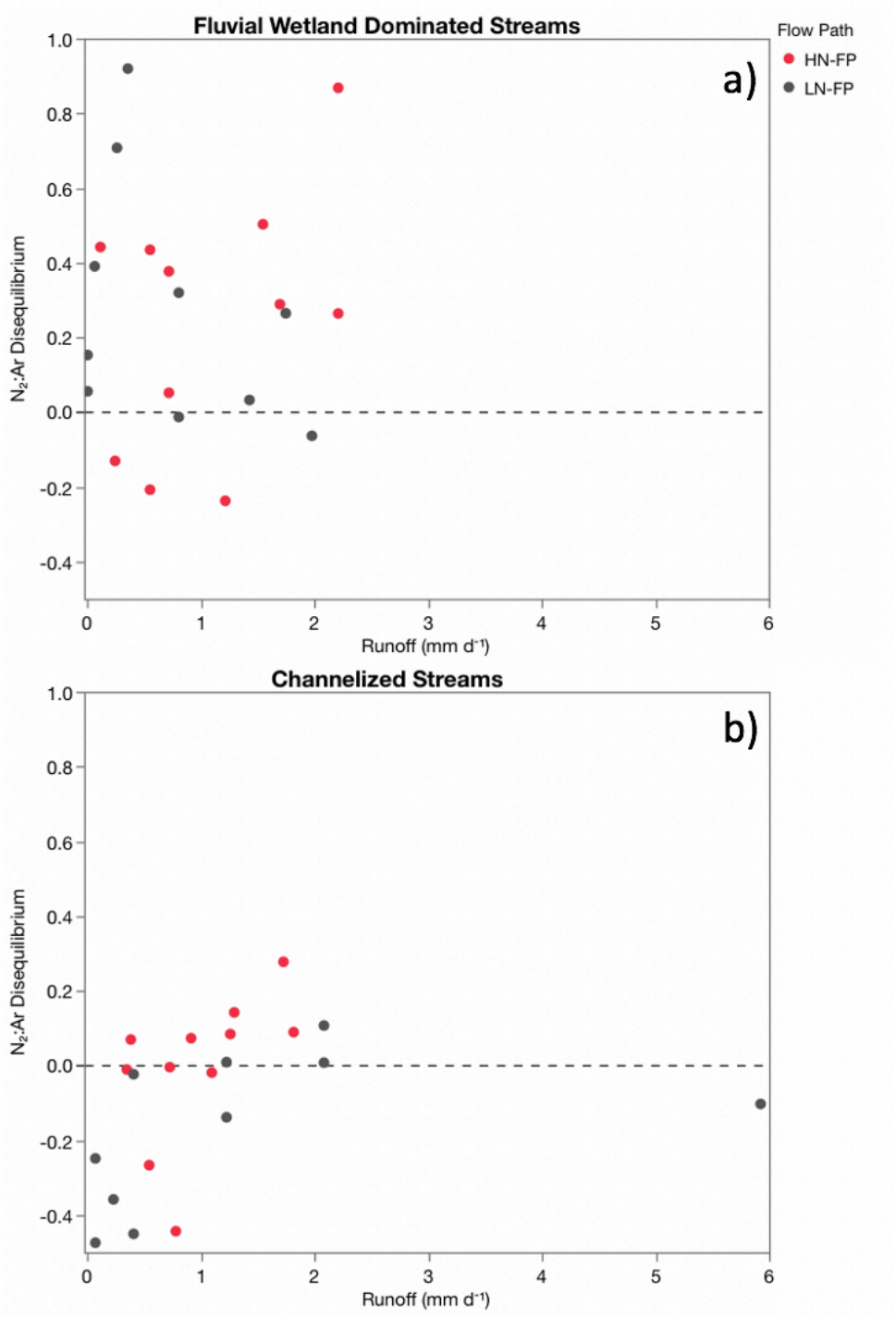

Figure 10. Relationships between mean N_2:Ar disequilibrium and estimated runoff rate for a) fluvial wetland dominated streams and b) channelized streams for each flow path across the 6-month study period. Each dot represents a sampling day. Red dots represent specific study sites along the HN-FP and grey dots represent those along the LN-FP. HN-FP and LN-FP are the higher nutrient and lower nutrient flow paths, respectively. Horizontal reference lines (dotted line) at N_2:Ar disequilibrium values of 0 for top and bottom plots are included.

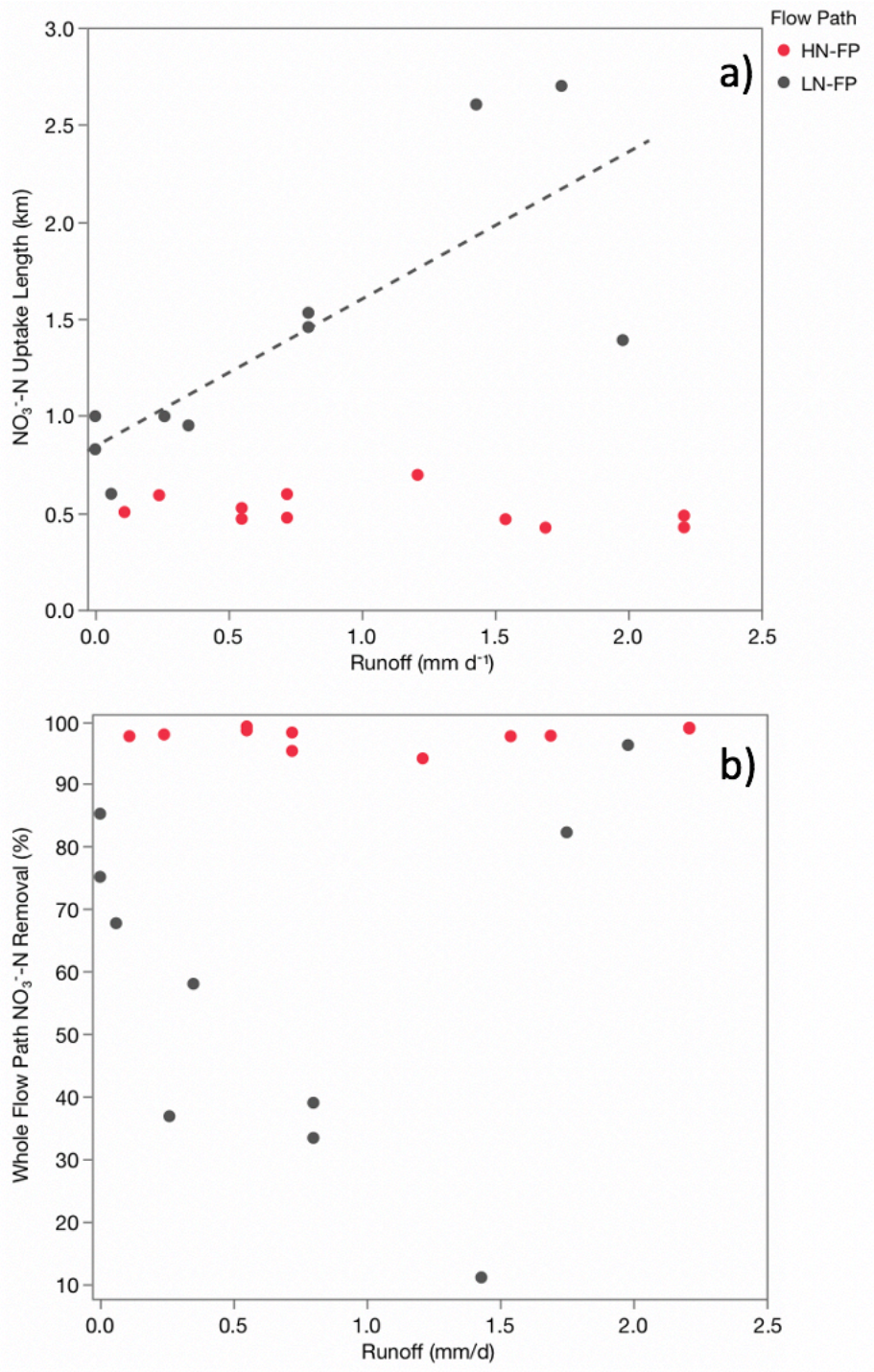

Figure 11. Relationships between a) NO_3^--N uptake length and b) NO_3^--N removal and runoff rate for each flow path across the 6-month study period. Each dot represents a sampling day. Red dots represent specific study sites along the HN-FP and grey dots represent those along the LN-FP. HN-FP and LN-FP are the higher nutrient and lower nutrient flow paths, respectively. Grey dashed line represents a significant bivariate relationship found between NO_3^--N uptake length and runoff rate for the LN-FP ($p = 0.0072$; $R^2 = 0.62$).

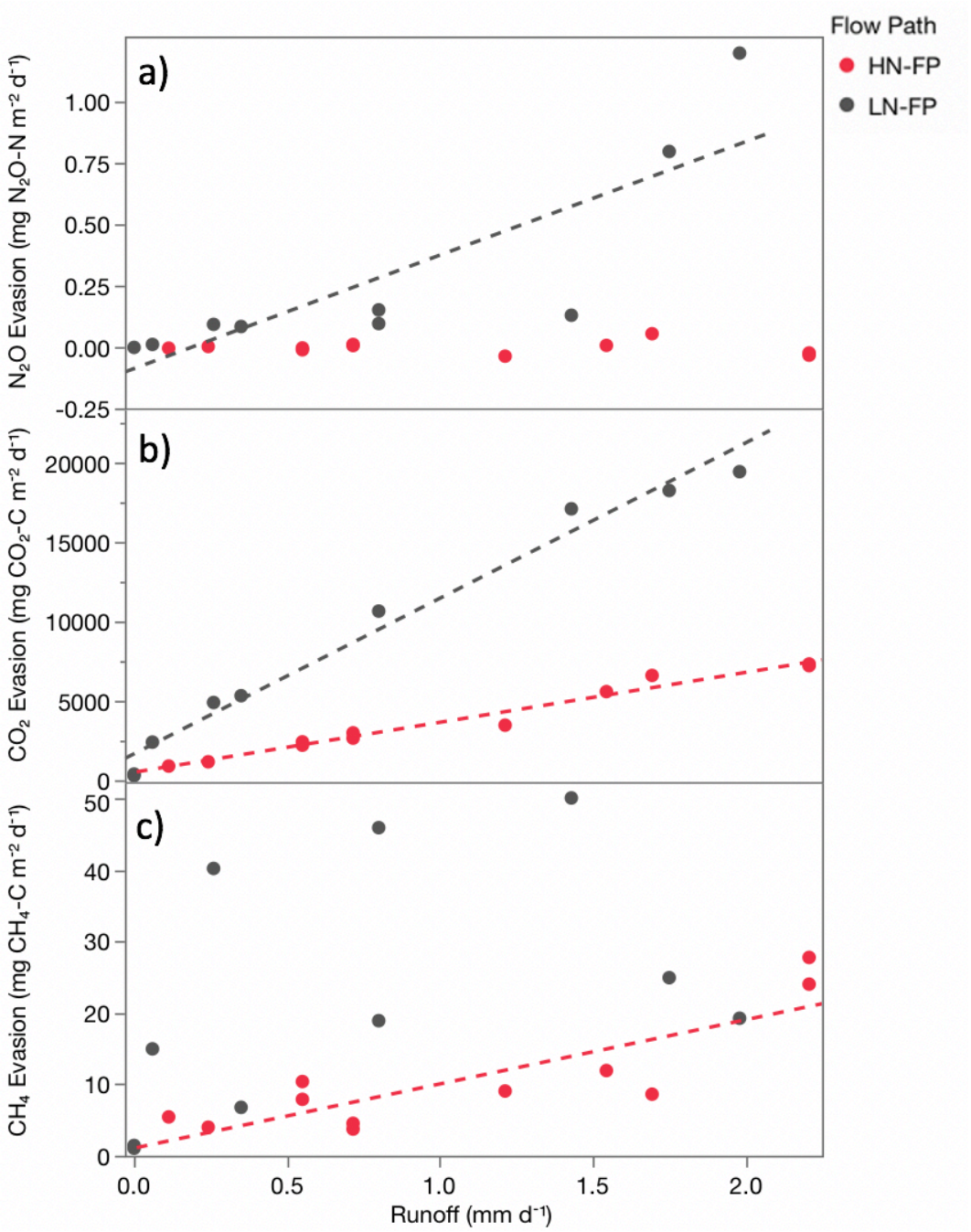

Figure 12. Relationships between mean nitrous oxide (N_2O) evasion, b) carbon dioxide (CO_2) evasion, and c) methane (CH_4) evasion and runoff rate for fluvial wetland dominated stream study sites along each flow path. Each dot represents the mean evasion for a sampling day. Red dots represent specific study sites along the HN-FP and grey dots represent those along the LN-FP. HN-FP and LN-FP are the higher nutrient and lower nutrient flow paths, respectively. Grey dashed lines represent significant bivariate relationships found between variables for the LN-FP (N_2O: $p = 0.0038$, $R^2 = 0.67$; CO_2: $p \leq .0001$, $R^2 = 0.98$). Red dashed lines represent significant bivariate relationships found between variables for the HN-FP (CO_2: $p \leq .0001$, $R^2 = 0.97$; CH_4: $p = 0.0012$, $R^2 = 0.70$).

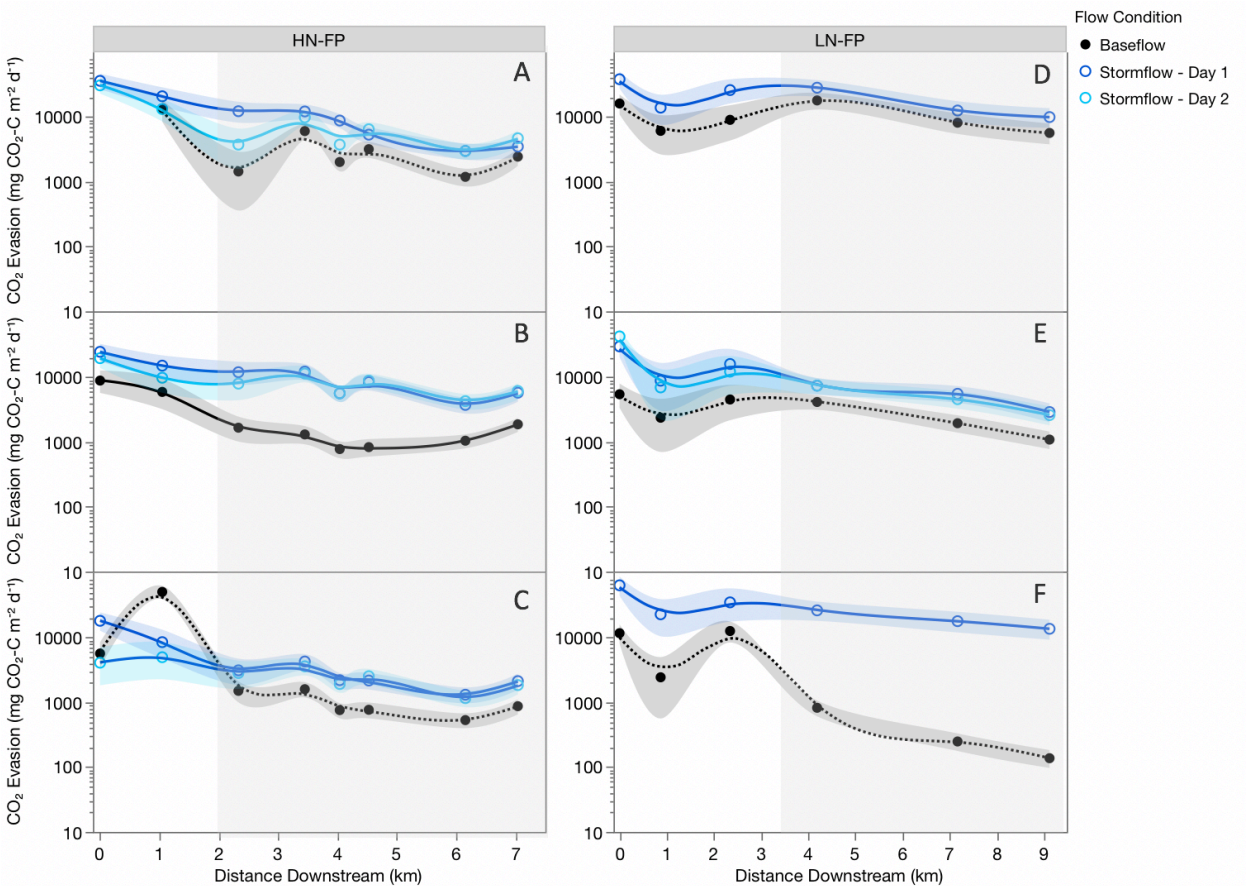

Figure 13. Carbon dioxide (CO_2) evasion rates along two surface water flow paths in the Ipswich River watershed before and after 6 storms (3 per flow path). HN-FP (left) and LN-FP (right) are the higher nutrient and lower nutrient flow paths, respectively. Storms on the left (A, B, C) represent the storms where study sites along the HN-FP were sampled, while storms on the right (D, E, F) represent the storms where study sites along the LN-FP were sampled. Storms top to bottom are in order of earliest date to latest date (A: 6/5/19, B: 7/22/19, C: 8/28/19, D: 6/20/19, E: 8/7/19, F: 10/16/19). Dots (solid black or hollow blue) are measured CO_2 evasion at study sites along the flow paths. Black dots and dashed lines represent baseflow evasion, usually prior to a storm. Stormflow – Day 1 (dark blue dots and solid lines) and Stormflow – Day 2 (light blue dots and solid lines) represent evasion measured typically 24 and 48 hours after a storm, respectively. Shaded regions around data points/lines represent estimated error associated with CO_2 evasion for each sampling day. Grey shaded regions indicate the fluvial wetland dominated portions of the flow paths. Non-shaded regions (between 0 and ~2-3.5 km) indicate the channelized portion of the flow paths.

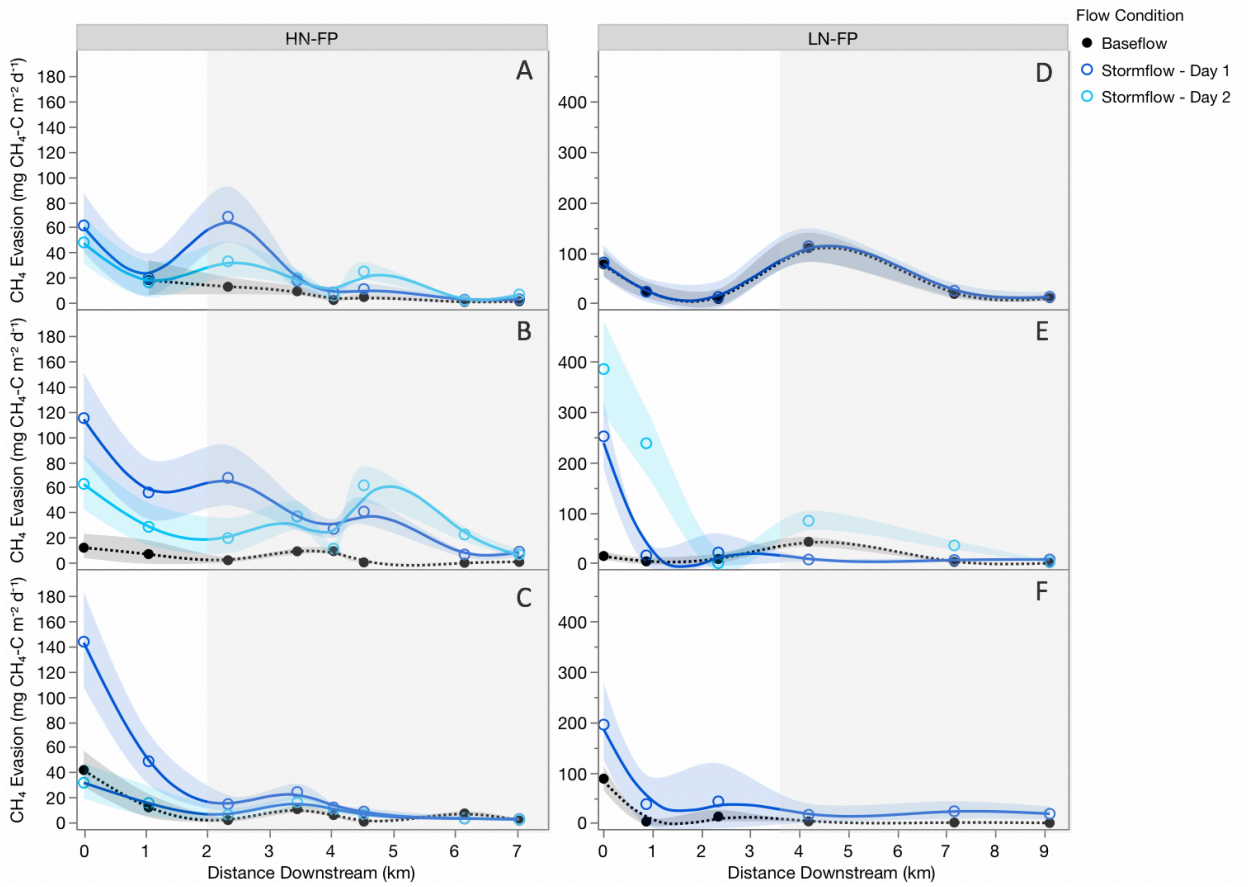

Figure 14. Methane (CH_4) evasion rates along two surface water flow paths in the Ipswich River watershed before and after 6 storms (3 per flow path). HN-FP (left) and LN-FP (right) are the higher nutrient and lower nutrient flow paths, respectively. Storms on the left (A, B, C) represent the storms where study sites along the HN-FP were sampled, while storms on the right (D, E, F) represent the storms where study sites along the LN-FP were sampled. Storms top to bottom are in order of earliest date to latest date (A: 6/5/19, B: 7/22/19, C: 8/28/19, D: 6/20/19, E: 8/7/19, F: 10/16/19). Dots (solid black or hollow blue) are measured CH_4 evasion at study sites along the flow paths. Black dots and dashed lines represent baseflow evasion, usually prior to a storm. Stormflow – Day 1 (dark blue dots and solid lines) and Stormflow – Day 2 (light blue dots and solid lines) represent evasion measured typically 24 and 48 hours after a storm, respectively. Shaded regions around data points/lines represent estimated error associated with CH_4 evasion for each sampling day. Grey shaded regions indicate the fluvial wetland dominated portions of the flow paths. Non-shaded regions (between 0 and ~2-3.5 km) indicate the channelized portion of the flow paths.

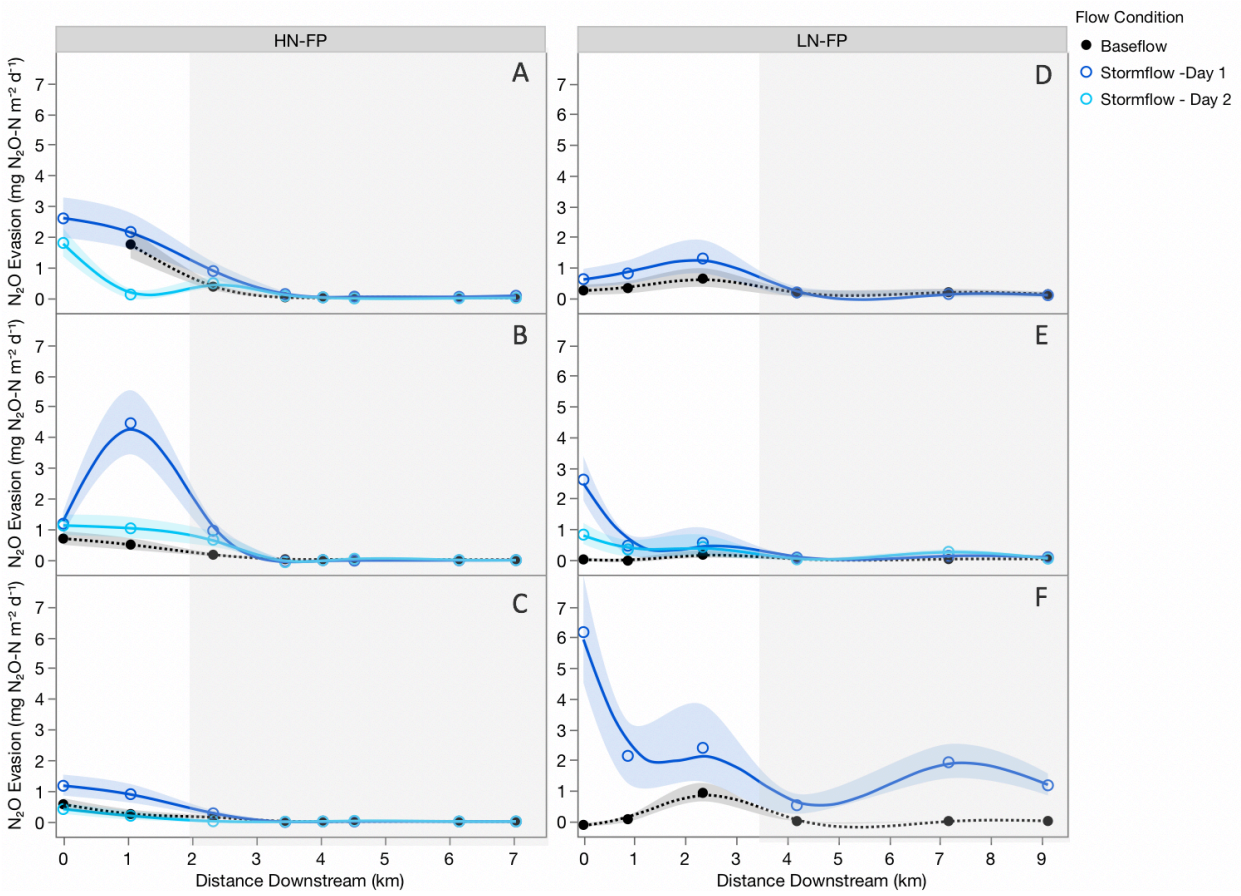

Figure 15. Nitrous oxide (N_2O) evasion rates along two surface water flow paths in the Ipswich River watershed before and after 6 storms (3 per flow path). HN-FP (left) and LN-FP (right) are the higher nutrient and lower nutrient flow paths, respectively. Storms on the left (A, B, C) represent the storms where study sites along the HN-FP were sampled, while storms on the right (D, E, F) represent the storms where study sites along the LN-FP were sampled. Storms top to bottom are in order of earliest date to latest date (A: 6/5/19, B: 7/22/19, C: 8/28/19, D: 6/20/19, E: 8/7/19, F: 10/16/19). Dots (solid black or hollow blue) are measured N_2O evasion at study sites along the flow paths. Black dots and dashed lines represent baseflow evasion, usually prior to a storm. Stormflow – Day 1 (dark blue dots and solid lines) and Stormflow – Day 2 (light blue dots and solid lines) represent evasion measured typically 24 and 48 hours after a storm, respectively. Shaded regions around data points/lines represent estimated error associated with N_2O evasion for each sampling day. Grey shaded regions indicate the fluvial wetland dominated portions of the flow paths. Non-shaded regions (between 0 and ~2-3.5 km) indicate the channelized portion of the flow paths.

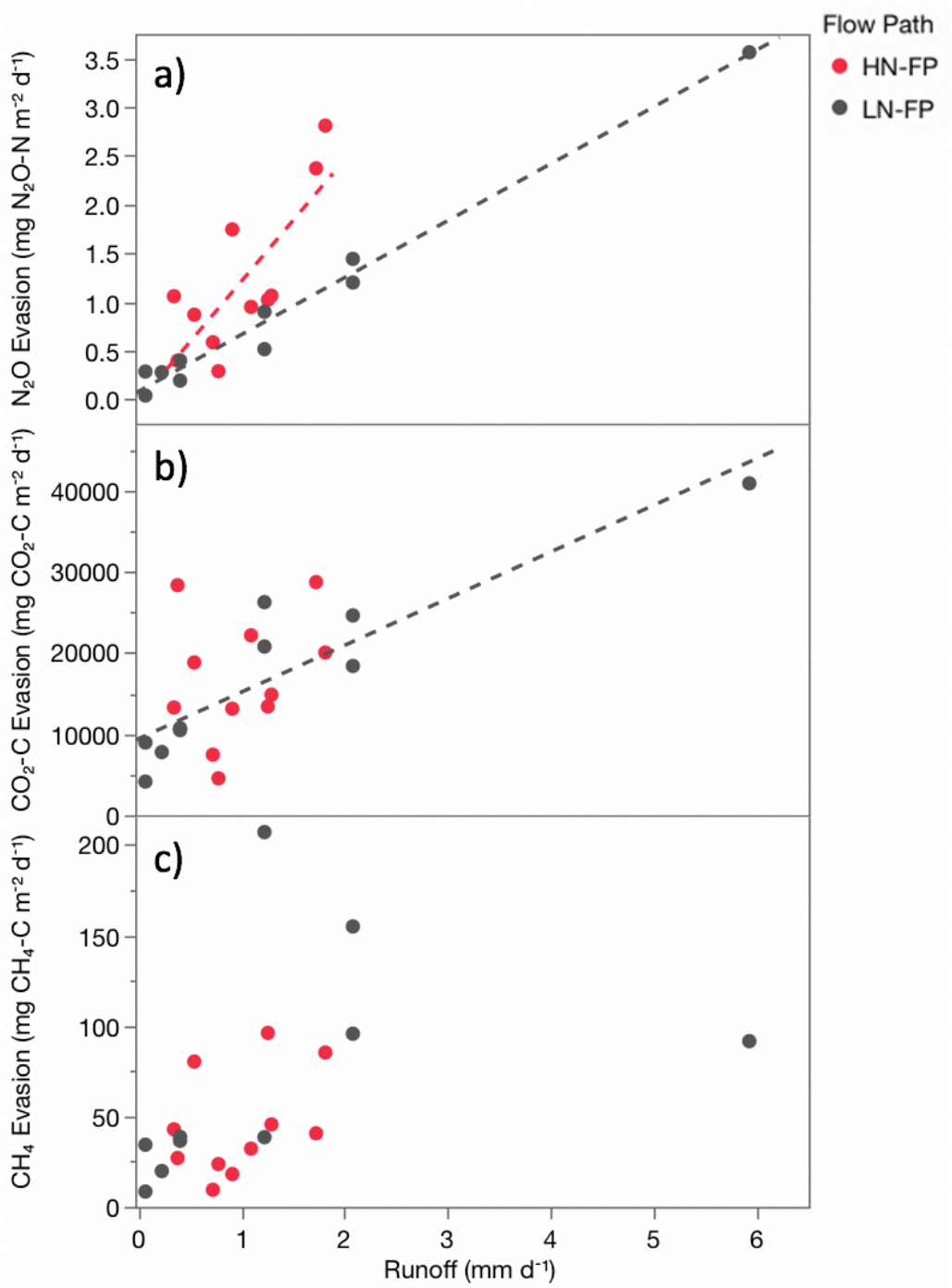

Figure 16. Relationships between mean nitrous oxide (N_2O) evasion, b) carbon dioxide (CO_2) evasion, and c) methane (CH_4) evasion and runoff rate for channelized stream study sites along each flow path. Each dot represents mean evasion on a sampling day. Red dots represent specific study sites along the HN-FP and grey dots represent those along the LN-FP. HN-FP and LN-FP are the higher nutrient and lower nutrient flow paths, respectively. Grey dashed lines represent significant bivariate relationships found between variables for the LN-FP (N_2O: $p \leq .0001$, $R^2 = 0.98$; CO_2: $p = 0.0002$; $R^2 = 0.84$). Red dashed line represents significant bivariate relationship found between variables for the HN-FP (N_2O: $p = 0.0045$, $R^2 = 0.61$).

APPENDIX

Table A1. GPS coordinate locations of study sites and the tributary on which each site lies. Tributary input sites to the main flow paths are indicated with an *. Study sites for each flow path are in order of distance downstream where distance downstream is benchmarked to the first sample locations.

Site	Tributary	Latitude	Longitude
IS_101	Sawmill Brook	42.516067	-71.191722
SB	Sawmill Brook	42.523322	-71.185925
SB-Chest	Sawmill Brook	42.527199	-71.172401
MMB-OldCanal	Maple Meadow Brook	42.533158	-71.162950
MMB-38	Maple Meadow Brook	42.537399	-71.160698
MMB-Lowell	Maple Meadow Brook	42.540858	-71.157336
Mill-Adams*	Mill Brook	42.553231	-71.164803
MMB	Maple Meadow Brook	42.552719	-71.157043
MMB-Federal	Maple Meadow Brook	42.552101	-71.150002
IS_135	Mosquito Brook	42.663750	-71.107460
MB-Johnston	Mosquito Brook	42.666425	-71.097603
MB-Salem	Mosquito Brook	42.669250	-71.083456
MB-Foster	Mosquito Brook	42.670533	-71.064222
Ogunquit_Trib*	Rocky Brook	42.673586	-71.042747
FB-Lawrence	Fish Brook	42.667872	-71.041542
FB-BV	Fish Brook	42.664928	-71.028481

Table A2. Slope and total percent upstream land cover (Urban, Forest, Wetland, and Agriculture) for each study site. Study sites for each flow path are in order of distance downstream where distance downstream is benchmarked to the first sample locations. Tributary input sites to the main flow paths are indicated with an *. Shaded sites are found along the higher nutrient flow path (HN-FP) and unshaded sites are found along the lower nutrient flow path (LN-FP).

Site	Slope	% Urban	% Forest	% Wetland	% Agriculture
IS_101	0.0052	38.6	41.9	4.0	0.0
SB	0.0052	37.3	44.4	4.9	0.0
SB-Chest	0.0067	33.2	49.2	6.2	0.0
MMB-OldCanal	0.0014	26.3	47.5	13.5	0.1
MMB-38	0.0005	27.5	45.6	14.8	0.0
MMB-Lowell	0.0006	28.9	44.3	15.3	0.0
Mill-Adams*	0.0020	29.2	43.3	24.3	0.0
MMB	0.0002	29.6	41.6	21.6	0.0
MMB-Federal	0.0003	29.5	41.0	23.4	0.0
IS_135	0.0122	32.1	42.6	15.2	0.3
MB-Johnston	0.0122	31.4	44.5	13.3	1.1
MB-Salem	0.0114	27.1	51.3	12.4	1.3
MB-Foster	0.0036	24.5	52.7	18.9	1.8
Ogunquit_Trib*	0.0190	6.6	61.3	28.0	2.0
FB-Lawrence	0.0014	16.4	54.4	28.1	2.1
FB-BV	0.0008	14.9	50.8	32.4	1.8

Table A3. Water depth (cm) from visual staff gauge along the flow paths at designated study sites for a) Storm A (6/5/19), b) Storm B (7/22/19), c) Storm C (8/28/19), d) Storm D (6/20/19), e) Storm E (8/7/19), and f) Storm F (10/16/19). The higher nutrient flow path (HN-FP) was sampled for storms A, B, and C, while the lower nutrient flow path (LN-FP) was sampled for storms D, E, and F. NA is used for sites where water depth with no visual staff gauge or if the gauge wasn't measured. Baseflow represents water depth before a storm. Stormflow day 1 and 2 represent water depth typically 24 and 48 hours after a storm, respectively. Study sites for each flow path are in order of distance downstream where distance downstream is benchmarked to the first sample locations.

a) Storm A: 6/5/19

Site	Baseflow Depth (cm)	Stormflow Day 1 Depth (cm)	Stormflow Day 1 Depth (cm)
IS_101	NA	NA	NA
SB	32	34	29
SB-Chest	66	70	67
MMB-OldCanal	26	30	30
MMB-38	45	50	53
MMB-Lowell	NA	NA	NA
MMB	63	68	67
MMB-Federal	49	52	54

b) Storm B: 7/22/19

Site	Baseflow Depth (cm)	Stormflow Day 1 Depth (cm)	Stormflow Day 1 Depth (cm)
IS_101	NA	NA	NA
SB	<25	34	29
SB-Chest	40	70	67
MMB-OldCanal	NA	38	31
MMB-38	36	60	53
MMB-Lowell	NA	NA	NA
MMB	54	71	69
MMB-Federal	43	58	58

c) Storm C: 8/28/19

Site	Baseflow Depth (cm)	Stormflow Day 1 Depth (cm)	Stormflow Day 1 Depth (cm)
IS_101	NA	NA	NA
SB	<20	27	23
SB-Chest	30	72	67
MMB-OldCanal	17	26	28
MMB-38	29	38	44
MMB-Lowell	NA	NA	NA
MMB	48	60	60
MMB-Federal	39	48	48

d) Storm D: 6/20/19

Site	Baseflow Depth (cm)	Stormflow Day 1 Depth (cm)
IS_135	36	38
MB-Johnston	12	18
MB-Salem	16	22
MB-Foster	44	50
FB-Lawrence	44	55
FB-BV	25	32

e) Storm E: 8/7/19

Site	Baseflow Depth (cm)	Stormflow Day 1 Depth (cm)	Stormflow Day 1 Depth (cm)
IS_135	33	39	38
MB-Johnston	8	18	16
MB-Salem	10	20	18
MB-Foster	26	39	44
FB-Lawrence	48	52	52
FB-BV	10	18	16

f) Storm F: 10/16/19

Site	Baseflow Depth (cm)	Stormflow Day 1 Depth (cm)
IS_135	33	48
MB-Johnston	8	39
MB-Salem	9	32
MB-Foster	20	35
FB-Lawrence	40	65
FB-BV	3	37

Table A4. Mean air-water gas transfer velocities for carbon dioxide (kCO_2), methane (kCH_4), and nitrous oxide (kN_2O) during baseflow and stormflow conditions at channelized and fluvial wetland dominated stream study sites throughout the 6-month study period. Standard deviation in parentheses.

Flow Path	Site Type	Flow Condition	kCO_2	kCH_4	kN_2O
HN-FP	Channelized	Baseflow	0.86 (0.18)	0.80 (0.17)	0.58 (0.14)
		Stormflow	1.17 (0.18)	1.08 (0.17)	0.79 (0.13)
	Fluvial wetland	Baseflow	0.06 (0.05)	0.06 (0.05)	0.04 (0.03)
		Stormflow	0.20 (0.11)	0.18 (0.10)	0.13 (0.07)
LN-FP	Channelized	Baseflow	0.99 (0.36)	0.92 (0.33)	0.66 (0.23)
		Stormflow	2.95 (1.35)	2.77 (1.33)	2.09 (1.20)
	Fluvial wetland	Baseflow	0.24 (0.30)	0.22 (0.28)	0.16 (0.20)
		Stormflow	0.70 (0.54)	0.66 (0.52)	0.51 (0.43)

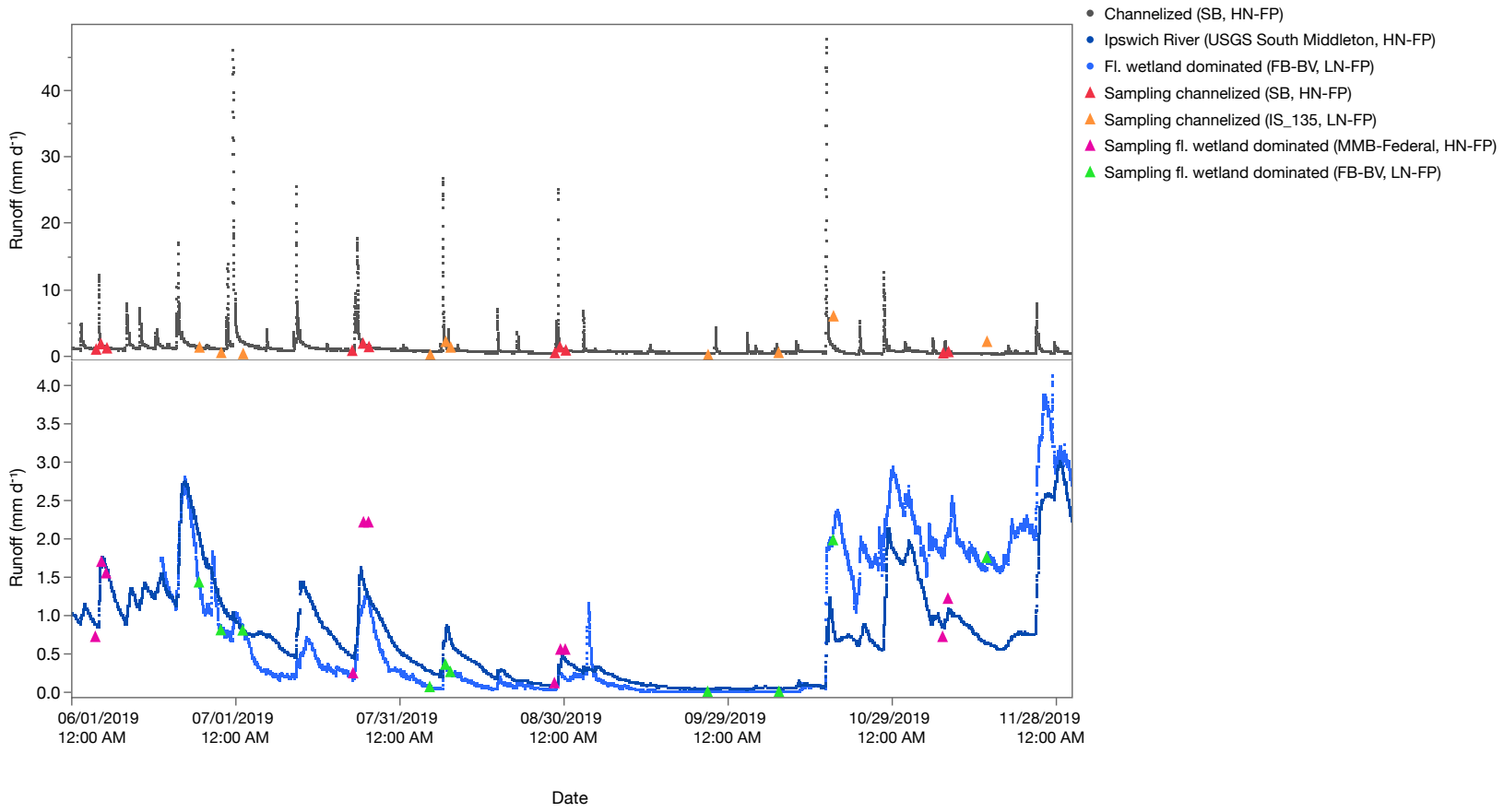

Figure A1. Runoff rates across the 6-month study period with estimated runoff at time of sampling for specific study sites. Continuous measurements of runoff using data loggers are depicted for the channelized stream study site (SB) in grey (top), fluvial wetland dominated stream study site (FB-BV) in light blue (bottom), and the Ipswich River (USGS South Middleton) in dark blue (bottom). Triangles represent runoff estimated at specific study sites at the time of sampling; red and orange triangles represent runoff estimated at one channelized stream study sites for each flow path – SB for the higher nutrient flow path (HN-FP) and IS_135 for the lower nutrient flow path (LN-FP), respectively. Pink and green triangles represent runoff estimated at the furthest downstream fluvial wetland dominated stream study sites for each flow path – MMB-Federal for HN-FP and FB-BV for LN-FP, respectively.

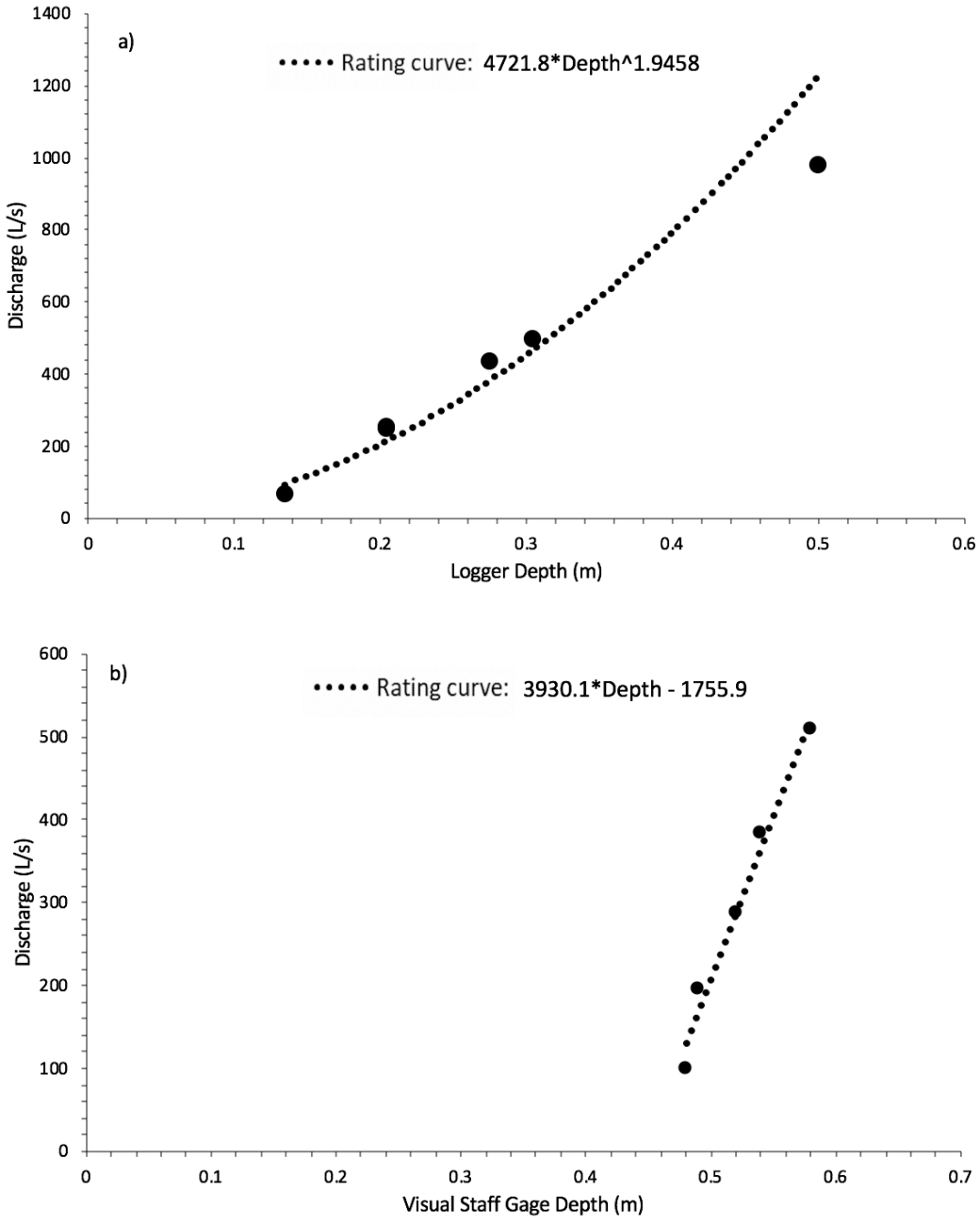

Figure A2. Rating curves used to estimate runoff at fluvial wetland dominated stream study sites using discharge and water depth data from FB-BV for the lower nutrient flow path (LN-FP) and MMB_Federal for the higher nutrient flow path (HN-FP). Panel a) depicts the power rating curve at FB-BV used to estimate runoff at fluvial wetland dominated stream sites along the LN-FP and panel b) depicts the linear rating curve at MMB-Federal used to estimate runoff at fluvial wetland dominated stream sites along the HN-FP. Equations for each curve are listed. Rating curve a) at FB-BV used continuous logger data for depth and b) at MMB-Federal used depth data from a visual staff gauge.

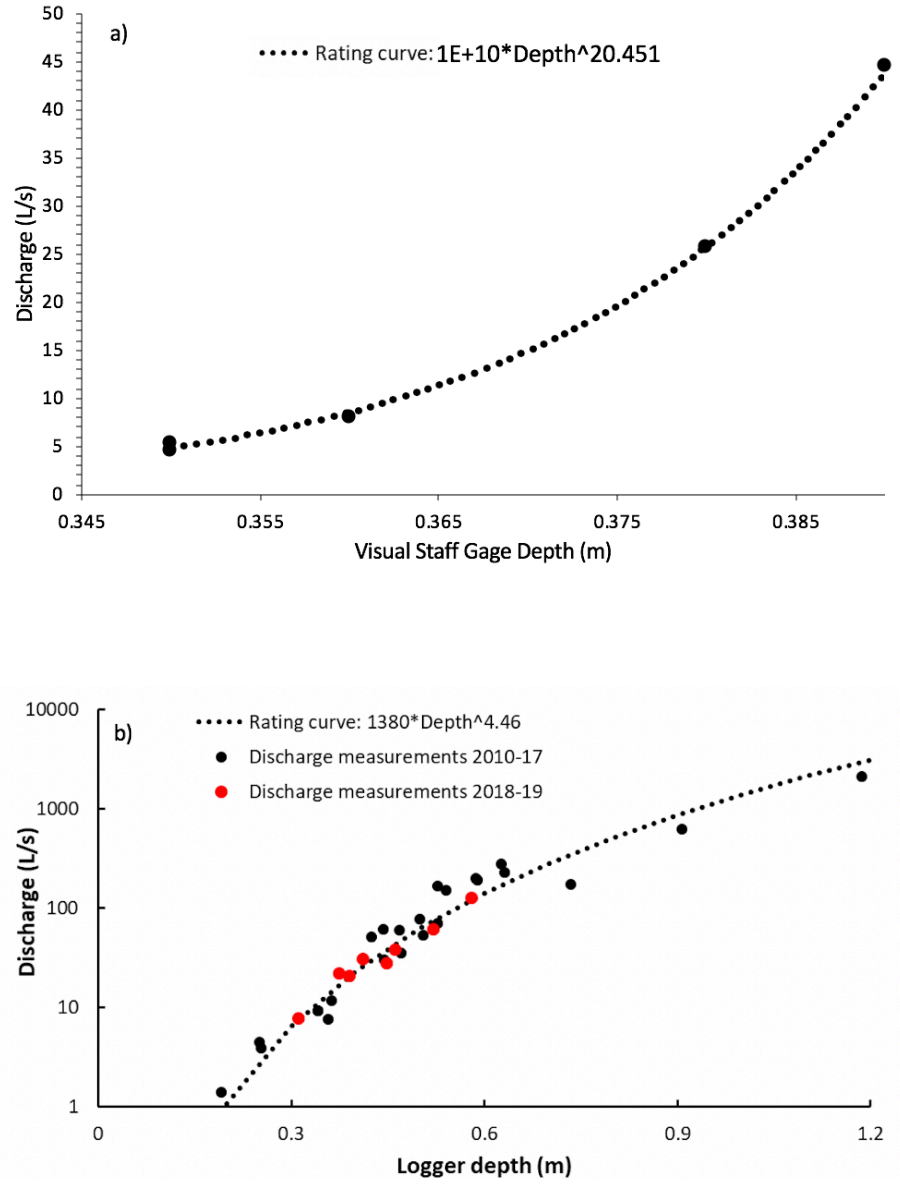

Figure A3. Rating curves used to estimate runoff at channelized stream study sites using discharge and water depth data from IS_135 for the lower nutrient flow path (LN-FP) and SB for the higher nutrient flow path (HN-FP). Panel a) depicts the power rating curve at IS_135 used to estimate runoff at channelized stream sites along the LN-FP and panel b) depicts the power rating curve at SB used to estimate runoff at channelized stream sites along the HN-FP. Equations for each curve are listed in each panel. Rating curve a) at FB-BV used depth data from a visual staff gauge while b) at SB used continuous logger data for depth. Rating curve b) (SB) was created by and obtained from Andrew Robison and is affiliated with the Plum Island Ecosystem Long Term Ecological Research (PIE-LTER) network.

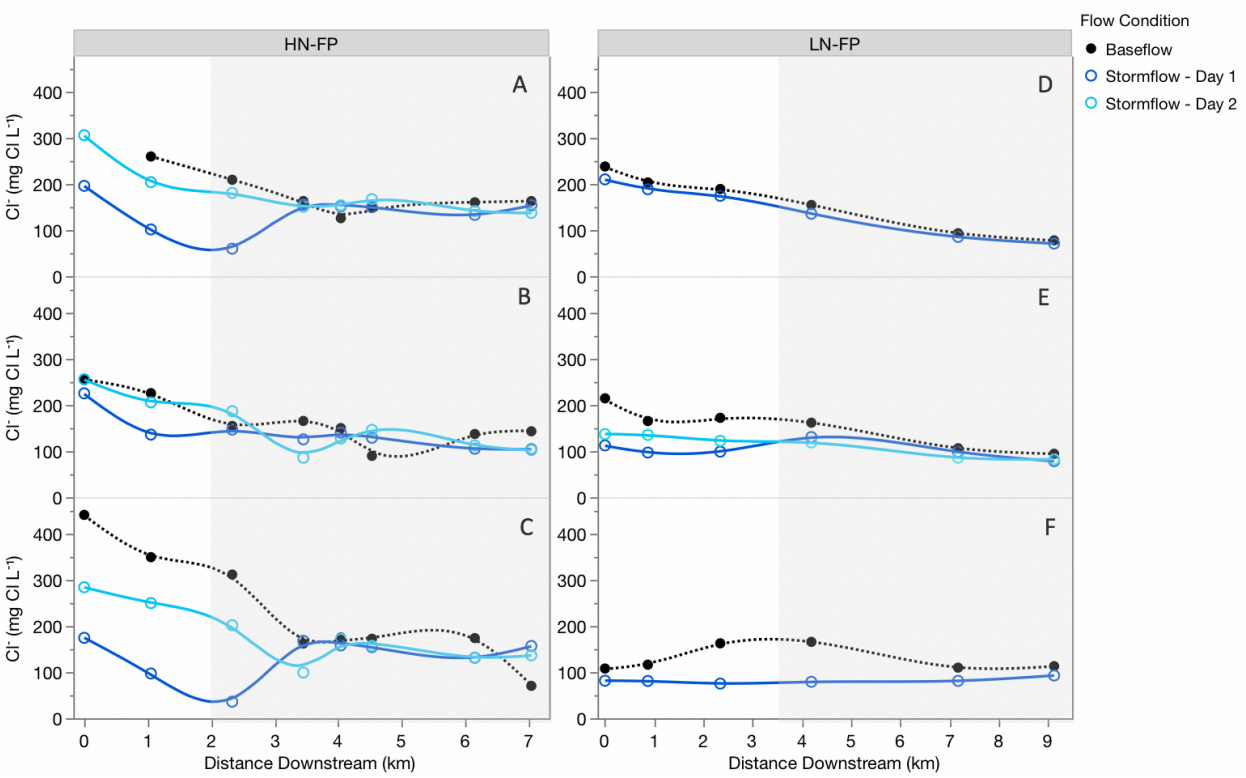

Figure A4. Chloride (Cl^-) concentrations at study sites along two surface water flow paths at baseflow and stormflows following 6 storms (3 per flow path). HN-FP (left) and LN-FP (right) are the higher nutrient and lower nutrient flow paths, respectively. Storms on the left (A, B, C) represent the storms where study sites along the HN-FP were sampled, while storms on the right (D, E, F) represent the storms where study sites along the LN-FP were sampled. Storms top to bottom are in order of earliest date to latest date (A: 6/5/19, B: 7/22/19, C: 8/28/19, D: 6/20/19, E: 8/7/19, F: 10/16/19). Dots (solid black or hollow blue) are measured values at study sites along the flow paths. Black dots and dashed lines represent baseflow concentrations, usually prior to a storm. Stormflow – Day 1 (dark blue dots and solid lines) and Stormflow – Day 2 (light blue dots and solid lines) represent concentrations measured typically 24 and 48 hours after a storm, respectively. Grey shaded regions indicate the fluvial wetland dominated portions of the flow paths. Non-shaded regions (between 0 and ~2-3.5 km) indicate the channelized portion of the flow paths.

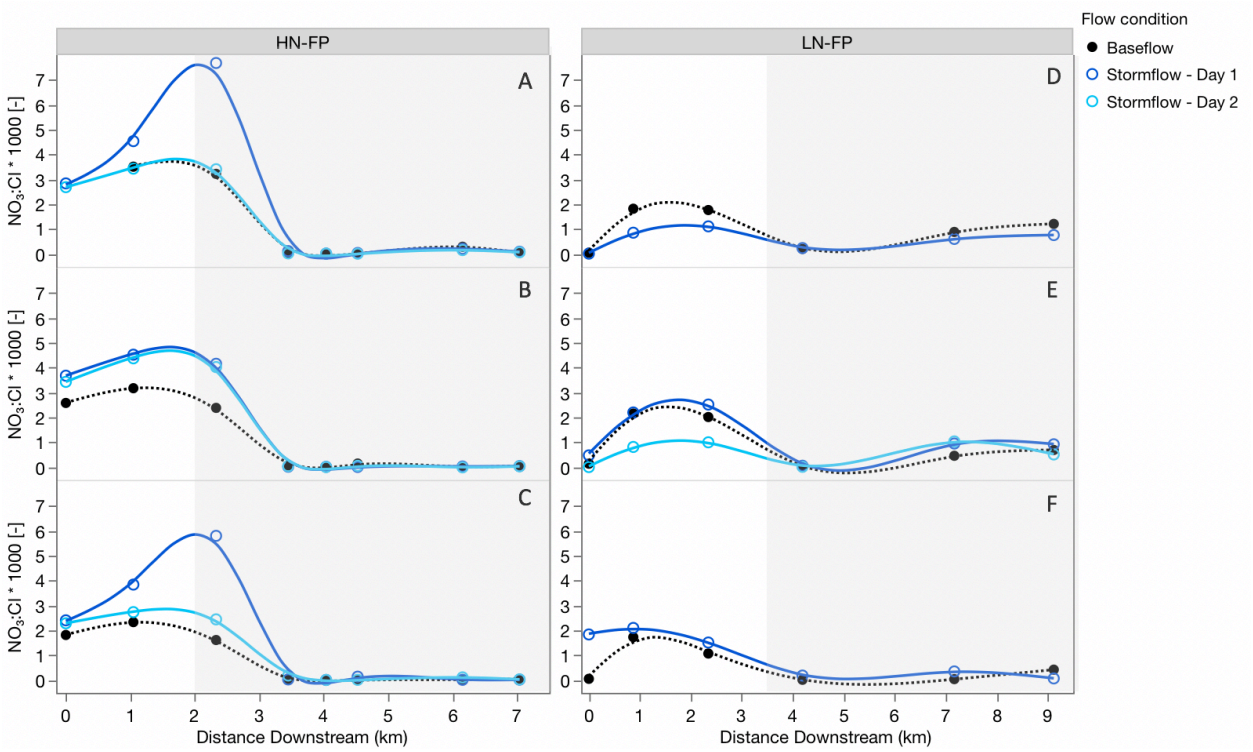

Figure A5. Ratios of nitrate to chloride concentrations (NO_3:Cl) multiplied by 1000 at study sites along two surface water flow paths at baseflow and stormflows following 6 storms (3 per flow path). HN-FP (left) and LN-FP (right) are the higher nutrient and lower nutrient flow paths, respectively. Storms on the left (A, B, C) represent the storms where study sites along the HN-FP were sampled, while storms on the right (D, E, F) represent the storms where study sites along the LN-FP were sampled. Storms top to bottom are in order of earliest date to latest date (A: 6/5/19, B: 7/22/19, C: 8/28/19, D: 6/20/19, E: 8/7/19, F: 10/16/19). Dots (solid black or hollow blue) are measured ratios at study sites along the flow paths. Black dots and dashed lines represent baseflow concentrations, usually prior to a storm. Stormflow – Day 1 (dark blue dots and solid lines) and Stormflow – Day 2 (light blue dots and solid lines) represent ratios measured typically 24 and 48 hours after a storm, respectively. Grey shaded regions indicate the fluvial wetland dominated portions of the flow paths. Non-shaded regions (between 0 and ~2-3.5 km) indicate the channelized portion of the flow paths.

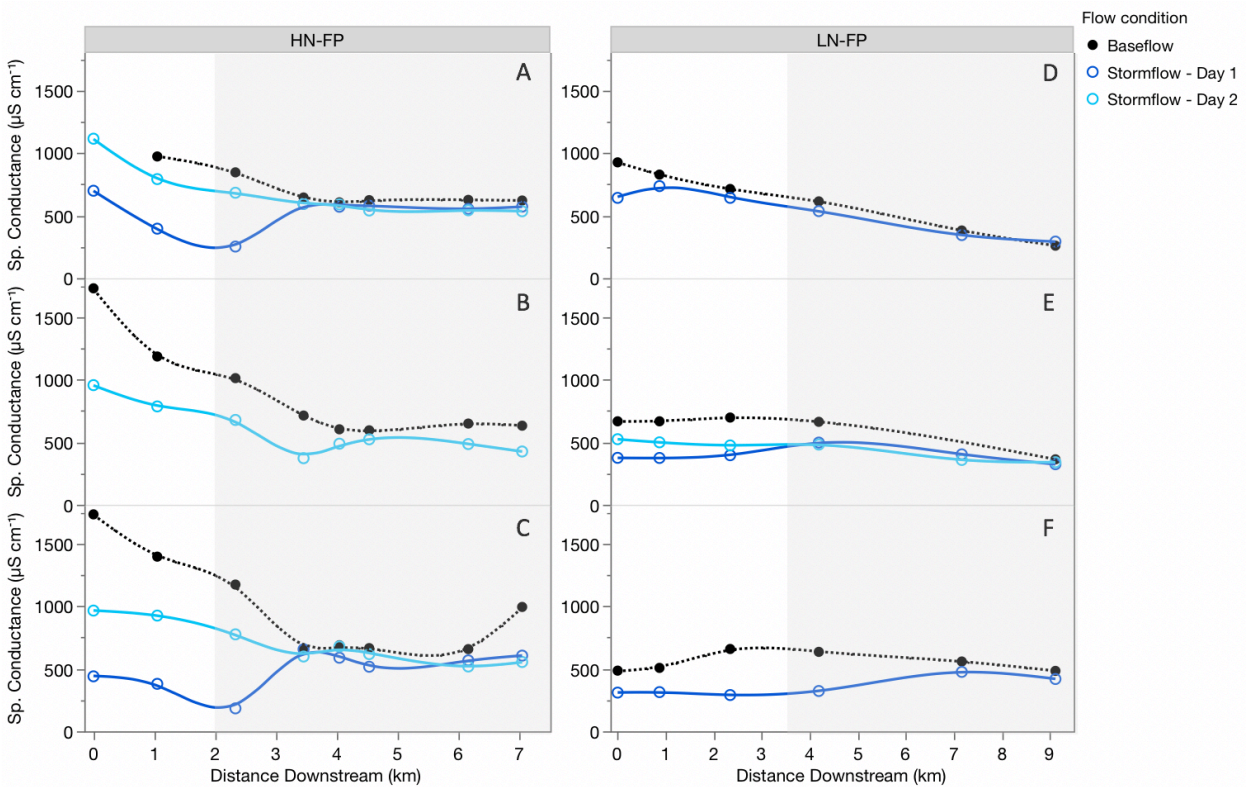

Figure A6. Specific conductance at study sites along two surface water flow paths at baseflow and stormflows following 6 storms (3 per flow path). HN-FP (left) and LN-FP (right) are the higher nutrient and lower nutrient flow paths, respectively. Storms on the left (A, B, C) represent the storms where study sites along the HN-FP were sampled, while storms on the right (D, E, F) represent the storms where study sites along the LN-FP were sampled. Storms top to bottom are in order of earliest date to latest date (A: 6/5/19, B: 7/22/19, C: 8/28/19, D: 6/20/19, E: 8/7/19, F: 10/16/19). Dots (solid black or hollow blue) are measured values at study sites along the flow paths. Black dots and dashed lines represent baseflow values, usually prior to a storm. Stormflow – Day 1 (dark blue dots and solid lines) and Stormflow – Day 2 (light blue dots and solid lines) represent values measured typically 24 and 48 hours after a storm, respectively. Grey shaded regions indicate the fluvial wetland dominated portions of the flow paths. Non-shaded regions (between 0 and ~2-3.5 km) indicate the channelized portion of the flow paths.

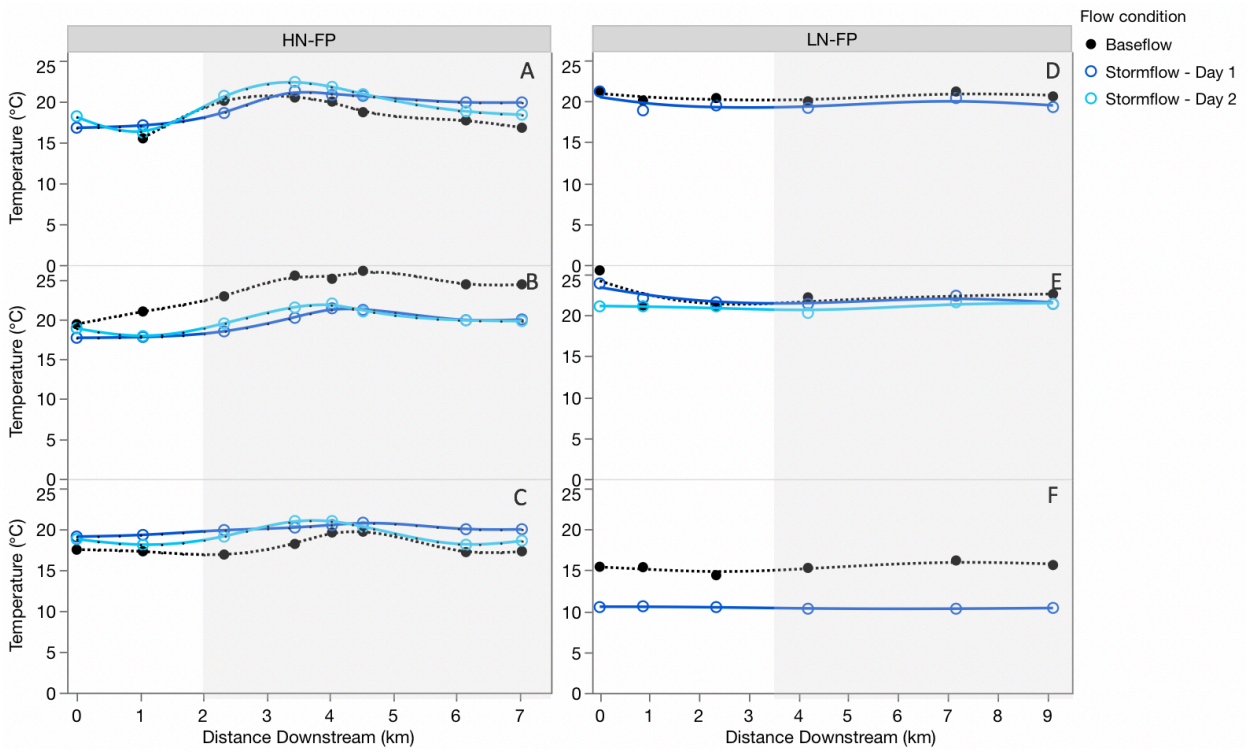

Figure A7. Temperature at study sites along two surface water flow paths at baseflow and stormflows following 6 storms (3 per flow path). HN-FP (left) and LN-FP (right) are the higher nutrient and lower nutrient flow paths, respectively. Storms on the left (A, B, C) represent the storms where study sites along the HN-FP were sampled, while storms on the right (D, E, F) represent the storms where study sites along the LN-FP were sampled. Storms top to bottom are in order of earliest date to latest date (A: 6/5/19, B: 7/22/19, C: 8/28/19, D: 6/20/19, E: 8/7/19, F: 10/16/19). Dots (solid black or hollow blue) are measured values at study sites along the flow paths. Black dots and dashed lines represent baseflow values, usually prior to a storm. Stormflow – Day 1 (dark blue dots and solid lines) and Stormflow – Day 2 (light blue dots and solid lines) represent values measured typically 24 and 48 hours after a storm, respectively. Grey shaded regions indicate the fluvial wetland dominated portions of the flow paths. Non-shaded regions (between 0 and ~2-3.5 km) indicate the channelized portion of the flow paths.

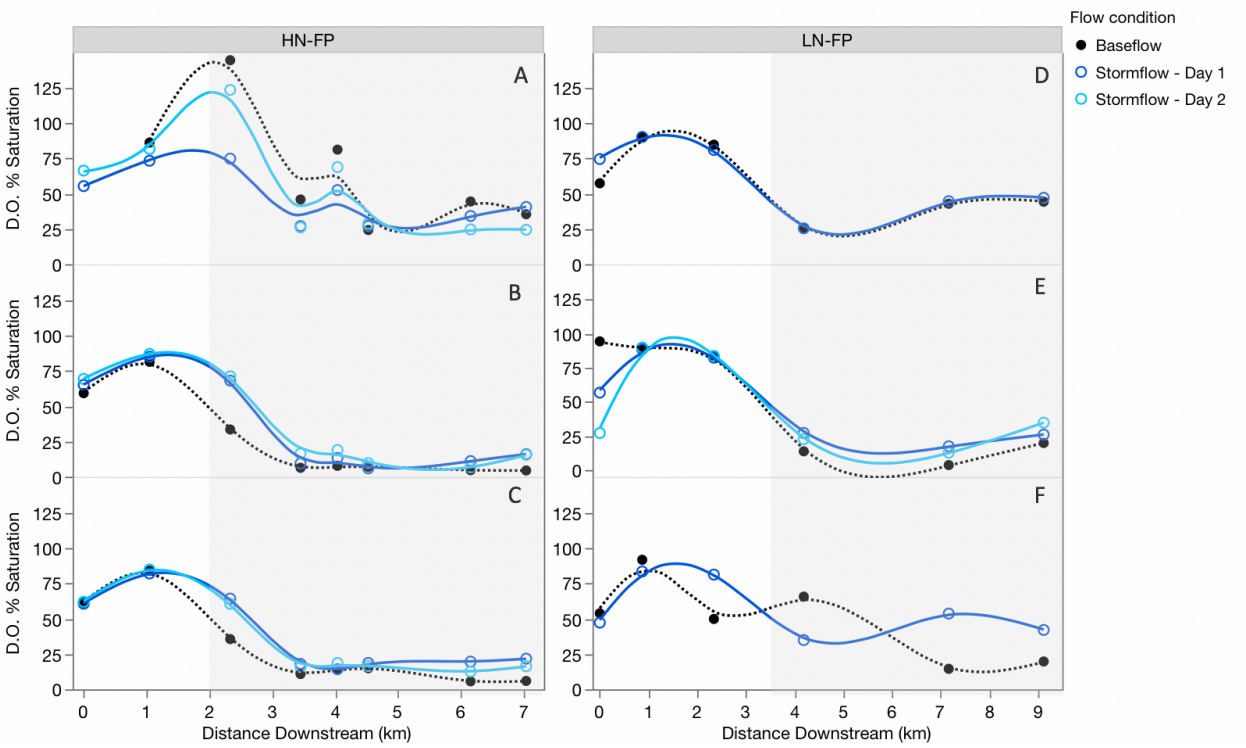

Figure A8. Dissolved oxygen (D.O.) percent saturation at study sites along two surface water flow paths at baseflow and stormflows following 6 storms (3 per flow path). HN-FP (left) and LN-FP (right) are the higher nutrient and lower nutrient flow paths, respectively. Storms on the left (A, B, C) represent the storms where study sites along the HN-FP were sampled, while storms on the right (D, E, F) represent the storms where study sites along the LN-FP were sampled. Storms top to bottom are in order of earliest date to latest date (A: 6/5/19, B: 7/22/19, C: 8/28/19, D: 6/20/19, E: 8/7/19, F: 10/16/19). Dots (solid black or hollow blue) are measured values at study sites along the flow paths. Black dots and dashed lines represent baseflow values, usually prior to a storm. Stormflow – Day 1 (dark blue dots and solid lines) and Stormflow – Day 2 (light blue dots and solid lines) represent values measured typically 24 and 48 hours after a storm, respectively. Grey shaded regions indicate the fluvial wetland dominated portions of the flow paths. Non-shaded regions (between 0 and ~2-3.5 km) indicate the channelized portion of the flow paths.

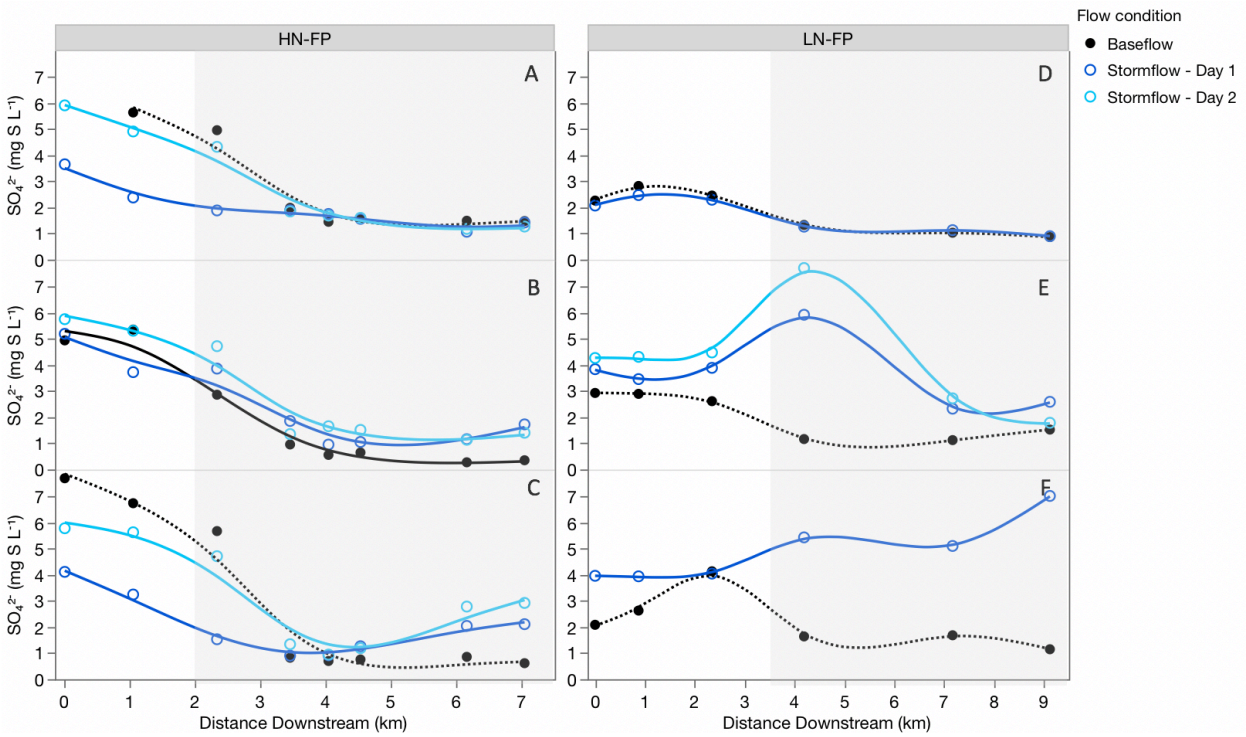

Figure A9. Sulfate (SO_4^{2-}) concentrations at study sites along two surface water flow paths at baseflow and stormflows following 6 storms (3 per flow path). HN-FP (left) and LN-FP (right) are the higher nutrient and lower nutrient flow paths, respectively. Storms on the left (A, B, C) represent the storms where study sites along the HN-FP were sampled, while storms on the right (D, E, F) represent the storms where study sites along the LN-FP were sampled. Storms top to bottom are in order of earliest date to latest date (A: 6/5/19, B: 7/22/19, C: 8/28/19, D: 6/20/19, E: 8/7/19, F: 10/16/19). Dots (solid black or hollow blue) are measured values at study sites along the flow paths. Black dots and dashed lines represent baseflow values, usually prior to a storm. Stormflow – Day 1 (dark blue dots and solid lines) and Stormflow – Day 2 (light blue dots and solid lines) represent values measured typically 24 and 48 hours after a storm, respectively. Grey shaded regions indicate the fluvial wetland dominated portions of the flow paths. Non-shaded regions (between 0 and ~2-3.5 km) indicate the channelized portion of the flow paths.

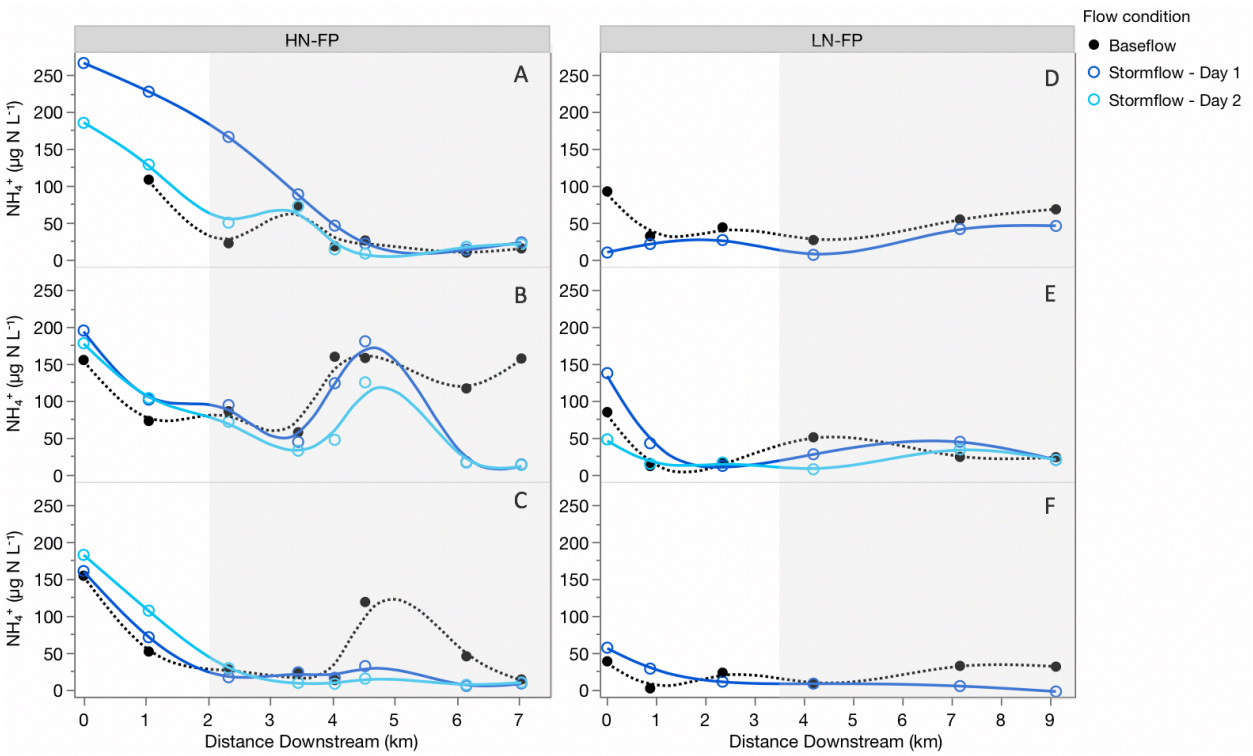

Figure A10. Ammonium (NH_4^+) concentrations at study sites along two surface water flow paths at baseflow and stormflows following 6 storms (3 per flow path). HN-FP (left) and LN-FP (right) are the higher nutrient and lower nutrient flow paths, respectively. Storms on the left (A, B, C) represent the storms where study sites along the HN-FP were sampled, while storms on the right (D, E, F) represent the storms where study sites along the LN-FP were sampled. Storms top to bottom are in order of earliest date to latest date (A: 6/5/19, B: 7/22/19, C: 8/28/19, D: 6/20/19, E: 8/7/19, F: 10/16/19). Dots (solid black or hollow blue) are measured values at study sites along the flow paths. Black dots and dashed lines represent baseflow values, usually prior to a storm. Stormflow – Day 1 (dark blue dots and solid lines) and Stormflow – Day 2 (light blue dots and solid lines) represent values measured typically 24 and 48 hours after a storm, respectively. Grey shaded regions indicate the fluvial wetland dominated portions of the flow paths. Non-shaded regions (between 0 and ~2-3.5 km) indicate the channelized portion of the flow paths.

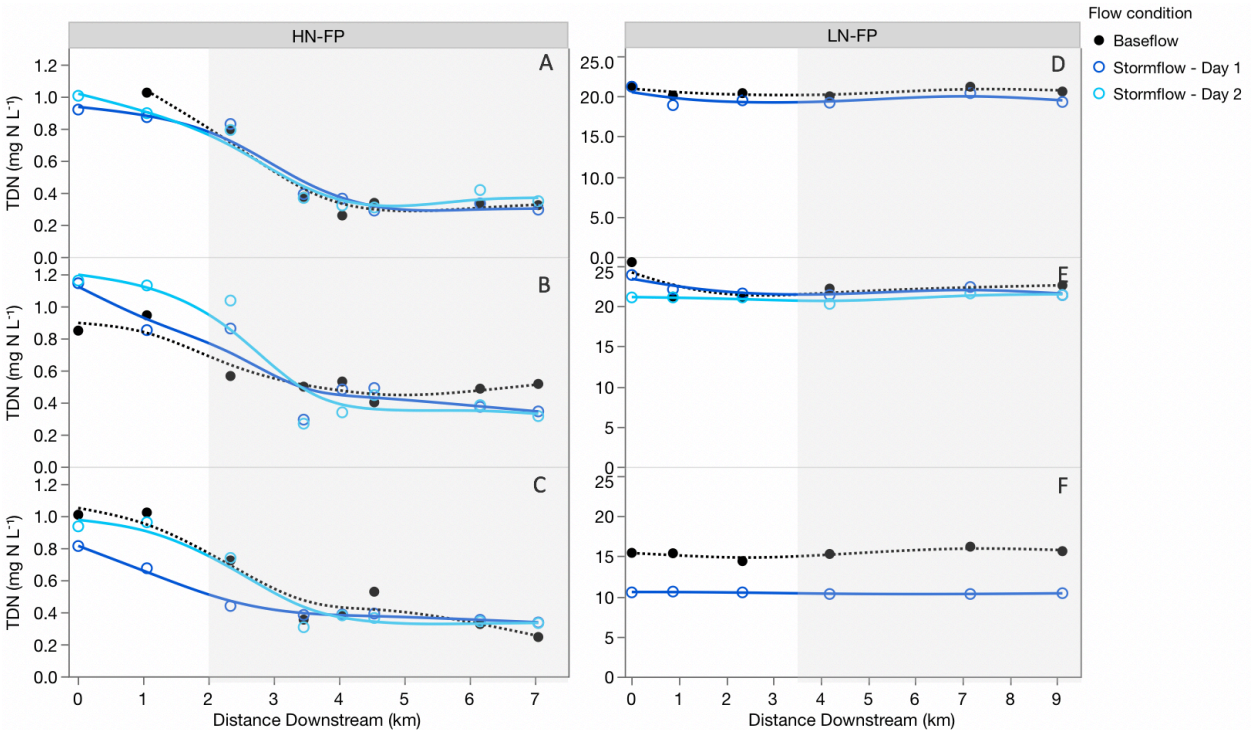

Figure A11. Total dissolved nitrogen (TDN) concentrations at study sites along two surface water flow paths at baseflow and stormflows following 6 storms (3 per flow path). HN-FP (left) and LN-FP (right) are the higher nutrient and lower nutrient flow paths, respectively. Storms on the left (A, B, C) represent the storms where study sites along the HN-FP were sampled, while storms on the right (D, E, F) represent the storms where study sites along the LN-FP were sampled. Storms top to bottom are in order of earliest date to latest date (A: 6/5/19, B: 7/22/19, C: 8/28/19, D: 6/20/19, E: 8/7/19, F: 10/16/19). Dots (solid black or hollow blue) are measured values at study sites along the flow paths. Black dots and dashed lines represent baseflow values, usually prior to a storm. Stormflow – Day 1 (dark blue dots and solid lines) and Stormflow – Day 2 (light blue dots and solid lines) represent values measured typically 24 and 48 hours after a storm, respectively. Grey shaded regions indicate the fluvial wetland dominated portions of the flow paths. Non-shaded regions (between 0 and ~2-3.5 km) indicate the channelized portion of the flow paths.

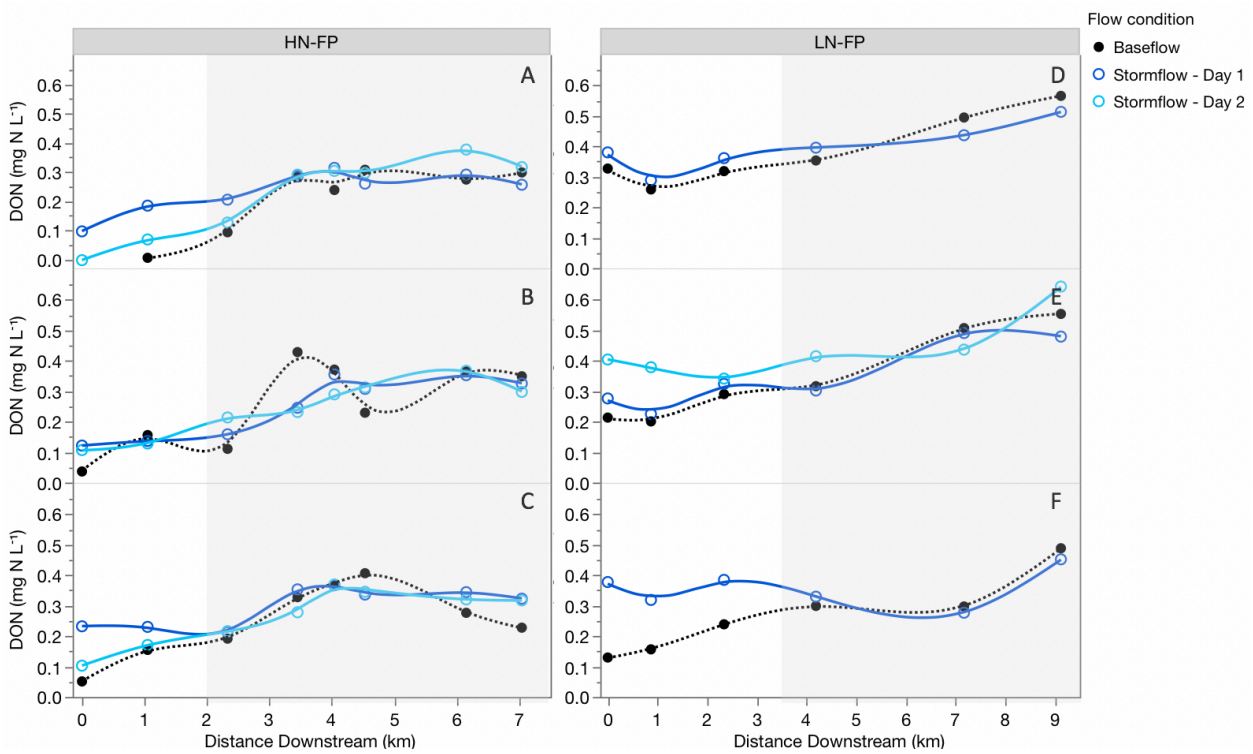

Figure A12. Dissolved organic nitrogen (DON) concentrations at study sites along two surface water flow paths at baseflow and stormflows following 6 storms (3 per flow path). HN-FP (left) and LN-FP (right) are the higher nutrient and lower nutrient flow paths, respectively. Storms on the left (A, B, C) represent the storms where study sites along the HN-FP were sampled, while storms on the right (D, E, F) represent the storms where study sites along the LN-FP were sampled. Storms top to bottom are in order of earliest date to latest date (A: 6/5/19, B: 7/22/19, C: 8/28/19, D: 6/20/19, E: 8/7/19, F: 10/16/19). Dots (solid black or hollow blue) are measured values at study sites along the flow paths. Black dots and dashed lines represent baseflow values, usually prior to a storm. Stormflow – Day 1 (dark blue dots and solid lines) and Stormflow – Day 2 (light blue dots and solid lines) represent values measured typically 24 and 48 hours after a storm, respectively. Grey shaded regions indicate the fluvial wetland dominated portions of the flow paths. Non-shaded regions (between 0 and ~2-3.5 km) indicate the channelized portion of the flow paths.

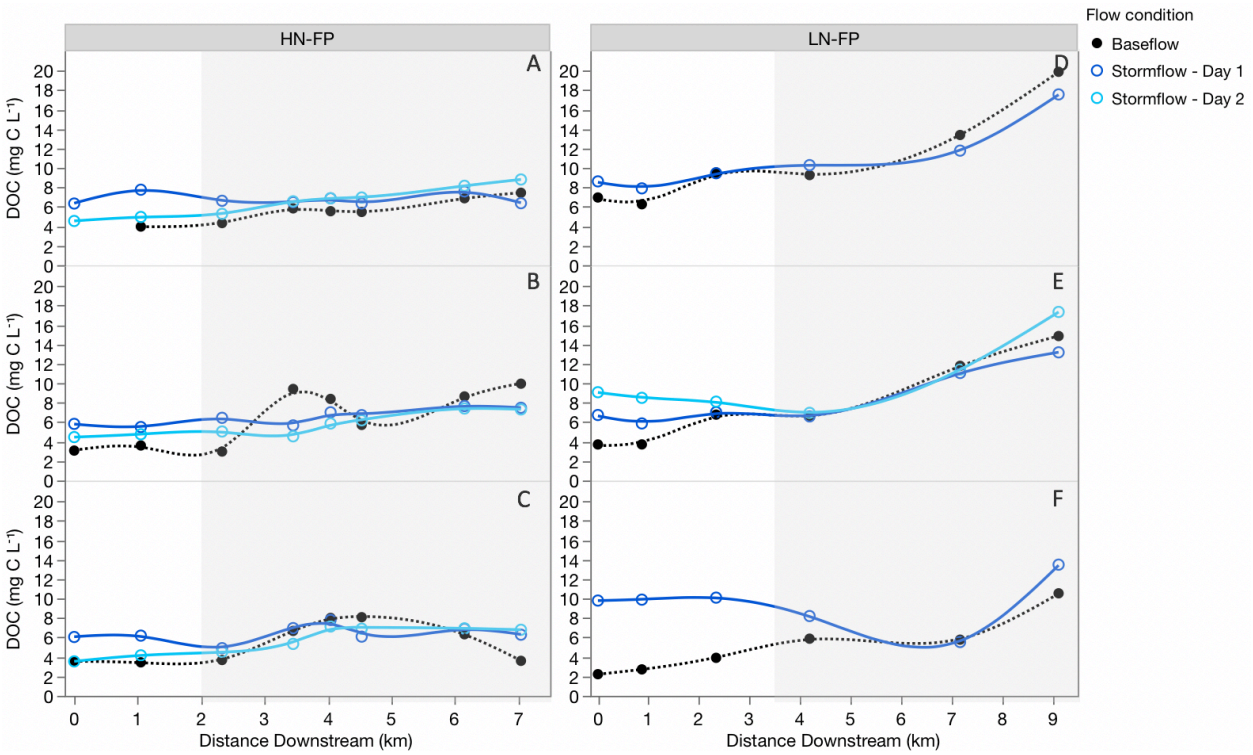

Figure A13. Dissolved organic carbon (DOC) concentrations at study sites along two surface water flow paths at baseflow and stormflows following 6 storms (3 per flow path). HN-FP (left) and LN-FP (right) are the higher nutrient and lower nutrient flow paths, respectively. Storms on the left (A, B, C) represent the storms where study sites along the HN-FP were sampled, while storms on the right (D, E, F) represent the storms where study sites along the LN-FP were sampled. Storms top to bottom are in order of earliest date to latest date (A: 6/5/19, B: 7/22/19, C: 8/28/19, D: 6/20/19, E: 8/7/19, F: 10/16/19). Dots (solid black or hollow blue) are measured values at study sites along the flow paths. Black dots and dashed lines represent baseflow values, usually prior to a storm. Stormflow – Day 1 (dark blue dots and solid lines) and Stormflow – Day 2 (light blue dots and solid lines) represent values measured typically 24 and 48 hours after a storm, respectively. Grey shaded regions indicate the fluvial wetland dominated portions of the flow paths. Non-shaded regions (between 0 and ~2-3.5 km) indicate the channelized portion of the flow paths.

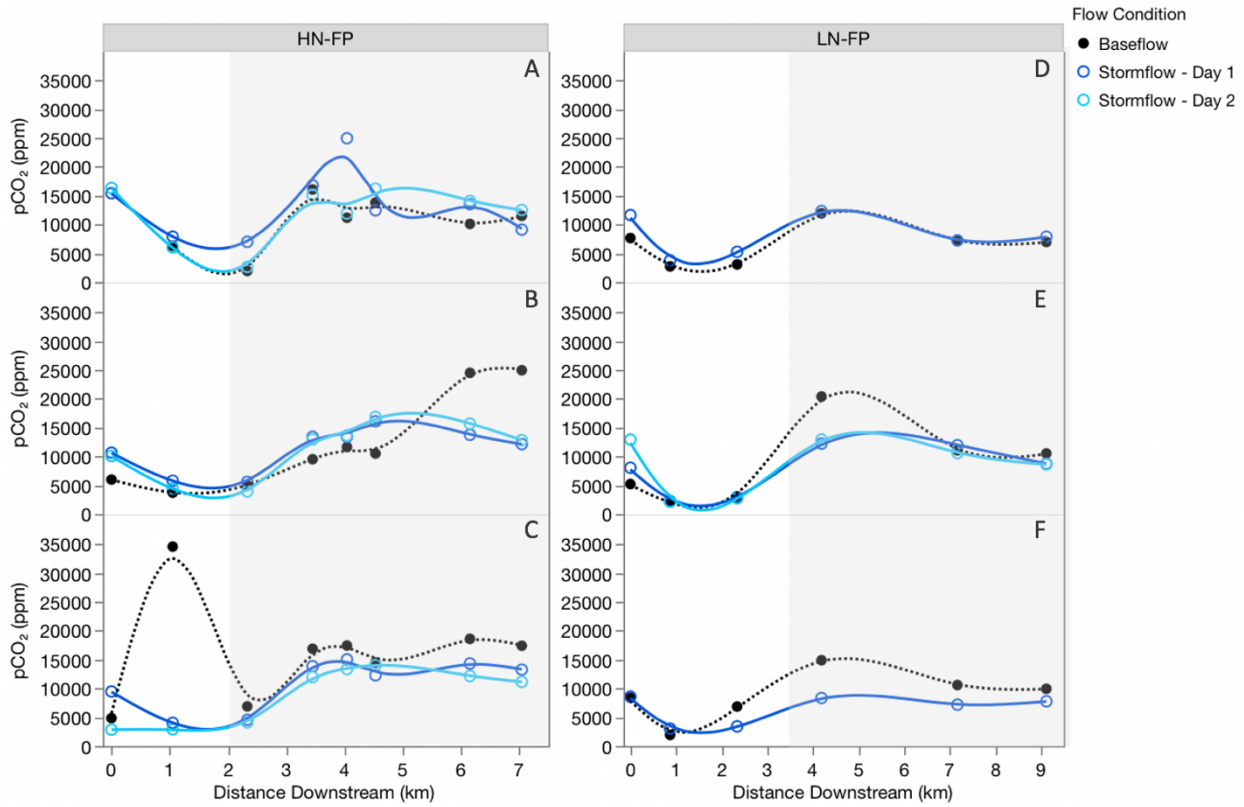

Figure A14. Partial pressure of carbon dioxide (pCO_2) at study sites along two surface water flow paths at baseflow and stormflows following 6 storms (3 per flow path). HN-FP (left) and LN-FP (right) are the higher nutrient and lower nutrient flow paths, respectively. Storms on the left (A, B, C) represent the storms where study sites along the HN-FP were sampled, while storms on the right (D, E, F) represent the storms where study sites along the LN-FP were sampled. Storms top to bottom are in order of earliest date to latest date (A: 6/5/19, B: 7/22/19, C: 8/28/19, D: 6/20/19, E: 8/7/19, F: 10/16/19). Dots (solid black or hollow blue) are measured values at study sites along the flow paths. Black dots and dashed lines represent baseflow values, usually prior to a storm. Stormflow – Day 1 (dark blue dots and solid lines) and Stormflow – Day 2 (light blue dots and solid lines) represent values measured typically 24 and 48 hours after a storm, respectively. Grey shaded regions indicate the fluvial wetland dominated portions of the flow paths. Non-shaded regions (between 0 and ~2-3.5 km) indicate the channelized portion of the flow paths.

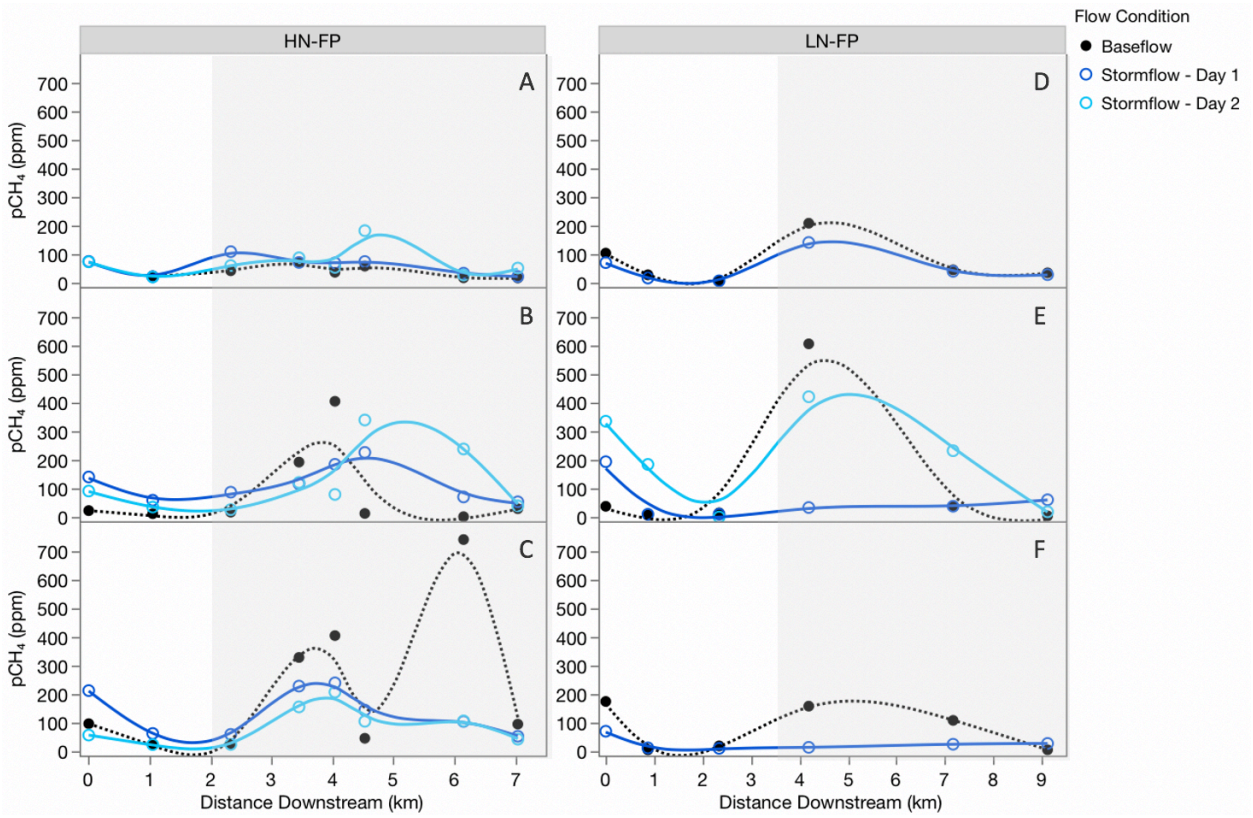

Figure A15. Partial pressure of methane (pCH_4) at study sites along two surface water flow paths at baseflow and stormflows following 6 storms (3 per flow path). HN-FP (left) and LN-FP (right) are the higher nutrient and lower nutrient flow paths, respectively. Storms on the left (A, B, C) represent the storms where study sites along the HN-FP were sampled, while storms on the right (D, E, F) represent the storms where study sites along the LN-FP were sampled. Storms top to bottom are in order of earliest date to latest date (A: 6/5/19, B: 7/22/19, C: 8/28/19, D: 6/20/19, E: 8/7/19, F: 10/16/19). Dots (solid black or hollow blue) are measured values at study sites along the flow paths. Black dots and dashed lines represent baseflow values, usually prior to a storm. Stormflow – Day 1 (dark blue dots and solid lines) and Stormflow – Day 2 (light blue dots and solid lines) represent values measured typically 24 and 48 hours after a storm, respectively. Grey shaded regions indicate the fluvial wetland dominated portions of the flow paths. Non-shaded regions (between 0 and ~2-3.5 km) indicate the channelized portion of the flow paths.

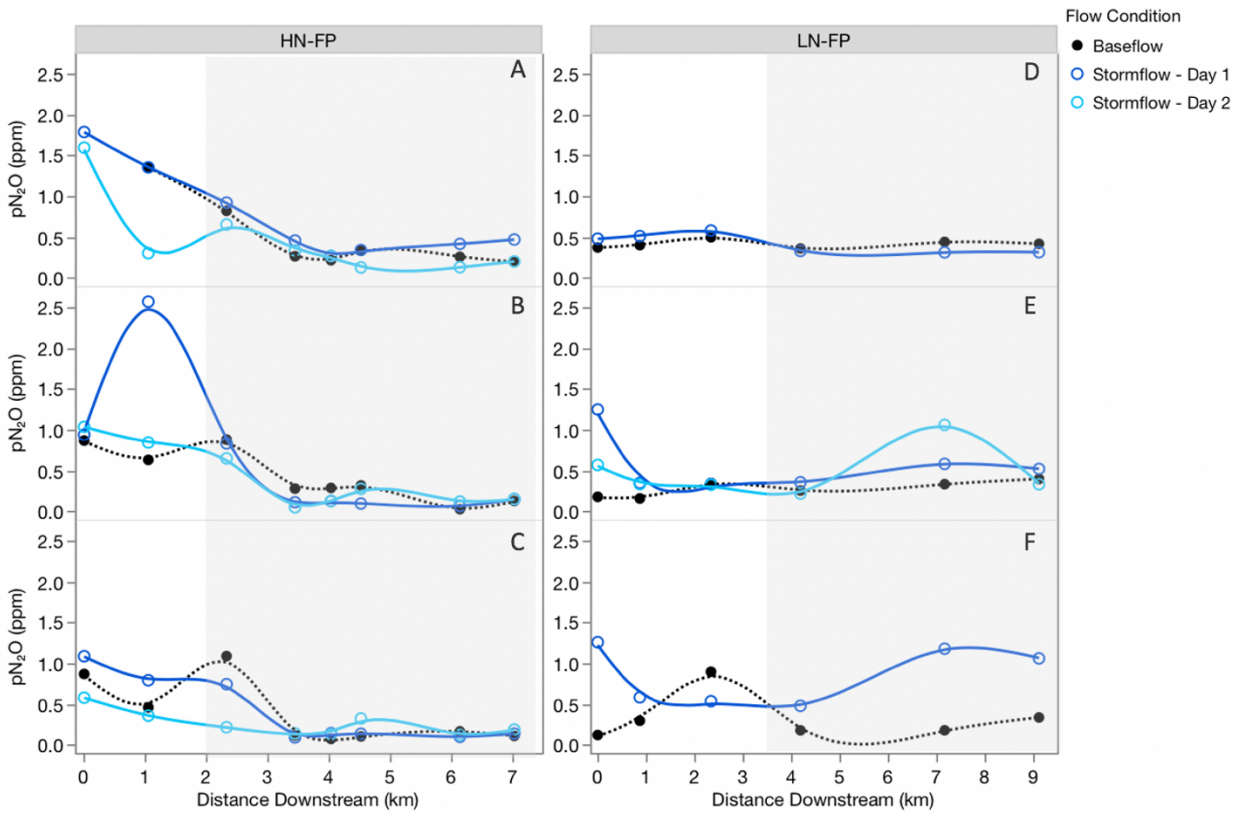

Figure A16. Partial pressure of nitrous oxide (pN_2O) at study sites along two surface water flow paths at baseflow and stormflows following 6 storms (3 per flow path). HN-FP (left) and LN-FP (right) are the higher nutrient and lower nutrient flow paths, respectively. Storms on the left (A, B, C) represent the storms where study sites along the HN-FP were sampled, while storms on the right (D, E, F) represent the storms where study sites along the LN-FP were sampled. Storms top to bottom are in order of earliest date to latest date (A: 6/5/19, B: 7/22/19, C: 8/28/19, D: 6/20/19, E: 8/7/19, F: 10/16/19). Dots (solid black or hollow blue) are measured values at study sites along the flow paths. Black dots and dashed lines represent baseflow values, usually prior to a storm. Stormflow – Day 1 (dark blue dots and solid lines) and Stormflow – Day 2 (light blue dots and solid lines) represent values measured typically 24 and 48 hours after a storm, respectively. Grey shaded regions indicate the fluvial wetland dominated portions of the flow paths. Non-shaded regions (between 0 and ~2-3.5 km) indicate the channelized portion of the flow paths.

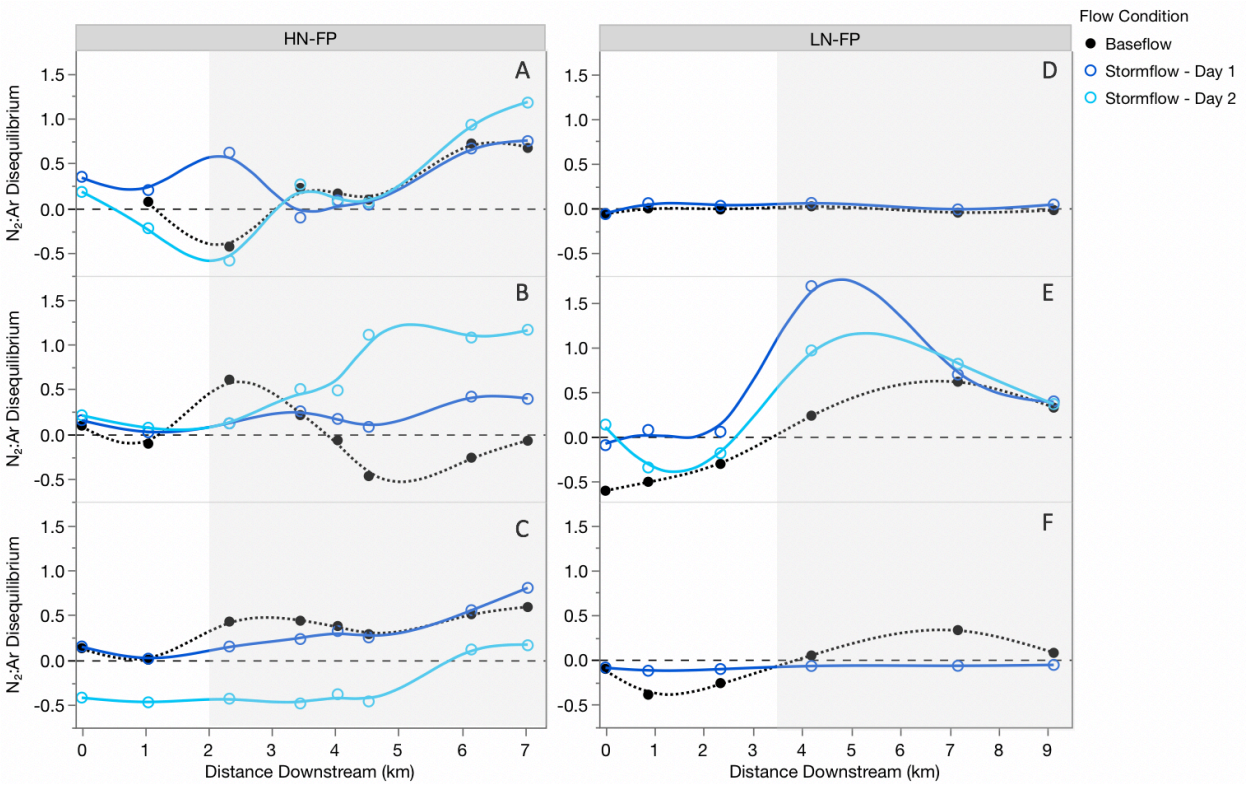

Figure A17. N_2:Ar disequilibrium at study sites along two surface water flow paths at baseflow and stormflows following 6 storms (3 per flow path). HN-FP (left) and LN-FP (right) are the higher nutrient and lower nutrient flow paths, respectively. Storms on the left (A, B, C) represent the storms where study sites along the HN-FP were sampled, while storms on the right (D, E, F) represent the storms where study sites along the LN-FP were sampled. Storms top to bottom are in order of earliest date to latest date (A: 6/5/19, B: 7/22/19, C: 8/28/19, D: 6/20/19, E: 8/7/19, F: 10/16/19). Dots (solid black or hollow blue) are measured values at study sites along the flow paths. Black dots and dashed lines represent baseflow values, usually prior to a storm. Stormflow – Day 1 (dark blue dots and solid lines) and Stormflow – Day 2 (light blue dots and solid lines) represent values measured typically 24 and 48 hours after a storm, respectively. Grey shaded regions indicate the fluvial wetland dominated portions of the flow paths. Non-shaded regions (between 0 and ~2-3.5 km) indicate the channelized portion of the flow paths. Dashed line at 0 is a reference line, where positive disequilibrium indicates N_2 production via denitrification and negative disequilibrium indicates N_2 consumption via N fixation.

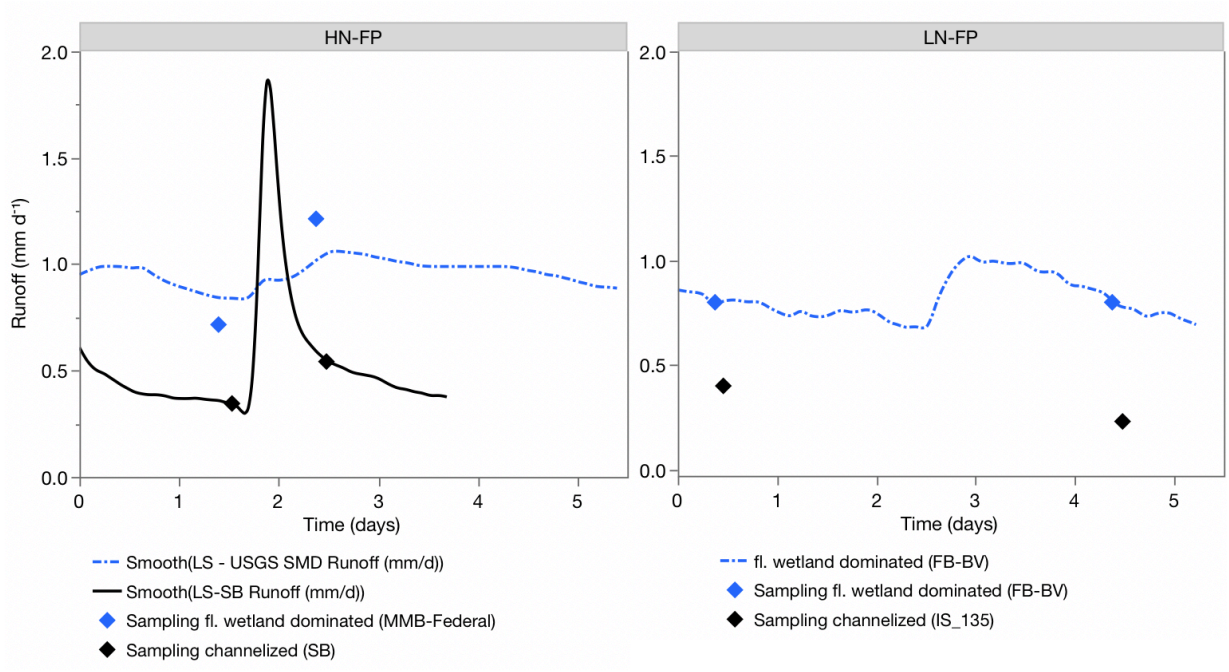

Figure A18. Runoff rate over time for the two storms excluded from storm-specific analyses (one per flow path). HN-FP (left) and LN-FP (right) are the higher nutrient and lower nutrient flow paths, respectively. Plot on the left represents the storm response at study sites along the HN-FP while the plot on the right represents the storm response at study sites along the LN-FP. The storm for the HN-FP (left) began on 11/7/19 and the LN-FP (right) on 6/30/19. Black lines represent the storm responses at Sawmill Brook (SB), which was used to characterize the responses at channelized streams along the HN-FP. Blue dashed lines in the HN-FP represent the storm responses at the USGS gauge at South Middleton along the Ipswich River (just downstream of the last fluvial wetland dominated site, MMB-Federal, in the HN-FP); the storm response at fluvial wetland dominated stream sites along the HN-FP were expected to be somewhere between SB and USGS South Middleton. Blue dashed lines in the LN-FP represent the storm response at FB-BV, the furthest downstream fluvial wetland dominated study site along the LN-FP. There was no continuous runoff data available to characterize the storm response in channelized streams of the LN-FP. Black and blue diamonds are estimated runoff at the representative channelized stream study sites (SB for HN-FP and IS_135 for LN-FP) and fluvial wetland dominated stream study sites (MMB-Federal for HN-FP and FB-BV for LN-FP), respectively, at the time of sampling. Ultimately, these two storms were excluded because stormflows did not meet criteria of at least 2x the baseflow condition.

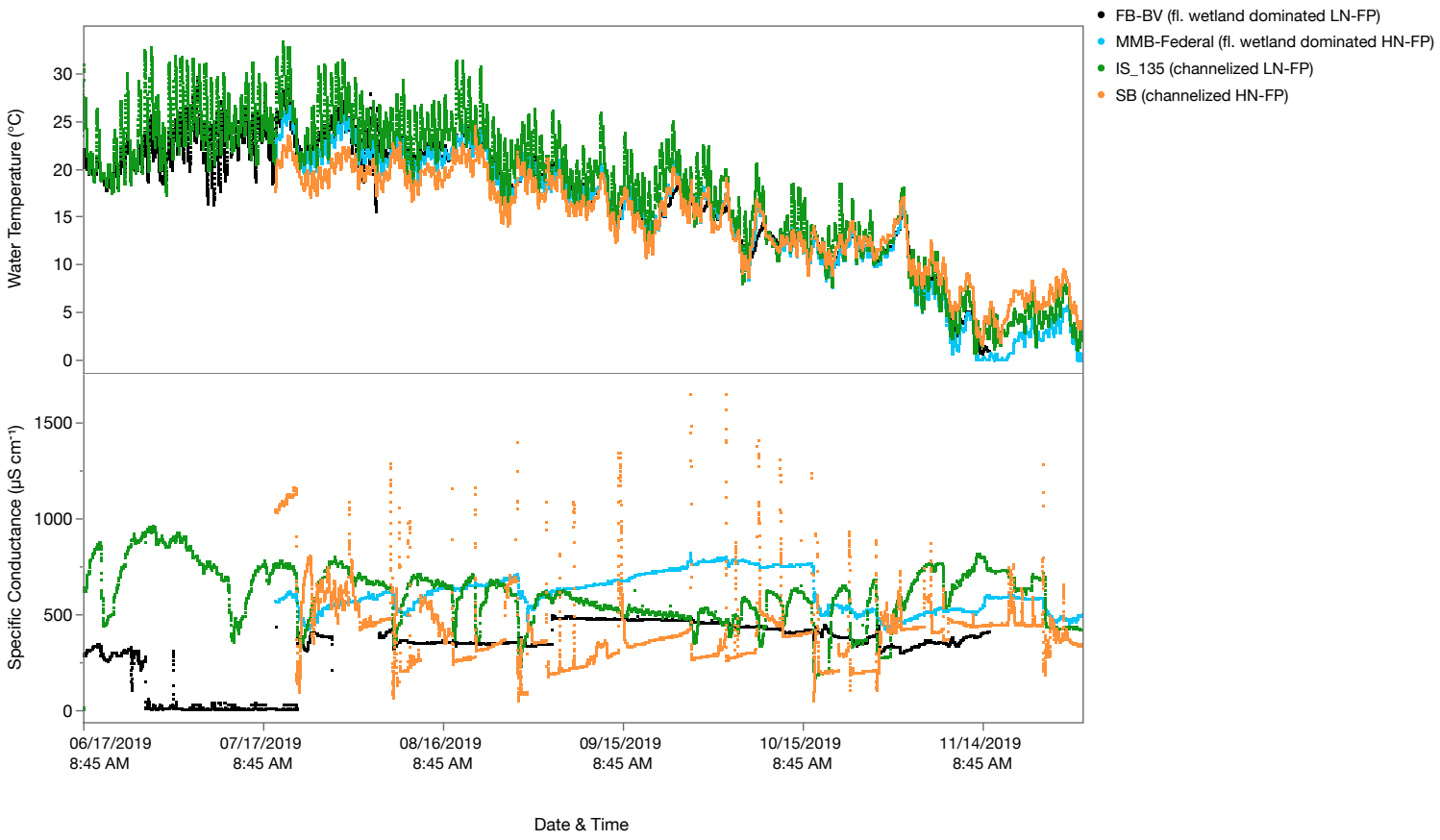

Figure A19. Continuous logger data of water temperature and specific conductance at four study sites (two from each flow path) across the study period. Study sites represented are FB-BV (fluvial wetland dominated stream in the LN-FP) in black, MMB-Federal (fluvial wetland dominated stream in the HN-FP) in blue, IS_135 (channelized stream in the LN-FP) in green, and SB (channelized stream in the HN-FP) in orange. HN-FP and LN-FP are the higher nutrient and lower nutrient flow paths, respectively. Logger data for specific conductance at study site SB was not consistent with data collected using a handheld YSI Pro30 conductivity meter at the time of sampling. Low specific conductance at FB-BV between late June and early July seems inconsistent with handheld data and is likely due to being out of the water (missing data from 7/28/19 until 8/5/19 due to logger being out of the water); logger was moved to deeper location on 8/5/19 and readings afterwards are consistent with handhelds. Specific conductance logger data for study sites MMB-Federal and IS_135 were mostly consistent with handheld data observed at the time of sampling.

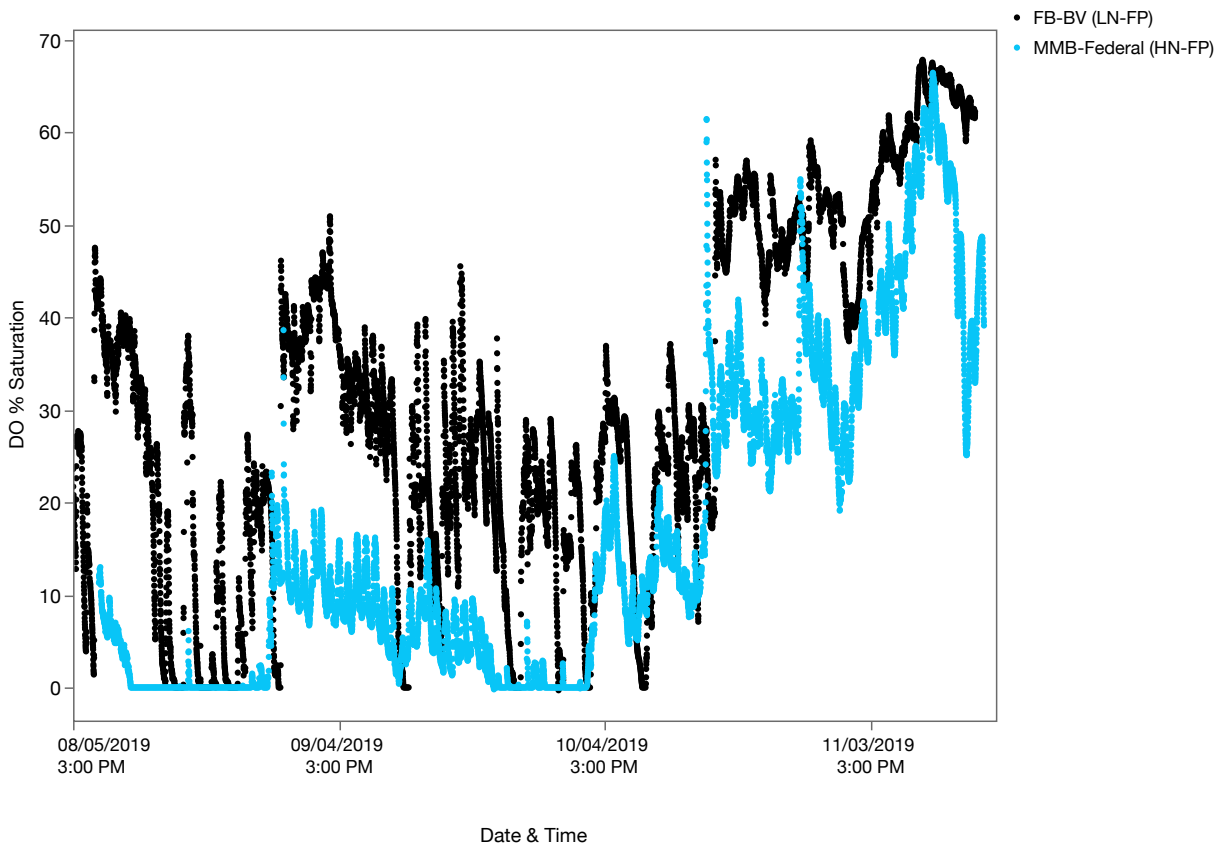

Figure A20. Continuous logger data of dissolved oxygen percent saturation at two fluvial wetland dominated stream study sites (one from each flow path) across the study period. Study sites represented are MMB-Federal for the HN-FP in blue and FB-BV for the LN-FP in black. HN-FP and LN-FP are the higher nutrient and lower nutrient flow paths, respectively. DO concentration data was adjusted using atmospheric pressure data from the Plum Island Ecosystem Long Term Ecological Research (PIE-LTER) Marshview Farm in Newbury, MA.